EFFECT OF Bi$_2$O$_3$ AND V$_2$O$_5$ ADDITION ON STUCTURAL, ELECTRICAL TRANSPORT AND ELECTROMAGNETIC PROPERTIES OF Ni-Cu-Zn FERRITES

M. Phil. Thesis

By

Md. ABDUL GOFUR

প্রভু!
আমায়
জ্ঞান দাও

DEPARTMENT OF PHYSICS

KHULNA UNIVERSITY OF ENGINEERING & TECHNOLOGY

KHULNA - 9203, BANGLADESH

DECEMBER - 2016

EFFECT OF Bi_2O_3 AND V_2O_5 ADDITION ON STUCTURAL, ELECTRICAL TRANSPORT AND ELECTROMAGNETIC PROPERTIES OF Ni-Cu-Zn FERRITES

BY

Md. ABDUL GOFUR

ROLL No. 1155551

SESSION: JULY - 2011

A THESIS SUBMITED TO THE DEPARTMENT OF PHYSICS, KHULNA UNIVERSITY OF ENGINEERING & TECHNOLOGY, KHULNA - 9203 IN PARTIAL FULFILMENT OF THE REQUIRMENT FOR THE DEGREE OF MASTER OF PHILOSOPHY

DEPARTMENT OF PHYSICS

KHULNA UNIVERSITY OF ENGINEERING & TECHNOLOGY

KHULNA - 9203, BANGLADESH

DECEMBER - 2016

TO

MY PARENTS

DECLARATION

This is to certify that the thesis work entitled as **"Effect of Bi$_2$O$_3$ and V$_2$O$_5$ addition on Structural, Electrical transport and Electromagnetic properties of Ni-Cu-Zn Ferrites "** has been carried out in partial fulfillment of the requirement for M. Phil. degree in the department of Physics, Khulna University of Engineering & Technology, Khulna - 9203, Bangladesh. The above research work or any part of this work has not been submitted anywhere for the award of any degree or diploma. No other person's work has been used without due acknowledgement.
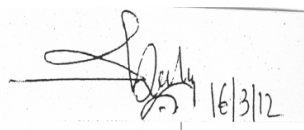
1. Supervisor   Candidate

----------------------------   ---------------------------------
(Prof. Dr. S. S. Sikder)   (Md. Abdul Gofur)

2. Joint-Supervisor

(Dr. Dilip Kumar Saha)

i

ABSTRACT

Ni-Cu-Zn ferrites are well-known technological magnetic materials used for manufacturing of multilayer chip inductor and applications in various electrical devices. The present work is focused on the influence of substitutions and sintering additive V_2O_5 and Bi_2O_3 on structural, transport and electromagnetic properties of Ni-Cu-Zn ferrites. Two series of ferrite samples of the composition $Ni_{0.28}Cu_{0.10}Zn_{0.62}Fe_2O_4$ + x wt.% the concentration sintering additives were varies 0.2wt.% to 0.8wt.% for (i) V_2O_5 and (ii) Bi_2O_3 were prepared by using the solid state reaction technique sintered at 1150^oC and 1200^oC with 6 hours holding time. The X-ray diffraction analysis revealed that all the samples of the two series are crystalline in single phase cubic spinel structure. Lattice parameter of $Ni_{0.28}Cu_{0.10}Zn_{0.62}Fe_2O_4$ + x wt.% V_2O_5 or Bi_2O_3 are slightly decrease with the increase of x content. The average grain size of the samples increases with the increase of V_2O_5 additive content. On the other hand grain growth by increasing Bi_2O_3 content inter diffusion as results after > 0.4wt.% Bi_2O_3 content abnormal grain growth. Curie temperature (T_c) and saturation magnetization (M_s) are slightly increase with increasing V_2O_5 doped ferrite samples up to x = 0.6 after decrease. On the other hand T_c decreases continuously with the increase of Bi_2O_3 additive in the same ferrite samples. The magnetization process all the samples are soft magnetic behavior. Initial permeability (μ_i) increases with the increase of V_2O_5 at both sintering temperatures attaining maximum value for x = 0.4. This enhancement of permeability may be correlated with improved microstructural features. But the μ_i decreases with increasing doped Bi_2O_3 content in ferrite samples and hence the highest value of quality factor is found for x = 0.4 within the range 20kHZ to 2MHz. The μ_i shows a flat profile from 1kHz to 4MHz indicating frequency stability for all the ferrite samples. The improved electromagnetic properties of the composition might be attributed to better densification and visible grain size. DC resistivity decreases with increasing temperature. The dielectric constant is found to decrease continuously with increasing frequency and remain almost constant at higher frequency range. The dielectric behavior of the experiment ferrite samples explained on the basis of the mechanism of the dielectric polarization and conduction process.

Contents

CHAPTER - I

INTRODUCTION

CHAPTER - II

THEROETICAL BACKGROUND

CHAPTER-III

EXPERIMENTAL PROCEDURE

CHAPTER-IV

RESULTS AND DISCUSSION

CHAPTER-V

CONCLUSIONS

List of Figures

List of Tables

List of Symbols

Absolute value of admittance = $|Y|$

Absolute value of impedance = $|Z|$

AC current $= I$

Angular frequency $= \omega$

Anisotropy field $= H_K$

Anisotropy constant $= K_1$

Average anisotropy $= <K>$

Bohr magneton $= \mu_B$

Bragg's angle $= \theta$

Bulk density $= d_B$

Charge of electron $= e$

Capacitance $= C$

Coercivity $= H_C$

Cross-sectional area of toroids $= S$

Curie temperature $= T_C$

DC resistivity $= \rho_{dc}$

Dielectric constant $= \epsilon'$

Diffraction angle $= \theta$

Energy per unit area of a 180^oBloch wall $= \Upsilon$

Exchange integral $= J$

Exchange coupling constant $= J_{ij}$

Exchange correlation length $= L_O$

Face centered cubic $= f_{cc}$

Frequency $= f$

Ferromagnetism $=FM$

Imaginary part of initial permeability $= \mu''$

Impedance $= Z$

Inductance $= L$

Initial permeability $= \mu_i$

Inter planner spacing $= d$

Loss factor $= \tan\delta$

Magnetization $= M$

Magnetic field $= H$

Magnetic induction $= B$

Magneto crystalline anisotropy constant $= K_l$

Nell temperature $= T_N$

Nelson-Riley function $= F(\theta)$

Number of turns $= N$

Peak temperature $= T_P$

Permeability of in free space $= \mu_O$

Quality factor $= QF$

Reactance $= X$

Real part of initial permeability $= \mu'$

Retentivity $= B_r$

Remanent ratio $= M_r$

Resistance $= R$

Resistivity $= \rho$

Saturation magnetization $= M_S$

Saturation induction $= B_S$

Saturation polarization $= J_S$

Susceptance $= B$

Susceptibility $= \chi$

X-ray density $= d_X$

X-ray diffraction $= XRD$

Yafet-Kittel $= Y\text{-}K$

Wavelength $= \lambda$

CHAPTER I

INTRODUCTION

CHAPTER II

THEROETICAL BACKGROUND

CHAPTER III

EXPERIMENTAL PROCEDURE

CHAPTER IV

RESULTS AND DISCUSSION

CHAPTER V

CONCLUSIONS

REFERENCES

INTRODUCTION

1.1 Introduction

Technological advances in a variety of areas have generated a growing demand for the soft magnetic materials in devices. These are now very well established group of magnetic materials. Today ferrites are employed in a truly wide range of applications and have contributed materially to the advances in electronics. In the area of new materials, ferrites with permeabilities up to 3×10^4 and power ferrites for frequencies up to 10MHz have been made available commercially [1.1]. Among the soft magnetic materials, polycrystalline ferrites have received special attention due to their good magnetic properties and high electrical resistivity over a wide range of frequencies; starting from a few hundred hertz (Hz) to several gigahertz (GHz). There are two basic types of magnetic materials, one is metallic and other is metallic oxides. Metallic oxide materials are called ferrites. Ferrites are ferromagnetic mixed oxides having the general formula $MO.Fe_2O_3$, where M is a divalent metal ion such as Mg^{2+}, Mn^{2+}, Zn^{2+}, Ni^{2+}, Co^{2+}, Fe^{2+}, Cd^{2+} and Cu^{2+} etc. [1.2]. Ferrites are more useful because of their high resistivity. The resistivity of ferrites varies from 10^2 to 10^{10} Ω-cm, which is about 15 orders of magnitude higher than that of iron. The ferrites were developed in to commercially important materials by Snoek [1.3] and his associates at the Philips Research Laboratories in Holland.

Spinel type ferrites are commonly used in many electronic and magnetic devices due to their high magnetic permeability and low magnetic losses [1.4-1.5] and also used in electrode materials for high temperature applications because of their high thermodynamic stability, electrical resistivity, electrolytic activity and resistance to corrosion [1.6-1.7]. Moreover, these low cost materials are easy to synthesize and offer the advantages of greater shape formability than their metal and amorphous magnetic counterparts. Almost every item of electronic equipment produced today contains some ferrimagnetic spinel ferrites materials. Loudspeakers, motors, deflection yokes, electromagnetic interface suppressors, radar absorbers, antenna rods, proximity sensors, humidity sensors, memory devices, recording heads, broadband transformers, filters, inductors, etc. are frequently based on ferrites. Soft ferrites still remain the best magnetic materials and cannot be replaced by any other magnetic materials with respect to their very high frequency application because they are

inexpensive, more stable, easily manufactured [1.8]. They have wide range of technological applications in transformer cores, inductors, high quality filters, radio frequency circuits, read/write heads for high speed digital tape and operating devices [1.9-1.11]. Microstructure and magnetic properties of ferrites are highly sensitive to preparation method, sintering conditions amount of constituent metal oxides, various additives including dopants and impurities [1.12-1.15].

Presently, Ni-Cu-Zn ferrites have been the dominant materials for multilayer ferrite chip inductor (MLFCI) component due to its low sintering temperature (<950°C) and good electromagnetic properties [1.16-1.18]. In addition, Ni-Cu-Zn ferrites have better high frequency properties compared to that of Mn-Zn ferrite and low densification temperature than Ni-Zn ferrites [1.19]. Since, the work is related to Ni-Cu-Zn ferrite is a spinel ferrite. The normal spinal ferrites MFe_2O_4 the divalent ions are all in 'A' sites and the Fe^{3+} ions occupy 'B' sites. In spinal structure the magnetic ions are distributed among two different lattices tetrahedral (A) and octahedral (B) sites and are ordered antiparallel to each other cubic spinel ferrites has two sub lattices: Tetrahedral (A) site and Octahedral (B) site in AB_2O_4 crystal structure.

The important structural, electrical and magnetic properties of spinels, responsible for their application in various fields are found to depend on the distribution of cations among to depend on the distribution of cations among the sites. Therefore the estimation of the cation distribution turns out to be important. Various cations can be replaced in A site and B site to tune its magnetic properties. Depending on A site and B site cations it can exhibit various magnetic structures. Ni-Cu-Zn ferrite is solid solution of inverse $NiFe_2O_4$, $CuFe_2O_4$ and normal $ZnFe_2O_4$ ferrites. Due to the favorable fit of charge distribution, Ni^{2+} and Cu^{2+}ions show strong preference to B-sites. Zn^{2+} ions show a strong preference for A-sites due to its electronic configuration. Cu is used in this ferrite to decrease the sintering temperature so that it can be co-fired with Ag internal electrode. However, Cu decreases the resistivity of the ferrite, which is not desirable for its high frequency applications. So, optimization of Cu content with respect to densification and resistivity of the ferrite is very important. Different ranges of electromagnetic properties have been reported with various Z concentrations in Ni-Cu-Zn ferrites. Optimization of Zn concentration with respect to Ni and Cu is essential to achieve desirable electromagnetic properties in the ferrites where Zn enters into the A-sites by displacing a proportion number of Fe^{3+}

from A to B-sites. Among the soft ferrites Ni-Cu-Zn, Mg-Cu-Zn and Mn-Zn ferrites with various additives have been carried out [1.20 - 1.24]. The addition of CuO in the Ni-Zn ferrite composition is known to play a crucial role in increasing the sintering density and lowering the sintering temperature [1.25]. The uses of nano particles in the starting materials for the synthesis of ferrites can also reduce sintering temperature and improve magnetic properties.

Recently, there has been a growing interest in the low temperature sintering of Ni-Zn ferrite doped with CuO for attaining high density and high permeability than undoped Ni-Zn ferrite. Several studies have been conducted to enhance the properties of Ni-Cu-Zn ferrite. Important approaches adopted are: (i) the reduction of the particle size to improve densification, (ii) using sintering aids for better densification and (iii) substitutions at tetrahedral and octahedral crystallographic site in the spinel ferrite to improve electromagnetic properties.

Influence of rare earths on the properties of different ferrites has been reported by many investigators. Rare earth ions can improve densification and increase permeability and resistivity in $(Ni-Cu-Zn)RE_zFe_{2-z}O_4$ ferrites where RE enters into the B-sites by displacing a proportion number of Fe^{3+} from B to A-sites. Various additives such as V_2O_5, Bi_2O_3, PbO, MoO_3, WO_3, Eu_2O_3, P_2O_5, Li_2O_3, Na_2O etc. having low melting point, facilitated to reduce the sintering temperature of these oxide materials due to liquid phase sintering. These additives form liquid phase either due to the melting of the additives or due to the eutectic liquid phase formation between the additives and the ferrite. Amount of the liquid phase increases with increasing amount of sintering aids which results in increased densification. However, excessive amount of sintering additives will deteriorate electromagnetic properties of the ferrites. So, optimum content of sintering aids is necessary to achieve good sinterability as well as better electromagnetic properties. Ni-Cu-Zn ferrites have potential application in the fabrication of MLCI and various electronic applications such as telecommunication because of their good electromagnetic properties at high density covering a wide range of compositions.

So, spinel ferrites of different compositions have been studied and used for a long time to get useful products. Many researchers have worked on different types of ferrites in order to improve their electrical and magnetic properties. There does not exist an ideal ferrite sample that meets the requirements of low eddy current loss and usefulness at frequencies of the GHz. Each one has its own advantages and

disadvantages. Scientists still continue their efforts to achieve the optimum parameters of ferrites, like high saturation magnetization, high permeability, high resistivity etc. Since the research on ferrites is so vast, it is difficult to collect all of the experimental results and information about all types of ferrites in every aspect. Till now researchers have not yet been able to formulate a rigid set of rules for ferrites about a single property. Among these V_2O_5 and Bi_2O_3 where the most effective sintering aids for Ni-Cu-Zn ferrites the systematic research is still necessary for a more comprehensive understanding and properties such materials. In the present work efforts has been under taken to prepare Ni-Cu-Zn ferrite doped with V_2O_5 and Bi_2O_3.

1.2   Application of Ferrites

Ferrites are very important magnetic materials because of their high electric resistivity; they have wide applications in technology, particular at high frequencies. Ferrites are used due to their following properties:

(i)   Ferrites are particularly used as inductive components in a large variety of electronic circuits such as low- noise amplifiers, filters voltage-controlled oscillators, impedance matching networks, for instance. The basic components to produce the inductance are very soft ferrite and a metallic coil.

(ii)   Ferrites are part of low power and high flux transformers which are used in television.

(iii)   Soft ferrites were used for the manufacture of inductor core in combination with capacitor circuits in telephone system, but now a day solid state device have replaced them. The soft Ni-Zn and Mn-Zn ferrites are used for core manufacture.

(iv)   Almost every item of electronic equipment produced such as electromagnets, electric motors, loud speakers, deflection Yokes, generators, radar absorbers, antenna rods, proximity, sensors, humidity sensors, memory devices, recording head, broad band transformer, filters, inductor etc are frequently based on ferrite.

(v)   In computer, non volatile memories are made of ferrite materials. They store information even if power supply fails. Non-volatile memories are made up of ferrite materials as they are highly stable against severe shock and vibrations.

(vi)   Ferrites are used in high frequency transformer core and computer memories i.e. computer hard disk, floppy disks, credit cards, audio cassettes, video cassettes and recorder heads.

(vii) Ferrites are primarily used as inductive components in a large variety of electronic circuits such as low-noise amplifiers, filters, voltage-controlled oscillators, impedance matching networks, for instance. The basic components to produce the inductance are a very soft ferrite and a metallic coil.

(viii) Ferrites are used in microwave devices like circulation, isolators, and switches phase shifters and in radar circuits.

(ix)   Nickel alloys are used in high frequency equipments like high speed relays, wide band transformers and inductors. They are used to manufacture transformers, inductors, small motors, synchors and relays. They are used for precision voltage and current transformers and inductive potentiometers.

(x)   Layered samples of ferrites with piezoelectric oxides can lead to a new generation of magnetic field sensors. These sensors can provide a high sensitivity, miniature size, virtually zero power consumption; sensors for AC and DC electric currents can be fabricated.

(xi)   Ferrites are used as electromagnetic wave absorbers at low dielectric value.

(xii) Ferrite beads are found on all cable types including USB cables, serial port cables and AC adaptor power supply cables. They also are placed on coaxial cables to form so called choke baluns. A choke balun can be used to reduce noise currents on the cable and if placed at the point where the cable connects to a balanced antenna such as a dipole, the beads transform the balanced antenna currents to unbalanced coaxial cable currents.

1.3   The Aims and Objectives of the Present Work

Soft ferrites are relatively cheap materials which are within our means and technical ability to develop. There are large numbers of applications of these soft magnetic materials where high frequency electromagnetic energy use is involved. At present, Bangladesh is totally dependent upon the imported ferrite cores and other soft magnetic materials. If can be develop a ferrite in our country, that may alleviate this

problem. Research in this field will provide information in choosing appropriate materials for the above applications and ultimately high quality materials with desired characteristics and will open up the possibility of indigenous development of ferrite technology.

The main objectives of the present research work are to synthesize Ni-Cu-Zn ferrites of composition $Ni_{0.28}Cu_{0.10}Zn_{0.62}Fe_2O_4$+ x wt.% additives such as

(i) $Ni_{0.28}Cu_{0.10}Zn_{0.62}Fe_2O_4$+ x wt.% V_2O_5 [x = 0.2, 0.4, 0.6 and 0.8] and

(ii) $Ni_{0.28}Cu_{0.10}Zn_{0.62}Fe_2O_4$+ x wt.% Bi_2O_3 [x = 0.2, 0.4, 0.6 and 0.8]

The raw oxide materials in the synthesis of ferrites samples are commercially available of nano particle size of 20- 70nm.

The low melting point additives as sintering aid would be optimized to a maximum value so that the magnetic properties are not jeopardized but an effective low temperature sintering is achieved. Finally structural, electrical transport and magnetic properties of all the prepared samples such as magnetization, Curie temperature, magnetic permeability, magnetic loss components, coercivity, resistivity, dielectric constant, etc. would be studied in detail to find out an optimum composition. Ni-Cu-Zn ferrites are generally used as magnetic materials for their better properties at high frequencies than for Mn-Zn and their lower densification temperature. It is expected that the use of nano particles as starting materials may give uniform microstructure exhibiting better magnetic and electrical transport properties. The addition of additives as sintering aid will reduce the sintering temperature which may affect to obtain homogeneous microstructure and enhanced electromagnetic properties. The accumulated results would be interpreted on the basis of existing theories of magnetism.

1.4   Experimental Reason for this Research Work

Ferrites samples would be prepared by conventional double sintering ceramic technique using high purity oxide nanomaterials. The experimental methods would be used in this research work as follows:

- The prepared sample has been characterized in terms of their crystal structure, unit cell parameters and phase presents in the prepared samples with the help of X-ray diffractometer (XRD).
- Sintering of the samples has been carried out in a micro processor controlled high temperature furnace.

- Permeability, magnetic loss factor and relative quality factor as a function of frequency and temperature has been determined using an impedance analyzer.
- Curie temperature/ magnetic phase transition has been determined by permeability versus temperature measurement with the help of a oven using a LCR meter.
- Magnetization of the samples has been measured as a function of field using vibrating sample magnetometer (VSM)
- DC electrical resistivity and dielectric properties as a function of frequency and temperature has been studied with the help of electrometer/ inductance meter.

1.5 Review of the Earlier Research Work

Spinel ferrites are extremely important for academic and technological applications. The physical properties such as structural, electrical and magnetic properties are governed by the type of magnetic ions residing on the tetrahedral A-site and B-site of the spinel lattice and the relative strength of the inter- and intra-sublattice interactions. In recent years, the design and synthesis of non-magnetic particles have been the focus of fundamental and applied research owing to their enhanced or unusual properties [1.26]. It is possible to manipulate the properties of spinel material to meet the demands of a specific application. A large number of scientists are involved in research on the ferrites materials. Before discussing our research work, we shall see the previous work done related to our through literature survey.

Khan *et. al* [1.27] and Low *et. al* [1.28] reported that Ni-Cu-Zn ferrites are well established soft magnetic material for MLCI applications because of their relatively low sintering temperature, high permeability in the RF frequency region and high electrical resistivity. Khan *et. al* [1.29] studied complex permeability spectra of Ni-Cu-Zn ferrites. The particle size increase the sintering temperature is raised. For the composition and different sintering temperature was found that the real permeability in that low frequency region decreases CuO. Manjurul Haque *et. al* [1.30] reported the effect of Zn^{2+} substitution on the magnetic properties of $Mg_{1-x}Zn_xFe_2O_4$ ferrites prepared by solid-state reaction method. They observed that the lattice parameter increases linearly with the increase in Zn content. The Curie

temperature decreases with the increase in Zn content. The saturation magnetization (M_s) and magnetic moment are observed to increase up to x = 0.40 and thereafter decreases due to the spin canting in B-sites. The initial permeability increases with the addition of Zn^{2+} ions but the resonance frequency shift towards the lower frequency.

Yue *et. al* [1.31] worked on the effect of Cu on the electromagnetic properties of $(Mg_{0.5-x}Cu_xZn_{0.5})O(Fe_2O_3)_{0.98}$ ferrites and found that the density, grain size, permeability, Curie temperature increased; resistivity decreased with Cu content up to x = 0.40. Rezlescu *et .al* [1.32] reported the effect of Cu substitution on the physical properties of $(Mg_{0.5-x}Cu_xZn_{0.5})Fe_2O_4 +0.5MgO$ ferrites. They found that the density increased up to x=0.30 whereas, resistivity increased up to x = 0.10 and permeability increased with Cu content as well. They [1.33] also reported that the sintered density and resistivity of $(Mg_{0.5-x}Cu_xZn_{0.5}O)Fe_2O_3$ ferrite increased up to x = 0.30 whereas, permeability increased up to x = 0.40.

Noor *et. al* [1.34-1.35] investigated composition dependence of $Co_{1-x}Cd_xFe_2O_4$ sintered at 1050°C/3hrs. They found variation of lattice parameter with Cd content obeys Vagard's law and the linear variation of X-ray densities with Cd-content. Bulk density is found to increase while porosity decreases with increasing Cd-content. Curie temperature decrease linearly with the addition of Cd-ions. The initial permeability increases with Cd content and sintering temperature has little effect on permeability. Saturation magnetization increases with increasing Cd content at x ≥ 0.40 and then it decreases. The hysteresis behavior and initial permeability reveals the softer ferromagnetic nature of the studied sample. DC electrical resistivity is found to increases with the increase of Cd content.

Ni-Cu-Zn ferrites are soft magnetic materials that are used for inductive multilayer devices because of their low sintering temperature and their good performance at intermediate at high frequencies, Ni-Cu-Zn ferrites are Co-fired with internal Ag conductor, because of the melting point of silver, the sintering temperature is limit T ≤ 950°C. The first MLCI were developed by Nomura *et. al.* [1.36] and Nakamura *et. al.*[1.37]. Multilayer chip LC filters and hybrid circuit devices appeared as second generation of inductive multilayer. SMD components reported by Yasuda et. al.[1.38]. The required low sintering temperature it is crucial to use powders with high activity at 900°C. Several soft chemistry routes have been explored in order to synthesize reactive powder, e.g. Sol-gel synthesis [1.28], auto-combustion synthesis studied [1.39] or Co-precipitation of oxalates [1.40]. Different

sintering additives have been proposed to enhance the densification behavior of Ni-Cu-Zn ferrites, e.g. V_2O_5 [1.40], PbO[1.41] and glasses[1.42].

The preparation of highly reactive sub-micron Ni-Cu-Zn ferrite powders by milling of calcined raw materials. The influence of powder particle size and bismuth oxide addition on the densification behavior ferrite microstructure and permeability are outlined, contrary to studied by Jeong *et. al.* [1.43] at intermediate concentration of Bi_2O_3 an inhomogeneous microstructure with large grains is formed causing maximum permeability. Wang *et. al.* [1.44] worked on the mixing of $(Ni_{0.38}Cu_{0.12}Zn_{0.50})Fe_2O_4$ powders with Bi_2O_3 using the solid state mixing as well as wet chemical coating processes such as ammonia precipitation coating, area precipitation coating and solution coating. Wang *et. al.* [1.45] used $PbO-SiO_2$, $PbO-Bi_2O_3$ and Bi_2O_3 flux systems to lower the sintering temperature of $(Ni_{0.38}Cu_{0.12}Zn_{0.50})Fe_2O_4$ ferrite and found that the $PbO-SiO_2$ posses higher resistivity, higher quality factor and higher coercivity compared with those obtained using other systems. The results also showed that the addition of Bi_2O_3 considerable deteriorated the quality factor of Ni-Cu-Zn ferrites, through benefited the densification and permeability.

Su *et. al.*[1.46] investigated the effects of mixed $Bi_2O_3-WO_3$ additives. The results showed that appropriate additives of mixed $Bi_2O_3-WO_3$ could enhance densification of the specimens, improve the initial permeability and the quality factor of Ni-Cu-Zn ferrites. Kawano *et. al.* [1.47] fabricated Bi, Si oxides-doped Ni-Cu-Zn ferrite composite materials. Analysis showed that the composite materials has mainly Ni-Cu-Zn ferrite and $Bi_4(SiO_4)_3$ phases. The optimum percentage of Bi_2O_3 content to improve the electromagnetic properties in Ni-Cu-Zn ferrite is 0.25wt.%. Kong *et. al.*[1.48] have prepared Bi_2O_3 doped $MgFe_{1.98}O_4$ ferrite by using the solid state reaction process and studied the effect of Bi_2O_3 and sintering temperature on the dc resistivity, complex relative permittivity and permeability. They found that the poor densification and slow grain growth rate of $MgFe_{1.98}O_4$ can be greatly improved by the addition Bi_2O_3, because liquid phase sintering was facilitated by the formation of a liquid phase layer due to the low melting point of Bi_2O_3. The average grain size has a maximum at a certain concentration, depending on sintering temperature.

Ping Hu *et. al.* [1.49] have considered the ways of reducing sintering temperature of high permeability Ni-Zn ferrites. It was found that optimum additions of CuO and V_2O_5 contributed to the grain growth and the densification of matrix in

the sintering process, leading to decrease in sintering temperatures of Ni-Zn ferrites. The post-sintering density and the initial permeability were also strongly affected by the average particle size of raw materials. Jingling Sun [1.50] measured the effects of La_2O_3 and Gd_2O_3 on some properties of Ni-Zn ferrites The R_2O_3 [r = La or Gd] substitutions decrees samples density and increase lattice parameter of higher sintering temperature is necessary for densification with R_2O_3. R_2O_3 substitution tends to flatten dielectric constant versus frequency curves, increase the value of dielectric constant and lower the value of loss factor.

One of the key parameters to increase the permeability in spinel ferrite is lowering the magnetostriction constant. As the magnetostriction constant of Mg-Cu-Zn ferrites is lower than Ni-Cu-Zn [1.51] and decreased with increasing Mg content [1.52]. Mg can be substituted for Ni to increase the permeability in Ni-Cu-Zn ferrites. Another important sintering aid is MoO_3 Seo *et. al.* [1.53] focused on the effect of MoO_3 addition on the sintering behavior and magnetic properties of $(Ni_{0.2}Cu_{0.2}Zn_{0.6})_{1.02}(Fe_2O_3)_{0.98}$ ferrite. Results showed that MoO_3 addition reduced the sintering temperature and magnetic loss of Ni-Cu-Zn ferrite and it is increased the bulk density and initial permeability up to additive content of 0.2wt.%. Gu et. al [1.54] reported the effect of MoO_3 and TiO_3 additions on the magnetic properties of Mn-Zn power ferrites fluctuate with increase of MoO_3 content and could be considerably improved with suitable amount of MoO_3 addition.

These additives form liquid phase which either due to the melting of the additives or eutectic liquid phase formation between the additives and ferrites. In addition, serving as a liquid phase to promote the densification, it is important to recognize that the additives components may also play an important role in the contribution to the magnetic properties of the sintered ferrites. Flux sintered ferrite may not always result in the desired magnetic properties.

From the above mentioned review works it is observed that physical, magnetic, electrical transport and microstructure properties are strongly dependent on addition substitution in a very complicated way and there is no straight forward relationship between the nature and the quantity of doping on the magnetic characteristic to be understood by any simple theory. There are strongly dependent on several factors like sintering condition preparation methods, compositions etc. In the present work it is aimed at determining experimental microstructure exhibiting better magnetic and electrical properties as affected by sintering temperature/time,

composition and the nature and amount of substations. The addition of additives as sintering aid will reduce the sintering temperature which may affect to obtain homogeneous microstructure and enhanced electromagnetic properties. Ni-Cu-Zn ferrites are generally used as magnetic materials for their better properties at high frequency than for Mn-Zn ferrites. So that Ni-Cu-Zn ferrites with appropriate substitution can be obtained in respect of improving electromagnetic properties.

1.6   Outline of the Thesis

The thesis has been configured into Six chapters which are as follows:

Chapter 1: Introduction

In this chapter, a brief introduction to Ni-Cu-Zn ferrites and organization of thesis. This chapter incorporates background information to assist in understanding the aims and objectives of this investigation, and also reviews recent reports by other investigators with which these results can compared.

Chapter II: Theoretical Background

In this chapter, a briefly describe theories necessary to understand the present work.

Chapter III: Experimental Background

In this chapter, the experiment procedures are briefly explained along with description of the sample preparation, raw materials. This chapter deals with mainly the design and construction of experimental and preparation of ferrite samples. The fundamentals and working principles of measurement set up are discussed.

Chapter IV: Result and Discussion

In this chapter, describes the   result and discussion about the structural, magnetic and electrical properties of $Ni_{0.28}Cu_{0.10}Zn_{0.62}Fe_2O_4$ doped with V_2O_5.

Chapter V: Result and Discussion

In this chapter, describes the   result and discussion about the structural, magnetic and electrical properties of $Ni_{0.28}Cu_{0.10}Zn_{0.62}Fe_2O_4$ doped with Bi_2O_3.

Chapter VI: Conclusion

In this chapter, the results obtained in this study are summarized. Suggestions for future works on these studies are included.

References are added at the end of each chapter.

THEROETICAL BACKGROUND

2.1   Introduction of Ferrites

Ferrites are ferromagnetic cubic spinels that posses the combined properties of magnetic materials and insulators. They form a complex system composed of grains, grain boundaries and pores. A ferrimagnetic material is defined as one which below a transition temperature exhibits a spontaneous magnetization that arises from non parallel arrangement of the strongly coupled magnetic moments. They have the magneto-dielectric property of material which is useful for high frequency (2 -30 MHz) antenna design. The usefulness of ferrite is influenced by the physical and chemical properties of the materials and depends on many factors including the preparation conditions, such as, sintering temperature, sintering time, rate of heating, cooling and grinding time. In the spinel structure, the magnetic ions are distributed among two different two lattice sites, tetrahedral (A) and octahedral (B) sites. The electromagnetic properties of these ferrites depend on the relative distribution of cations at the different sites as well as the preparation condition.

Ferrites are electrically non-conductive ferrimagnetic ceramic compound materials, consisting of various mixtures of iron oxides such as Hematite (Fe_2O_3) or Magnetite (Fe_3O_4) and the oxides of other metal like NiO, CuO, ZnO, MnO, CoO, MgO. The prime property of ferrites is that, in the magnetized state, all the spin magnetic moments are not oriented in the same direction few of them are in the opposite direction. But at the spin magnetic moments are of two types with different values. The net magnetic moments will have some finite value. The molecular formula at ferrites is $M^{2+}O.Fe_2^{3+}O_3$, where M stands for the divalent metal such as Fe, Mn, Co, Ni, Cu, Mg, Zn or Cd. There are 8 molecules per unit cell in a spinel structure. There are 32 oxygen (O^{2-}) ions, $16Fe^{3+}$ ions and $8M^{2+}$ions, per unit cell. Out of them $8Fe^{3+}$ and $8M^{2+}$ ions occupy the octahedral sites. Each ion is surrounded by 6 oxygen ions.

The spin of all such ions are parallel to each other. The rest $8Fe^{3+}$ ions occupy the tetrahedral site which means that each ion is surrounded by 4 oxygen ions. The spin of these 8 ions in the tetrahedral sites, are all oriented antiparallel to the spin in the octahedral sites. The net spin magnetic moment of Fe^{3+} ions is zero as the 8 spin in

the tetrahedral sites cancel the 8 antiparallel spins in the octahedral site. The spin magnetic moment of the $8M^{2+}$ ions contribute to the magnetization of ferrites [2.1]

Ferrites have been studies since 1936. They have an enormous impact over the application of magnetic materials. Ferrites are essentially ceramic materials, compound of iron, boron, barium, strontium, lead, zinc, magnesium or manganese. The ingredients are mixed, preferred, milled/crushed, dried, shaped and finally pressed and fired into their final hand a brittle state. Now a days newer family of ferrite materials have been discovered, which are rare-earth types. Additives of rare earth metals like vanadium oxide (V_2O_5) are used to study the effect of enhancing the magnetic properties. Therefore, hard ferrites constitute the major fraction since they are used whether energy per unit eight and cost are important considerations [2.2]. Ferrite are a class of chemical compounds with the formula AB_2O_4 where A and B represent various metal cations usually including iron. These ceramic materials are used in applications ranging from magnetic components in micro electronics. The DC electrical resistivity of ferrites at room temperature can vary depending upon the chemical composition between about $10^{-2}\Omega$-cm and higher than $10^{11}\Omega$-cm [2.3] Ferrites are classified into two categories based on their coercive field strength. They are:

(i)   Soft ferrite with coercive field strength <10 Oe.
(ii)   Hard ferrite with coercive field strength >125 Oe.

2.2   Types of Ferrites

According to the crystallographic structures ferrites can be classified into three different types [2.4]

(i)   Cubic ferrites of spinel
(ii)   Hexagonal ferrites
(iii)   Cubic ferrites of garnets.

Ferrites fallen into two groups with different crystal structures are shown in the following block diagram shown in figure-2.1.

The present research work is on spinal ferrites therefore it has been discussed in detail the spinel ferrites only.

```
                      ┌─────────────────┐
                      │     FERRITE     │
                      └─────────────────┘
                               │
             ┌─────────────────┴─────────────────┐
   ┌───────────────────┐              ┌───────────────────────┐
   │       CUBIC       │              │      HEXAGONAL         │
   │                   │              │                        │
   │  e.g. MeO. Fe₂O₃  │              │  e.g. BaO.6Fe₂O₃       │
   └───────────────────┘              └───────────────────────┘
             │
     ┌───────┴───────────────────────────┐
┌──────────────────┐          ┌────────────────────────────┐
│     SPINEL       │          │         GARNET             │
│  e.g. MgAl₂O₄    │          │  e.g. 3MnO. Al₂O₃. 3SiO₂   │
└──────────────────┘          └────────────────────────────┘
```
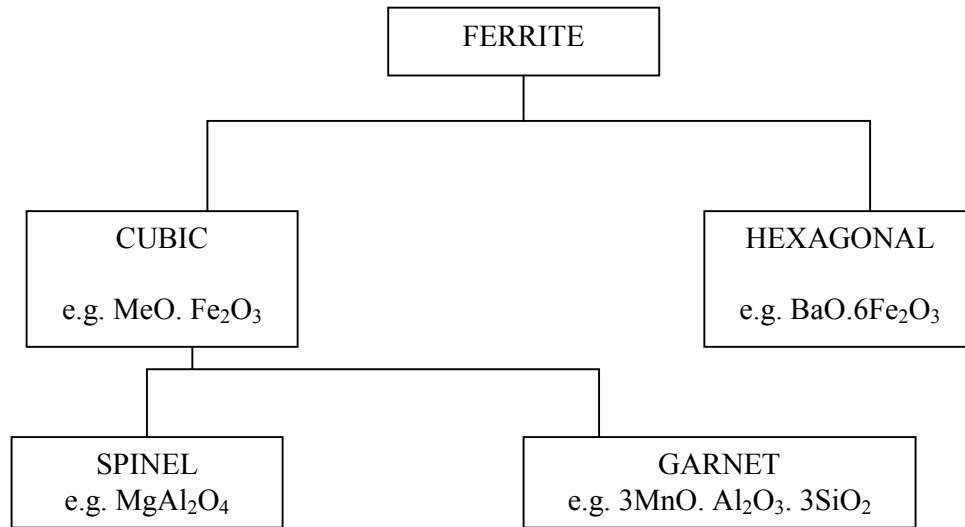
Figure 2.1: Classification of Ferrites

2.2.1 Cubic Ferrites with Spinel Structure

They are also called cubic ferrites. Spinel is the most widely used family of ferrites and are sometimes called ferrospinels because their crystal structure is closely related to that of the natural mineral spinal. High values of electrical resistivity and low eddy current losses make them ideal for their use at microwave frequencies. The spinal structure of ferrites as possessed by mineral spinel $MgAl_2O_4$ was first determined by Bragg [2.5]. Ni-Cu-Zn ferrite is a spinel ferrite. Magnetic spinels have the general formula $MO.Fe_2O_3$ or MFe_2O_4, where M is one of the divalent cations of the transition elements such as Mn, Ni, Mg, Zn, Cd, Co etc. A combination of these ions is also possible and it can named as solid solution of two ferrites or mixed spinel ferrites. Ni-Cu-Zn ferrite in spinel notation can be represented as $(NiCuZn)_1Fe_2O_4$. The spinel lattice is composed of a closed-packed oxygen arrangement in which 32 oxygen ions from a unit cell. There are two kinds of interstices in between the closed-packed anions as shown in figure 2.2; (a) tetrahedral coordinated interstices (called A-site) which are surrounded by 4 nearest neighboring oxygen ions and (b) octahedral coordinated interstices (called B-site) which are coordinated by 6 nearest neighboring oxygen ions. Structurally spinel can be represented as AB_2O_4. One unit cell of it contains eight formula units of AB_2O_4, where out of 64 A-sites 8 and out of 32 B-sites 16 are occupied by cations.

The crystal structure of ferrite is based on a fcc lattice of the oxygen ions. Each unit cell contains eight formula units. Therefore there are $32O^{2-}$ anions $16Fe^{3+}$ cations and $8M^{2+}$ cations in the cell and the order of 8.50 in each unit cell there are 64 tetrahedral or A-sites and 32 octahedral or B-site. These sites are so named because they are surrounded by four and six oxygen ions at equal distances respectively.

AB_2O_4

⊗ A   ◎ B   ◯ O
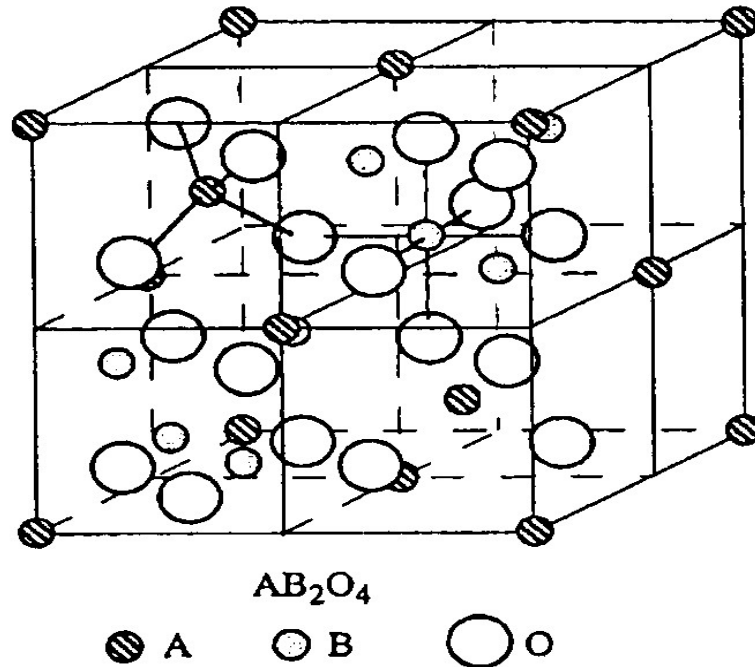
Figure 2.2: Schematic of two sub cells of a unit cell of the spinal structure, showing octahedral or tetrahedral sites.

The lattice characteristics of a spinel include a fcc site for the oxygen atoms and two cationic sites occupying A and B sites [2.6-2.7]. In a spinel, there are 64 A sites 32 B sites and 32 oxygen sites in a unit cell. Due to their exchange coupling, spinel ferrites are ferromagnetically aligned where all of the moments of A-sites 34 are aligned parallel with respect to one another while moments of A and B sites are antiparallel to each other. The change neutrality requires the presence of the cations within the structure to counter balance the change of these oxygen anions. These cations rest on two types of interstitial sites to preserve the charge neutrality namely A and B sites. The magnetic properties of spinel ferrites are generally influenced by composition and cation distribution. Variation of cation distribution between the

cationic sites leads to different electrical and magnetic properties even if the composition of the spinel is the same. The distribution of cations over A and B sites is determined by their ionic radius, electronic configuration and electrostatic energy in the spinel lattice. The octahedral sites are large than the tetrahedral sites, thus, the divalent ions are localized in the octahedral sites where trivalent ions are in the tetrahedral sites [2.8]. Each type of lattice sites will accept other metal ions with a suitable, 0.65 - 0.80Å at B-sites and 0.40 - 0.64Å at A sites.

The spinal ferrites have been classified into three categories due to the distribution of cation on tetrahedral (A) and octahedral (B) sites.

(i)   Normal spinel ferrites
(ii)   Inverse spinal ferrites
(iii) Intermediate or Mixed spinal ferrites.

2.2.1.1 Normal Spinel Ferrites

In normal spinel ferrite MFe_2O_4, the divalent ions are all in A-sites and the Fe^{3+} ions occupy B-sites. If there is only one kind of cations on octahedral (B) sites, the spinel is normal. In these ferrites the divalent cations occupy tetrahedral (A) sites while the trivalent cations are on octahedral (B) sites. The divalent cation (M^{2+}) are the tetrahedral A-sites and two trivalent (Fe^{3+}) cations are in octahedral B-sites which is represented as $(M^{2+})_A[Fe^{3+}Fe^{3+}]_BO_4$. A typical example of normal spinel ferrite is bulk $ZnFe_2O_4$.

2.2.1.2 Inverse Spinal Ferrites

In inverse spinel the divalent ions occupy some of the B-sites and the Fe^{3+} ions are divided equally between A- and B-sites. These structure half of the trivalent (A) sites and half octahedral (B) sites, the remaining cations being randomly distributed among the octahedral (B) sites. In this case divalent (M^{2+}) cations are in octahedral B- sites and the trivalent (Fe^{3+}) cations are equally divided between A and B sites. The divalent and trivalent ions normally occupy the B-sites in a random fashion i.e. they are disordered. These ferrites are represented by the formula $[Fe^{3+}]_A[M^{2+}Fe^{3+}]_BO_4$. A typical example of inverse spinal ferrite is Fe_3O_4 in which divalent cations of Fe occupy the octahedral (B) sites [2.9]. Most of the magnetic spinels are inverse type like $NiFe_2O_4$, $CuFe_2O_4$, $MnFe_2O_4$ etc.

2.2.1.3 Intermediate or Mixed Spinel Ferrites

X-ray and neutron diffraction experiments and magnetization measurements show that there is a whole range of cation distribution between the normal and inverse structure spinel with ionic distribution, intermediate between normal and inverse are known as mixed spinel. The arrangement of the form $(M_\delta^{2+}Fe^{3+}_{1-\delta})[M^{2+}_{1-\delta}Fe^{3+}_{1+\delta}]_BO_4^{2-}$, where δ is called inversion parameter. Quantity δ depends on the method of preparation and nature of the constituents of the ferrites. $\delta = 0$ for completely normal ferrites, $\delta = 1$ for completely inverse spinal ferrites and $0 < \delta < 1$ for intermediate spinels. For completely mixed ferrites $\delta = \frac{1}{3}$. If there unequal number of each kind of cations on octahedral sites, the spinal is called mixed. Typical example of mixed spinal ferrite is $MgFe_2O_4$ and $MnFe_2O_4$ [2.10].

2.2.2 Hexagonal ferrites

This was first identified by Went, Rathenau Gorter and Van Oostershout in 1952 [2.3] and Jonken, Wijin Z Braunin 1956. Hexaferrite are hexagonal or rhombohedral ferromagnetic oxides with formula $MFe_{12}O_4$, where M is an element like Barium, Lead or Strontium. The third type of ferrites are often called the barium ferrites these compounds usually contain BaO, in addition to Fe_2O_3, as the basic component oxide. They are also known as magneto plumbites. The common chemical formula of barium ferrites is $l(BaO) . m(MO). N(Fe_2O_3)_n$ or $Ba^{3+}M_m^{2+}Fe_{2n}^{3+}O_{l+m+3n}$, where l is much more complex than the previous two in both in terms of composition of barium ferrites may be changed one is to vary the M^{3+} ions. Mg, Mn, Fe, Co, Ni, Cu, and Zn are found suitable for the formation of hexagonal ferrites. Another way is to alter the values of l, m, and n. Basic combinations are found at 1-0-6 (M), 1-2-8 (M_2W), 2-2-6 (M_2Y) and 3-2-12 (M_2Z). Compounds formed under these combinations are termed classical hexagonal ferrites. Still another way is to substitute for Ba with Pb or Sr and or substitute for Fe with Al, Ga, Cr or Mn. A fourth way to vary the composition of barium ferrites is to mix two or more of the classical hexagonal ferrite in different proportions. They are widely used as permanent magnets and have high coercivity. They are used at very high frequency. Their hexagonal ferrite lattice is similar to the spinal structure with closely packed oxygen ions, but there are also metal ions at some layers with the same ionic radii as that of oxygen ions, hexagonal ferrites have larger ions than that of garnet ferrites and are formed by the replacement of oxygen ions. Most of these ions are Ba, Sr, or lead.

2.2.3 Cubic Ferrites of Garnet

Yoder and Keith reported [2.3] in 1951 that substituted can be made in ideal mineral garnet $Mn_3Al_2Si_{13}O_{12}$, or equivalently $3MnO.Al_2O_3.3Si_2O_3$ single magnetic garnets have the general formula $3M_2O_3.5Fe_2O_3 = 2M_3^{3+}Fe_5^{3+}O_{12}$. It is to be noted that in magnetic garnets, the 24 positive charge units per formula units are divided unequally between the ferrites ions (15 units) and another species of trivalent ions (9 units). Technically useful garnets are those with M = Sm, Eu, Gd, Tb, Dy, Ho, Er, Tm, Yb or Y. They are known as rare earth garnets. Figure 2.3 shows the cubic ferrite of garnet.
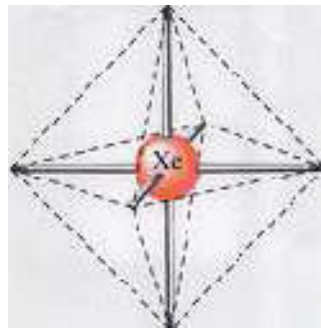
. Figure 2.3: Cubic ferrite of garnet

Bertaut and Forret prepared [2.3] YIG for the Yttrium-iron garnet ($Y_3Fe_5O_{12}$) in 1956 and measured their magnetic properties. In 1957 Geller and Gilleo prepared [2.1] and investigated REG stands for the rare-earth garnet, GdIG for the gadolinium-iron-garnet ($Gd_3Fe_5O_{12}$) which is also a magnetic compound. Garnets crystallize in the cubic system with two fifths of the ferric ions forming a bcc lattice, like ferrospinals, the garnets too, pace a large number (160) of ion in eight units formula unit cell. The lattice constant is ≈ 12.5Å about 50% larger than those ferrospinal. Also the crystal structure of garnets is more complicated than the spinal structure because of the size (0.85-1.10Å) of the M^{3+} ions. They are too large to be accommodated at the interstitial sites between the oxygen ions. Hence the oxygen ions are prohibited from forming a close packed structure as in the spinal. The general formulas for the unit cell of a pure iron garnet have eight formula units of $M_3Fe_5O_{12}$, where M is trivalent rare earth ions (Y, Gd, Dy). Their cell shape is cubic and the edge length is about 12.5 Å. They have complex crystal structure. They are important due to their application in memory structure.

2.3   The Spinel Structure

The ferrites have general formula $M^{2+}Fe^{3+}O_4$ where M^{2+} represents a divalent metal cation such as Mn, Fe, Co, Ni, Zn, Cd and Mg or combination of two divalent ions and Fe^{3+} is the trivalent iron cation. Ferrite's structure is derived from the mineral $MgAl_2O_4$ determined by Bragg [2.5]. The unit cell consists of eight formula units ($8Me^{2+}Fe^{2+}O_4$) as shown in Fig. (2.5a). The 32 oxygen ions form an fcc lattice in which two types of interstitial sites are present namely (a) 64 tetrahedral sites surrounded by 4 oxygen (A-sites) and (b) 32 octahedral sites surrounded by 6 oxygen ions (B-sites). The space group is (O^7_h-F3dm), with following cationic position [2.11-2.12].

8-fold positions, 8 metal cations

$$000, \quad \frac{1}{4}\,\frac{1}{4}\,\frac{1}{4}$$

16-fold positions, 16 metal ions

$$\frac{5}{8}\,\frac{5}{8}\,\frac{5}{8}, \quad \frac{5}{8}\,\frac{7}{8}\,\frac{7}{8}, \quad \frac{7}{8}\,\frac{5}{8}\,\frac{7}{8}, \quad \frac{7}{8}\,\frac{7}{8}\,\frac{5}{8}$$

32- fold positions, 32 oxygen ions

$uuu, u\,\bar{u}\,\bar{u}$

$$\frac{1}{4} - u, \quad \frac{1}{4} - u, \quad \frac{1}{4} - u, \quad \frac{1}{4} - u, \quad \frac{1}{4} - u, \quad \frac{1}{4} - u,$$

$\bar{u}\,u\,\bar{u}, \bar{u}\,\bar{u}\,u$

$$\frac{1}{4} + u, \quad \frac{1}{4} + u, \quad \frac{1}{4} + u, \quad \frac{1}{4} + u, \quad \frac{1}{4} + u, \quad \frac{1}{4} + u,$$

with fcc translations $\left(0\;0\;0, \; 0\frac{1}{2}\,\frac{1}{2}, \; \frac{1}{2}\,0\,\frac{1}{2}, \; \frac{1}{2}\,\frac{1}{2}\,0 \right)$ and $u = \frac{3}{8}$

It is useful to divide the cubic lattice into two groups [2.8, 2.13];

(i) subshell consisting of four cubes with edge lengths, $\frac{a}{2}$, called octants. As shown in Figure (2.5a), where two adjacent octants are illustrated, each of these small cubes contains four oxygen ions. In one of these octants, the oxygen ions lie along the main diagonal and are halfway from the divalent cations in the corner sites.

19
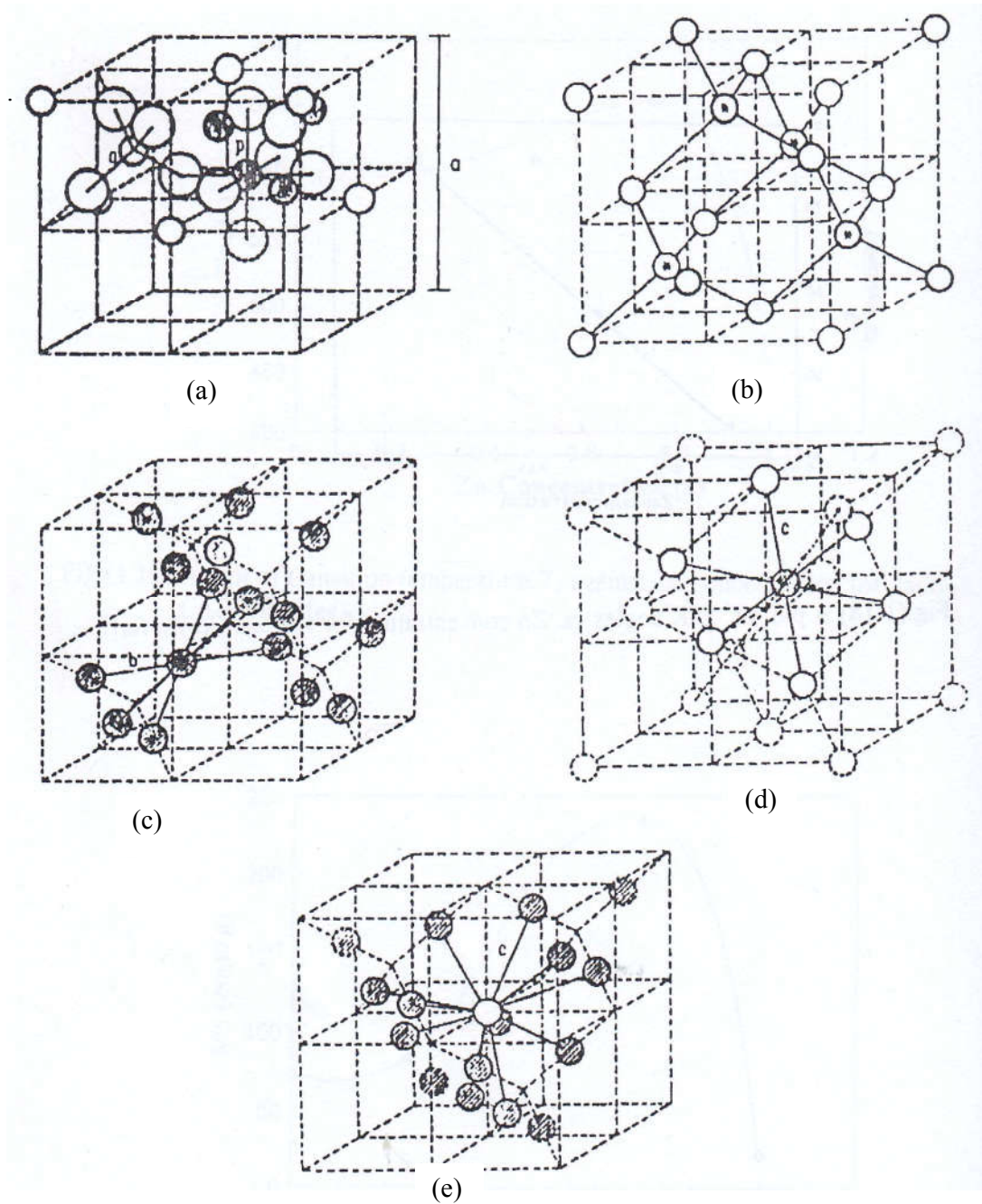
Figure 2.4: Unit cells of the spinel structure (a) showing the tetrahedral and octahedral sites in two adjacent octants. Large circles: Oxygen ions; small hatched circles octahedral metal ions; small unhitched circles: tetrahedral metal ions, (b) positions of metal cations of tetrahedral sites only (c) positions of metal cations on octahedral sites only (d) position of one octahedral cation with its six nearest-neighbour tetrahedral cations (e) position of one tetrahedral cation with its six nearest-neighbour tetrahedral cations

(ii) For the other type of octant the oxygen ions still lie along the main diagonal but lies half towards the divalent metal cations in the corners.

The left hand octant contains, in the center, a metal ion, in 8-fold position, which lies in the center of a tetrahedron of oxygen ions (A-sites). The right hand octant shows four metal cations in (16-fold) position, each surrounded by six oxygen ions (B-sites). Various features of the spinel structure are further illustrated in figure 2.4(b-e)

It is further concluded that each A-ion has 12 nearest-neighbors of B-type, while each B 6 nearest-neighbors of A-type surround ion. The shortest distances are;

$$\Gamma_{AB} = \frac{a}{8}\sqrt{11}$$

$$\Gamma_{AB} = \frac{a}{4}\sqrt{3}$$

$$\Gamma_{AB} = \frac{a}{8}\sqrt{2}$$

The M-O distances between nearest-neighbors are given by 0.216a and 0.25a, for tetrahedral and octahedral environments.

2.3.1 Cation Distribution Effect in Spinel Ferrites

Ferrites are posses the combined properties of magnetic materials and insulator. They from a complex composed of grains, grain boundaries and pores. Ferrites exhibit a substantial spontaneous magnetization at room temperature, like the normal ferromagnetic. They have two unequal sublattice called tetrahedral (A-site) and octahedral (B-site) and are ordered antiparallel to each other. In ferrites, the cations occupy the tetrahedral A-site and octahedral B-site of the cubic spinel lattice and experience competing nearest neighbor (J_{AB}) and the next nearest neighbor (J_{AA} and J_{BB}) interactions with $|J_{AB}| \gg |J_{BB}| > |J_{AA}|$. The magnetic properties of ferrites are dependent on the type of magnetic ions residing on the A- and B-sites and the relative strengths of the inter (J_{AB}) and intra sublattice (J_{BB}, J_{AA}) interactions. When the J_{AB} is much stronger then J_{BB} and J_{AA} interactions, the magnetic spins have a collinear structure in which the magnetic moments on the A sublattice are antiparallel to the moments on the B sublattice. But when J_{BB} or J_{AA} becomes comparable with $J_{AB,}$ it may lead to non-collinear spin structure.

When magnetic dilution of the sublattice is introduced by substituting nonmagnetic ions in the lattice, frustration and/or disorder occurs leading to collapse of the collinear of the ferromagnetic phase by local spin canting exhibiting a wide spectrum of magnetic ordering e.g. antiferromagnetic, ferrimagnetic, re-entrant spin-glass, spin-glass, cluster spin-glass properties [2.14-2.15]. Small amount of site distribution i.e. cations redistribution between A- and B-site is sufficient to change the super-exchange interactions which are strongly dependent on thermal history i.e. on sintering temperature, time and atmosphere as well as heating/cooling rates during materials preparation. Microstructure and magnetic properties of ferrites are highly sensitive to preparation method, sintering conditions, amount of constituent metal oxides, various additives including dopants and impurities.

The factors affecting the cation distribution over A and B-sites are as follows [2.16, 2.17];

- the size of the cations
- the electronic configurations of the cations
- the electronic energy
- the saturation magnetization of the lattice

Smaller cations (trivalent ions) prefer to occupy the A-sites. The cations have special preference for A and B-sites and the preference depends on the following factors.

- ionic radius
- size of interstices
- temperature
- Orbital preference for the specific coordination

The preference of cations is according to Verway-Heilman scheme [2.18-2.19];

- ions with preference for A-sites Zn^{2+}, Cd^{2+}, Ga^{2+}, In^{3+}, Ge^{4+}
- ions with preference for B-sites Ni^{2+}, Cr^{3+}, Ti^{4+}, Sn^{4+}
- Indifferent ions Mg^{2+}, Al^{3+}, Fe^{2+}, Co^{2+}, Mn^{2+}, Fe^{3+}, Cu^{2+}

Moreover the electrostatic energy also affects the cation distribution in the spinel lattice. The cations of the smallest positive charge reside on the B-sites having six anions in surrounding i.e. the most favorable electrostatic conduction.

2.4 Types of Ferrites with respect to their Hardness

Due to the persistence of their magnetization, the ferrites are of two types i.e. hard and soft. This classification is based on their ability to be magnetized or demagnetized. Soft ferrites are easily magnetized or demagnetized whereas hard ferrites are difficult to magnetize or demagnetize [2.20].

2.4.1 Soft Ferrites

Soft ferrites are those that can be easily magnetized or demagnetized. This shows that soft magnetic materials have low coercive field and high magnetization that is required in many applications. The hysteresis loop for a soft ferrite should be thin a long, therefore the energy loss is very low in soft magnetic material. At high frequency metallic soft magnetic materials simply cannot be used due to the eddy current losses. Therefore, soft ferrites, which are ceramic insulators, become the most desirable material. These materials are ferrimagnetic with a cubic crystal structure and the general composition $MO.Fe_2O_3$, where M is a transition metal such as nickel, manganese, magnesium or zinc. The magnetically soft ferrites first came into commercial production in 1948. Soft ferrites have certain advantages over other electromagnetic materials including high resistivity and low eddy current losses over wide frequency range. They have high permeability and are stable over a wide temperature range. These advantages make soft ferrites paramount over all other magnetic materials.

2.4.2 Hard Ferrites

Hard ferrites are difficult to magnetize or demagnetize. They are used as permanent magnets. A hard magnetic material has high coercive field and a wide hysteresis loop. Examples are alnico, rare earth metal alloys. The development of permanent magnets begun in 1950s with the introduction of hard ferrites. Hard magnets are characterized by high remanent inductions and high coercivities. They generally exhibit large hysteresis losses. Hard ferrite referred to as permanent magnets retain their magnetism after being magnetized. Hard ferrite likes Ba-ferrite, Sr-ferrite, Pb-ferrite are used in communication device operating with high frequency currents because of their high resistivity, negligible eddy currents and lower loss of energy due to Joule heating and hysteresis. These are found useful in many applications including fractional horse-power motors, automobiles, audio- and video-recorders, earphones, computer peripherals, and clocks.

2.5   Magnetic Exchange Interaction

The difference of energy of two electrons in a system with anti-parallel and parallel spins is called the exchange energy. The electron spins of the two atoms S_i and S_j which is proportional to their products. The exchange energy can be written as universally in terms of Heisenberg Hamiltonian [2.21]

$$H = - \Sigma J_{ij} S_i S_j = - \Sigma J_{ij} S_i S_j \cos \phi \tag{2.1}$$

Where, J_{ij} is the exchange integral represents the strength of the coupling between the spin angular momentum i and j and ϕ is the angle between the spins. It is well known that the favored situation is the one with the lowest energy and it turns out that there are two ways in which the wave functions can combine i.e. there are two possibilities for lowering the energy by $E_{ex.}$

These are:

   (i)   If J_{ij} is positive and the spin configuration is parallel, then ($\cos \phi = 1$) the energy is minimum. This situation leads to ferromagnetism.

   (ii)   If J_{ij} is negative and the spins are antiparallel ($\cos \phi = -1$) then energy is minimum. This situation leads to antiferromagnetism or ferromagnetism.

2.5.1 Superexchange Interactions in Spinel Ferrites

Superexchange interactions appear, i.e. indirect exchange via anion p-orbital's that may be strong enough to order the magnetic moments. Apart from the electronic structure of cations this type of interactions strongly depends on the geometry of arrangements of the two interacting cations and the intervening anion. Both the distance and the angles are relevant. Magnetic interactions in spinel ferrites as well as in some ionic compounds are different from the one considered above because the cations are mutually separated by bigger anions (oxygen ions). These anions obscure the direct overlapping of the cation charge distributions, sometimes partially and sometimes completely making the direct exchange interaction very weak. Cations are too far apart in most oxides for a direct cation-cation interaction. The magnetic interaction in magnetic oxide cannot be explained on the basis of direct reaction because of the following facts:

   (i)   The magnetic ions are located too far apart from each other shielded by the non magnetic anion i.e. oxygen. This is because these are not band type semiconductor [2.16]. The non magnetic anion such as oxygen is situated in the line joining magnetic cations.

(ii)   Super exchange interaction appears, i.e. indirect exchange via anion P-orbital that may be strong enough to order the magnetic moments. The P orbital of an anion (center) internet with the d-orbital of the transitional metal cations.

Three major types of superexchange interactions in spinel ferrites are: J_{AB}, J_{BB} and J_{AA}.

Ferromagnetic oxides are one kind of magnetic system in which there exist at least two in equivalent sublattice for the magnetic ions. The antiparallel alignment between these sublattices (ferrimagnetic ordering) may occur provided the inter sublattice (J_{AB}) exchange interaction are antiferromagnetic and some requirements concerning the signs and strength of the intra-sublattice (J_{AA}, J_{BB}) exchange interaction are fulfilled since usually in ferromagnetic oxides the magnetic cations are surrounded by bigger oxygen anion (almost excluding the direct overlap between cation orbital) magnetic interaction occur via indirect superexchange interaction depends both on the electronic structure of the cations and their geometrical arrangement [2.22].
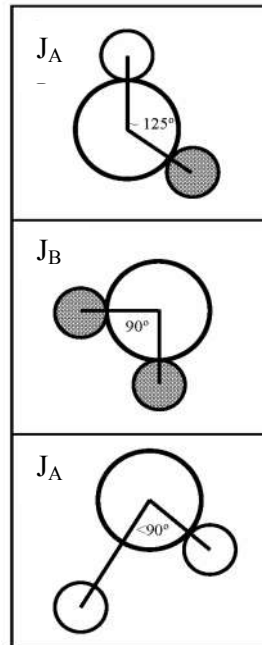
Figure 2.5: Three major types of superexchange interactions in spinel ferrites are as follows: J_{AB}, J_{BB} and J_{AA}. The small empty circle is A-site, the small solid circle is B-site, and the large empty circle is oxygen anion.

The magnitude of negative exchange energies between two magnetic ions M and M' depend upon the distances from these ions to the oxygen ion O^{2-} via which the super exchange take place and on the angle M-$OM'(\phi)$. According to the super exchange theory the angle $\phi=180°$ gives rise to the greatest exchange energy, and this energy decrease vary rapidly as the distance between the ions increases. The magnetic properties of the spinel ferrites are governed by the type of magnetic ions residing on the A and B sites and relative strengths of the inter-sublattice (J_{AB}) and intra-sublattice (J_{AA}, J_{BB}) exchange interaction are shown in figure 2.5

2.5.2 Two Sublattices in Spinel Ferrites

Ferrimagnetic materials are considerably more complex and the application of the molecular field theory to spinels has pointed to the problem of a clear definition of the concept of magnetic sublattices. In spinel ferrites the metal ions are separated by the oxygen ions and the exchange energy between spins of neighboring metal ions is found to be negative, that is, antiferromagnetic. This is explained in terms of superexchange interaction of the metal ions via the intermediate oxygen ions [2.23]. There are a few points to line out about the interaction between two ions in tetrahedral (A) sites:

- The distance between two A ions (~3.5 Å) is very large compared with their ionic radius (0.67 Å for Fe^{3+}).
- The angle A–O^{2-} –A (ϕ = $79^0 38'$) is unfavorable for superexchange interaction.
- The distance from one A ion to O^{2-} is not the same as the distance from the other A ion to O^{2-} as there is only one A nearest neighbor to an oxygen ion (in Figure 2.6, M and M' are A ions, r = 3.3 Å and q = 1.7 Å). As a result, two nearest A ions are connected via two oxygen ions.

These considerations led us to the conclusion that superexchange interaction between A ions is very unlikely. This conclusion together with the observation that direct exchange is also unlikely in this case support the assumption that $J_{AA} = 0$ in the spinel ferrites. According to Neel's theory, the total magnetization of a ferrite divided into two sublattices A and B is:

$$M_T(T) = M_B(T) - M_A(T) \tag{2.2}$$

where, T is the temperature, $M_B(T)$ and $M_A(T)$ are A and B sublattice magnetizations.
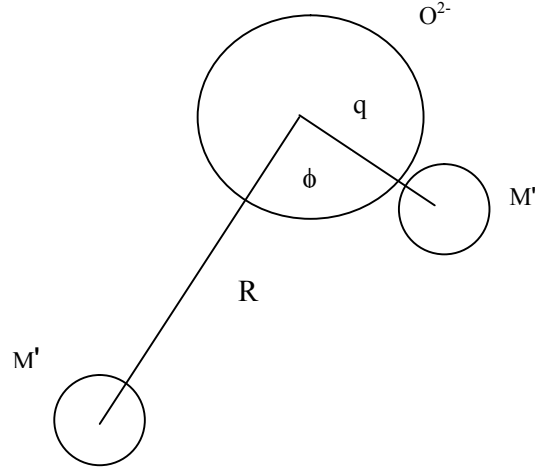
Figure 2.6:   Schematic representation of ions M and M' and the O^{2-} ion through which the superexchange is made. R and q are the centre to centre distances from M and M' respectively to O^{2-} and ϕ is the angle

Both $M_B(T)$ and $M_A(T)$ are given in terms of the Brillouin function $B_{S_i}(x_i)$;

$$M_B(T) = M_B(T=0)B_{SB}(x_B)$$ (2.3)

$$M_A(T) = M_A(T=0)B_{SA}(x_A)$$ (2.4)

with $$x_A = \frac{\mu_B g_A S_A}{k_B T} M_B N_{AB}$$ (2.5)

$$x_B = \frac{\mu_B g_B S_B}{k_B T}(M_B N_{BB} + M_A N_{AB})$$ (2.6)

The molecular field coefficients, N_{ij}, are related to the exchange constants J_{ij} by the following expression:

$$J_{ij} = \frac{n_j g_i g_j \mu_B^2}{2z_{ij}} N_{ij}$$ (2.7)

with n_j the number of magnetic ions per mole in the jth sublattice, g the Lande factor, μ_B is the Bohr magneton and z_{ij} the number of nearest neighbors on the jth sublattice that interact with the ith ion.

According to Neel's theory and using $J_{AA} = 0$, equating the inverse susceptibility $\frac{1}{\chi} = 0$ at $T = T_c$ we obtain for the coefficients of the molecular field theory N_{AB} and N_{BB} of the following expression:

$$N_{BB} = \frac{T_c}{C_B} - \frac{C_A N_{AB}^2}{T_c} \tag{2.8}$$

where, C_A and C_B are the Curie constants for each sublattice. Eq[n] (2.2) and eq[n] (2.8) constitute a set of equations with two unknown, N_{AB} and N_{BB}, provided that M_A and M_B are a known function of T.

2.5.3 Neel's Collinear Model of Ferrites

Soft ferrites belong to the cubic spinel structure. According to Neel's theory [2.11], the magnetic ions are assumed to be distributed among the tetrahedral A-sites and octahedral B-sites of the spinel structure. The magnetic structure of such crystal essentially depends upon the type of magnetic ions residing on the A- and B-sites and the relative strengths of inter- and intra-sublattice exchange interactions. A ferromagnetic crystal lattice could be split into two sublattices such as A - and B-sites. He supposed the existence of only one type of magnetic ions in the material of which a fraction λ appeared on A-sites and the rest fraction μ on B-sites.

Thus $\lambda + \mu = 1$ \tag{2.9}

The remaining lattice sites were assumed to have ions of zero magnetic moments. A-ion as well as B-ion have neighbors of both A and B types there are several interaction between magnetic ions as A-A, B-B, A-B and B-A. it is supposed that A-B and B-A interactions are identical and predominant over A-A or B-B interaction and four the alignment of the magnetic moment of each A-ion more . Neel defined the interactions within the material from the Weiss molecular field viewpoint as

$$H = H_0 + H_m \tag{2.10}$$

Where H_0 is the external applied field and H_m is the internal field arises due to the interaction of other atoms or ions in the material. When the molecular field concept is applied to a ferromagnetic material we have

$$H_A = H_{AA} + H_{AB} \tag{2.11}$$

$$H_B = H_{BB} + H_{BA} \tag{2.12}$$

Here molecular field H_A on A-sites is equal to the sum of the molecular field H_{AA} due to neighboring A-ions and H_{AB} due to neighboring B-sites. The molecular field components can be written as,

$$H_{AA} = \gamma_{AA}M_A, \quad H_{AB} = \gamma_{AB}M_B \tag{2.13}$$

A similar definition holds for molecular field H_B, acting on B-ions. Molecular filed components can also be written as

$$H_{BB} = \gamma_{BB}M_B, \quad H_{BA} = \gamma_{BA}M_A \tag{2.14}$$

Here J's are molecular field Co-efficient and M_A and M_B are magnetic moments of A and B sublattice or an identical sublattices

$$\gamma_{AB} = \gamma_{BA}, \text{ but } \gamma_{AA} \neq \gamma_{BB} \tag{2.15}$$

In the presence of the applied magnetic field H_a, the total magnetic field on the sublattice, can be written as

$$H_a = H_o + H_A$$
$$= H_o + \gamma_{AA}M_A + \gamma_{AB}M_B \tag{2.16}$$
$$H_b = H_o + H_B$$
$$= H_o + \gamma_{BB}M_B + \gamma_{AB}M_A \tag{2.17}$$

2.5.4 Non-collinear Model of Ferrimagnetism

In general, all the interactions are negative (anti ferromagnetic) with $|J_{AB}| \gg |J_{BB}| > |J_{AA}|$. In such situation, collinear or type of ordering is obtained. Yafet and Kittel [2.24] theoretically considered the stability of the ground state of magnetic ordering, taking all the three exchange interactions into account and concluded that beyond a certain value of $\dfrac{J_{BB}}{J_{AB}}$, the stable structure was a non-collinear triangular configuration of moment where in the B-site moments are oppositely canted relative to the A-sites moments. Later on Leyons *et.al.* [2.25] extending these theoretical considerations showed that for the value of $\dfrac{3J_{BB}S_B}{2J_{BB}S_A}$ greater than unity. Initially one can understand why the collinear Neel structure gets perturbed when $\dfrac{J_{BB}}{J_{AB}}$ increases. Since all these three exchange interactions are negative (favoring anti ferromagnetic alignment of moments) the inter- and intra-sublattice exchange interaction complete with each other in aligning the moment direction in the sublattice. This is one of the

origins of topological frustration in the spinel lattice. By selective one can effectively decreases the influence of J_{AB} vis – a - vis J_{BB} and thus perturb the Neel ordering.

It was found that ferrites which have been substituted sufficiently with non magnetic atoms showed significant departure from Neel collinear model. These theoretical models have been used to explain thus departures:

(i)   A paramagnetic center model in which a number of magnetic nearest neighbors determine whether a magnetic ion remains paramagnetic or contributes to the magnetization.

(ii)   A uniform spin canting relative to the average magnetization and

(iii)   A localized canting where the canting angle of a magnetic ion spin depends on the local magnetic environment.

The discrepancy in the Neel's theory was resolved by Yafet and Kittel [2.24] and they formulated the non-collinear model of ferrimagnetism. They concluded that the ground state at 0K might have one of the following configurations:

- Have an antiparallel arrangement of the spins on two sites.
- Consists of triangular arrangements of the spins on the sublattices and
- An antiferromagnetic in each of the sites separately.

2.6   Magnetic Properties of Ferrites

Ferromagnetic materials are characterized by a high magnetization (Magnetic moments per unit volume) which can be achieved even in polycrystalline materials by the application of relatively small magnetic field. In a ferromagnetic material the individual atomic (atom with partially filled 3d or 4f shells) or ionic moment arising from unpaired spins are permanent and interact strongly with one another in a manner which tends to cause parallel alignment of the nearby moments.

The moment of a large number of neighboring ions are thus parallel, even in the absence of an applied field. These regions or domains, of spontaneous magnetization exit in both single and polycrystalline materials and within a domain the value of the saturation magnetization, M_s is the maximum that can be achieved in the material at interaction lies in the so-called quantum mechanical exchange [2.26-2.27], but in a phenomenological description of magnetism, it is possible to regard that the obliging forces are arising from an internal magnetic field called the molecular filed [2.28]. Weiss assumed that spontaneous magnetization properties

disappear at the Curie point when the thermal energy is equal to the energy of the individual ionic moment in Weiss induction field. Then,

$$B_W = k_B T_C + \mu B_m \qquad (2.18)$$

Where k_B is Boltzmann constant, T_c is Curie temperature, μ is permeability and B_m is the Weiss molecular field. It is convenient to write $B_m = \mu_0 H$, below the Weiss molecular field H is used. Weiss assumed that that the molecular field H_m was proportional to the magnetization M

$$H_m = \gamma M \qquad (2.19)$$

Where M is the magnetization is the material and γ is the constant proportionality called molecular field co-efficient.

A ferrite may be defined as the one which below a certain temperature bears a spontaneous magnetization that arise from non-parallel arrangement of the strongly coupled atomic dipole. Ferrites are the substance consists of two sublattices with magnetic moments of one sublattice tending to antiparallel to those of other. The term ferromagnetism has been used in broad sense in order to include the material with more than two sublattices and with other spin configuration, such as triangular or spinel configuration. It is usually assumed that a ferromagnetic material has an appreciable net magnetization although no precise definition of the term appreciable has been given. The two sublattice are denoted by A- and B-sites are denoted by A and B. If the magnetic moment of the ions at A and B sites are unequal, this inequality may be due to

(i)   Presence of elements indifferent ionic state, e.g. Fe^{3+} and $Fe^{2}+$

(ii)   Different elements in the same or different ionic states, e.g. Fe^{3+} and Mg^{2+}

(iii)   Different crystalline field acting at two sites

The competition between the forces on the B spins may lead to the triangular configuration.

2.6.1 Magnetic Dipole

A dipole is a pair of electric charges or magnetic poles of equal magnitude but opposite polarity, separated by a small distance. Dipoles can be characterized by their dipole moment, a vector quantity with a magnitude equal to the product of the charge as magnetic strength of one of the poles and the distance separating the two poles. The Earth's magnetic field which is approximately a magnetic dipole. However, the N-

pole and S-pole are labeled here geographically, which is the opposite of the convention for labeling the poles of a magnetic dipole moment. In physics, there are two kinds of dipoles:

(i) An **electric dipole** is a separation of positive and magnetic charges. The simplest example of this is a pair of electric charges of equal magnitude but opposite sign, separated by some (usually small) distance. A permanent electric dipole is called electrets.

(ii) A **magnetic dipole** is a closed circulation of electric current. A simple example of this is a single loop of wire some constant current flowing through it [2.29-2.30].

2.6.2 Magnetic Field

A magnetic field (H) is a vector field which is created with moving charges or magnetic materials. It is also be defined as a regions in which the magnetic lines of force is present. The magnetic field vector at a given points in space is specified by two properties:

(i) Its direction which is along the orientation of a compass needle.

(ii) Its magnitude (also called strength), which is proportional to how strength the compass needle orients along that direction.

In matter, atomic circular currents may occur. Their strength is characterized by the magnetization **M**, which is the magnetic moment per cm^3. Then the matter provide the magnetic field is

$$H = 4\pi M \tag{2.20}$$

The S.I. units for magnetic field strength Am^{-1}.

2.6.3 Magnetic Moment

A magnet's magnetic moment (μ) is a vector that characterizes the magnets overall magnetic properties. For a bar magnet; the direction of the magnetic moment points from the magnetic south pole to its north pole; and the magnitude relates to how strong and how far apart these poles are. In S.I. units, the magnetic moment is specified interms of $A\text{-}m^2$. A magnet both produces its own magnetic field and it responds to magnetic fields. The magnetic moment is a measure of the strength of a magnetic source. In the simplest case of a current loop, the magnetic moment is defined as

$$\mu_m = I \int dA \qquad\qquad (2.21)$$

Where, A is the vector area of the current loop, and the current, I is constant.

In the more complicated case of a spinning charged solid, the magnetic moment can be found by the following equation:

$$\mu_m = \frac{1}{2} \int r \times J d\tau \qquad\qquad (2.22)$$

Where, $d\tau = r^2 \sin\theta dr d\theta d\varphi$, J is the current density. In addition, when the magnet is put into an external magnetic field, produced by a different source, it is subject to a torque tending to orient the magnetic moment parallel to the field. The amount of this torque is proportional both to the magnetic moment and the external field. A magnet may also be subject to a force driving it in one direction or another according to the positions and orientations of the magnetic and source. If the field is uniform in space, the magnet is subject to no net force, although it is subject to a torque.

2.6.4 Magnetic Moment of Ferrites

The determination of saturation moments of simple ferrites having the formula $M^{2+}Fe^{3+}O_4$, where M^{2+} is the divalent cation, such as Cu, Co, Ni, Fe, Mg, Mn etc agrees with the Neel's collinear model. The A-B interaction is much larger than the A-A and B-B interaction respectively. The two kinds of magnetic ion from two sublattices each saturated and magnetized in opposite direction at absolute zero.

Saturation magnetic moments of some selected spinels [2.11] are listed in the Table:2.1, the first six ferrites are the inverse type i.e $Fe^{3+}[Me^{2+}Fe^{3+}]O_4$. The magnetic moments of two Fe^{+3} cations compensate each other and the ferrite magnetization becomes equal to $M^{2+}(\mu_B) = 2 S_M^{+2}(cal)$. These values are listed in the Table 2.1 and the experimental and calculated shows good agreement, except Cobalt and copper series. The Li ferrite is also completely inverse and its moment is calculated based on the cation distribution Fe [$Li_{0.5}Fe_{2.25}$] O_4 is equal to 2.5 (μ_B); per molecule is in good agreement with the measured value. These are two possible reasons for the discrepancies observed between calculated and observed magnetic moments are mentioned in the Table 2.1.

(i)   The orbital moments of the divalent ions may not be neglected: the crystal field effects therefore become important.

(ii)   The cation distribution must be taken into account.

Table 2.1: Experiment and calculated saturation moments of spinals

Ferrites	M (μ_B)	$2S_M^{2+}$(cal)
$MnFe_2O_4$	5 - 4.4	5
$FeFe_2O_4$	4.2 - 4.08	5
$Co\ Fe_2O_4$	3.3 - 3.9	3
$Ni\ Fe_2O_4$	2.3 - 2.40	2
$Cu\ Fe_2O_4$	1.3 - 1.37	1
$Mg\ Fe_2O_4$	1.1 - 0.86	1.1
$Li_{0.5}\ Fe_{2.5}O_4$	2.6	2.5

2.7 Magnetization Process

A review of magnetization process, namely the response of ferromagnetic or ferrimagnetic material (bulk) to an applied field with a semi-microscopic approach is presented. In ferromagnetic or ferrimagnetic material, the magnetization curves, especially in low magnetic fields differ widely from sample to sample and as a function of the magnetic history of the sample i.e. of the previous fields which have been successively applied.

2.7.1 Magnetization Curve

For unmagnetization bulk material, there is a zero net magnetic moment. It can be predicted that there will be an infinite number of degree of magnetization between the unmagnitized and saturation condition, when the material is subjected to an external magnetic field. These extreme situations correspond respectively to random orientation of domains complete alignment is one direction with elimination of domain walls. If we start with the applied magnetic field, the bulk material will be progressively magnetized by the domain dynamics, the magnetization of the sample will follow the course as shown in figure 2.7 (2.31).

The slop from the origin to a point on the curve or the ratio $\left(\frac{M}{H}\right)$ is defined as magnetic susceptibility. The curve is called magnetization curve. This curve is greatly perceived as being made of three major portions.

The first, the lower section, is in the initial susceptibility region and is characterized by reversible domain wall movements and rotations. By reversible
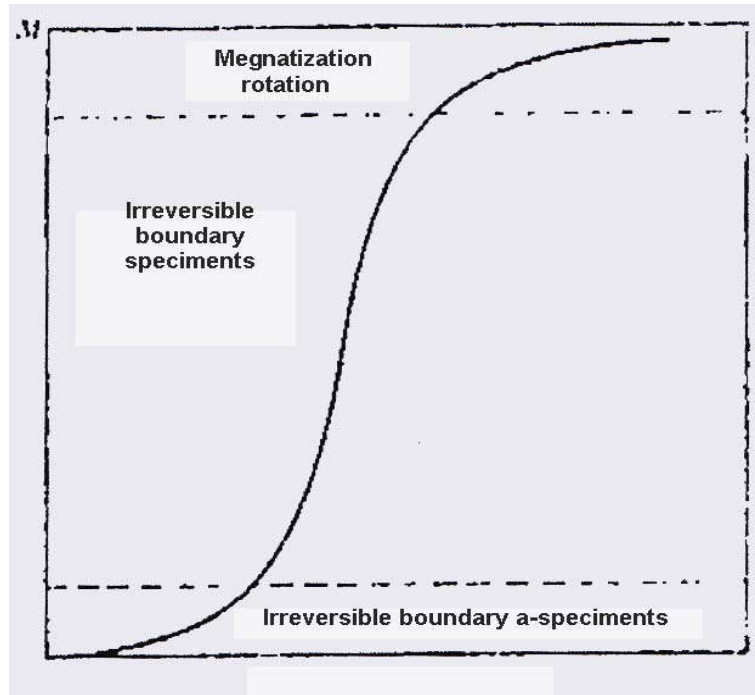
Figure 2.7: Domain dynamics during various parts of the magnetization curve.
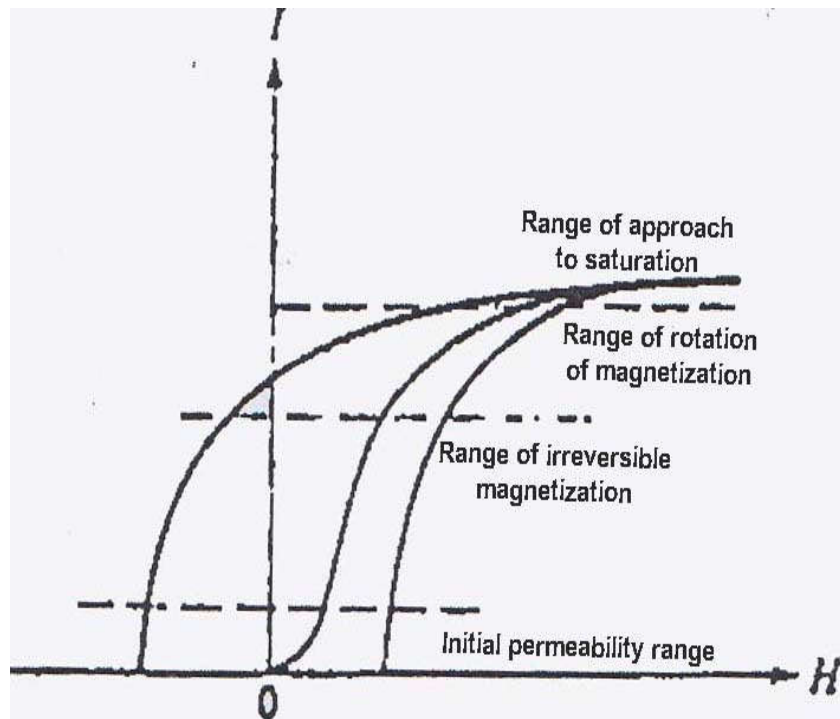
Figure 2.8: Magnetization curve and the classification of magnetization mechanism.

means that after the magnetization slightly with an increase in field the origin at magnetization conditions can be reversed if the field is reduced to initial value. The combination of the displacement walls to an initial permeability is entirely dependent on the short of material studied.

In the second stage magnetization curve, of the field is increased, the intensity of the magnetization increases more drastically, is called the irreversible magnetization range. This range is obtained mainly by the irreversible domain will motion from one stable state to another.

If the field is increased further, the magnetization curve becomes less steep and its process become reversible once more. In the third section of magnetization take place by rotation magnetization. This range is called rotation magnetization range. Beyond this range the magnetization gradually approaches to saturation magnetization shown in figure 2.8.

2.7.2 Magnetization and Temperature

The influence of temperature on magnetic material can be determinate in the magnetic properties of dose materials. Rising the temperature of a solid, result in the increase of the thermal vibration of atoms, with this the atomic magnetic moments are free to rotate. This phenomenon the atoms tend to randomize the directions of any moments that may be aligned [2.32]. With increasing temperature, the saturation magnetization diminishes gradually and abruptly drops to zero at what called the Curie temperature (T_c). The Curie point of a ferromagnetic material is the temperature above which it loses its characteristic ferromagnetic ability. At temperature below the Curie point the magnetic moments are partially aligned within magnetic domains in ferromagnetic materials. As the temperature is increased from below the Curie point, thermal fluctuations increasingly destroy this alignment, until the net magnetization becomes zero at and above the Curie point.

Above the Curie point, the material is purely paramagnetic. At temperature below the Curie point, an applied magnetic field has a paramagnetic effect on the magnetization, but the combination of paramagnetism leads to the magnetization following a hysteresis curve with the applied field strength.
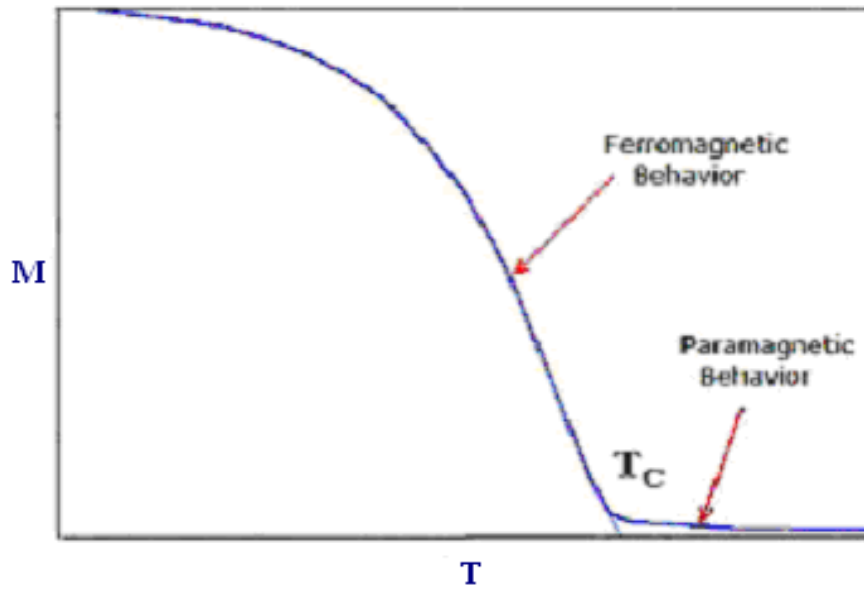
Figure 2.9: Typical M-T curve for magnetic material.

2.8   Theories of Permeability

Permeability is namely defines as the proportional constant between the magnetic field induction B and applied intensity H:

$$B = \mu H \tag{2.24}$$

If a magnetic material is subjected to an AC magnetic field as given below:

$$H = H_0 e^{i\omega t} \tag{2.25}$$

Then it is observed that the magnetic flux density B experiences a delay. The delay is caused due to presence of various losses and is thus expressed as

$$B = B_0 e^{i(\omega t - \delta)} \tag{2.26}$$

where δ is the phase angle and marks the delay of B with respect to H. The permeability is then given by

$$\mu = \frac{B}{H} = \frac{B_0 e^{i(\omega t - \delta)}}{H_0 e^{i\omega t}} \tag{2.27}$$

$$= \frac{B_0 e^{-i\delta}}{H_0} = \mu' - i\mu'' \tag{2.28}$$

Where $\mu' = \dfrac{B_0}{H_0}\cos\delta$ $\qquad\qquad\qquad\qquad\qquad\qquad$ (2.29)

$\mu'' = \dfrac{B_0}{H_0}\sin\delta$ $\qquad\qquad\qquad\qquad\qquad\qquad$ (2.30)

The real Part μ' of complex permeability μ as expressed in eq[n]. (2.28) represent the component of B which is in phase with H, so it corresponds to the normal permeability. If there is no losses , we should have $\mu = \mu'$, The imaging part μ'' corresponds to the part of B which is delayed by phase angle arranging up to 90° from H . The presence of such a component requires a supply of energy to maintain the alternating magnetization regardless of the origin of delay.

The ratio of μ'' to μ' gives

$$\frac{\mu'}{\mu''} = \frac{\dfrac{B_0}{H_0}\sin\delta}{\dfrac{B_0}{H_0}\cos\delta} = \tan\delta \qquad\qquad\qquad\qquad (2.31)$$

This $\tan\delta$ is called the loss Factor or loss tangent. The Q-Factor or quality factor is defined as the reciprocal of this loss factor, i.e

$$Q = \frac{1}{\tan\delta} \qquad\qquad\qquad\qquad\qquad\qquad (2.32)$$

2.9   Transport Properties

Ferrites are ferromagnetic semiconductors that could be used in electronic devices. The increasing demand for low loss ferrites resulted in detailed investigations on conductivity and on the influence of various substitutions on the electrical conductivity, thermoelectric power, etc. The conduction mechanism in ferrites is quite different from that in semiconductors. In ferrites, the temperature dependence of mobility affects the conductivity and the carrier concentration is almost unaffected by temperature variation. In semiconductors, the band type conduction occurs, where in ferrites, the cations are surrounded by closed pack oxygen anions and as a first approximation can well be treated as isolated from each other. There will be a little direct overlap of the anion charge clouds or orbital. In other words, the electrons associated with particular ion will largely remain isolated and hence a localized electron model is more appropriate than a collective electron (band) model. This accounts for the insulating nature of ferrites.

These factors led to the hopping electron model [2.33]. An appreciable conductivity in these ferrites is found to be due to the presence of iron ion ions with different valence states at crystallographically different equivalent lattice sites [2.34]. Conduction is due to exchange of 3d electron, localized at the metal ions, from Fe^{3+} to Fe^{2+}. Various models have been suggested to account for the electrical properties. These are as follows

- Hopping model of electrons
- Small polaron model

2.9.1 DC Resistivity of Ferrites

Extensive investigation into the origin of the electrical conductivity of the spinels has been carried out by Verwey [2.35] and later on by Van Uitert [2.36] and Jonker [2.37]. The resistivity of ferrites at room temperature can vary , depending on chemical composition between about 10^{-2} to higher than 10^{+11} ohm-cm [2.1]. The low value of resistivity is due to the simultaneous presence of ferrous and ferric ions on equivalent lattice sites (octahedral) as proposed by Verwey [2.35]. For example Fe_3O_4 at room temperature has resistivity of approximately 7×10^{-3} Ohm-cm and Fe_2O_4 with some deficiency in iron and sintered in a sufficiently oxidizing atmosphere so that the product contains no ferrous ions can have a resistivity higher than 7×10^6 ohm-cm. To make high resistivity ferrites one must sure that there are no ferrous ions in the stoichiometric ferrites.

Temperature dependent resistivity of ferrites follows Arrhenius relation [2.1]:

$$\rho = \rho_0 e^{\frac{E_a}{kT}},$$ (2.33)

Where ρ is the resistively and E_a is the activation energy required for hopping of an electron from one lattice site to another.

2.9.2 AC Resistivity Ferrites

AC resistivity is an important property of ferrites material. Ferrites material has high intrinsic resistivity. It can be changed with change of frequency and temperature.

2.9.3 Thermopower

The Hall effect and the thermoelectric measurements usually describe the conduction mechanism in semiconductors. The Hall effect gives precise results, but in case of low mobility materials such as ferrites, it is sometime difficult to measure the Hall effect. Under such circumstances the thermoelectric power is the only alternative. The sign of the thermo-emf gives vital information about the type of conduction in semiconductors whether it is p- or n-type. There are two methods of thermopower measurement [2.38];

    (i)   Integral Method

    (ii)   Differential Method

2.9.3.1   Integral Method

One end of the specimen is kept at a fixed temperature T_1 while the temperature T_2 of the other end is made to vary through the desired range. The thermoelectric power voltage V developed across the sample is measured as a function of the temperature T, i.e.

$$V(T) = \int_{T_1}^{T_2} a\, dT$$

(2.34)

2.9.3.2   Differential method

A small temperature difference ΔT is established across the sample to induce a small thermoelectric voltage $\Delta V(T)$. The Seebeck coefficient is then determined from the relation:

$$\alpha(T) = \lim_{\Delta T \to o} \frac{\Delta V(T)}{\Delta T}$$

(2.35)

The accuracy of the this method demands that the ΔT to be sufficiently small, so that $\alpha(T)$ changes in the temperature interval ΔT. On the other hand ΔT must be large enough to generate a voltage that can be detected to the desired precision.

2.9.4 Conduction Mechanisms

Ferrites are ferrimagnetic semiconductors and exhibit interesting properties that could be used in electronic devices. That is why ferrites attracted the attention of the physicist. The increasing demand for low loss ferrites resulted in detailed

investigations on conductivity and on the influence of various substitutions on the electrical conductivity, thermoelectric power, etc.

The conduction mechanism in ferrites is quite different from that in semiconductors. In ferrites the temperature dependence of mobility affects the conductivity and the carrier concentration is almost unaffected by temperature variation. In semiconductors the band type conduction occurs, where in ferrites, the cations are surrounded by closed pack oxygen anions and as a first approximation can well be treated as isolated from each other. There will be a little direct overlap of the anion charge clouds or orbital. In other words the electrons associated with particular ion will largely remain isolated and hence a localized electron model is more appropriate than a collective electron (band) model.

This accounts for the insulating nature of ferrites. These factors led to the hopping electron model [2.39]. An appreciable conductivity in these ferrites is found to be due to the presence of iron with different valence states at crystallographically different equivalent lattice points [2.40]. Conduction is due to exchange of 3d electrons, localized at the metal ions, from Fe^{3+} to Fe^{2+}. Assuming that all the Fe^{2+} ions in the B-site to participate in the in hopping transport, the number of charge carriers (n) worked out to be ~ $10^{22}/cm^3$. Since mobility is low, even though n is large.

Many models have been suggested to account for the electrical properties. These are as follows;

    (i) Hopping Model of Electrons
    (ii) Small Poloron Model
    (iii)Phonon Induced Tunneling

2.9.4.1 Hopping Model of Electrons

Jonker [2.45] suggested that in materials like ferrites there is a possibility of exchanging the valency of a considerable fraction of metal ions and especially that of iron ions.

In the presence of lattice vibrations however the ions occasionally come close enough together for transfer to occur with a high degree of probability. Thus only the lattice vibrations induce the conduction and the consequence the carrier mobility shows temperature dependence characterized by activation energy. For such a process of jumping of electrons and holes the motilities are given by;

$$\mu_1 = el_1 \, f_1 \left[\frac{e^{-\frac{E_1}{k_B T}}}{kT} \right] \text{ and} \qquad (2.36)$$

$$\mu_2 = el_2 \, f_2 \left[\frac{e^{-\frac{E_2}{k_B T}}}{kT} \right] \qquad (2.37)$$

where subscripts represent the parameters for electrons and holes, I represent jumping length, f_t and f_2 lattice frequencies active in the jumping process, E_1 and E_2 are activation energies involved in the required lattice deformation.

The general expression for the total conductivity in this case where we have two types of charge carriers can be given as;

$$\sigma = n_1 e \, \mu_1 + n_2 e \mu_2 \qquad (2.38)$$

The temperature dependence of conductivity arises only due to mobility and not due to the number of charge carriers in the sample. It was concluded that for hopping conduction;

- The mobility has a minimum value much lower than the limiting value (0.1 cm^2/Vs) taken as minimum for band conduction [2.41].
- The independence of Seebeck coefficient on temperature is due to fact that in hopping model the number of charge carriers is fixed.
- Thermally activated process with activation energy E_a called hopping activation energy.
- Occurrence of n-p transitions with charge carriers in the Fe^{2+} or oxygen concentration in the system.

2.9.4.2 Small Polaron Model

A small polaron is a defect created when an electronic carrier becomes trapped at a given site as a consequence of the displacement of adjacent atoms or ions. The entire defect (carrier plus distortion) then migrates by an activated hopping mechanism. Small polaron formation can take place in materials whose conduction electrons belong to incomplete inner (d or f) shells which due to small electron overlap, tend to form extremely narrow bands [2.42-2.45]. The migration of small polaron requires the hopping of both the electron and the polarized atomic

configurations from one site to an adjacent site. For a fcc lattice the drift mobility takes the form;

$$\mu = (1 - c)e\ a^{\frac{2\Gamma}{kT}}$$ (2.39)

where e is the electronic charge, a is the lattice constant, c is the fraction of sited which contain an electron $C = \dfrac{n}{N}$, n is the number of electrons and N is the jump rate of the polaron from one site to the particular neighboring site given by;

$$\Gamma = P\mu_0\ e^{-\frac{E_a}{kT}}$$ (2.40)

Here μ_o is the appropriate optical phonon frequency; E_a is the activation energy; p is the probability of the electron transfer after the polarized configuration has moved to the adjacent site. The small polaron model also explains the low mobility, temperature independence of the Seebeck coefficient and thermally activated hopping.

EXPERIMENTAL PROCEDURE

3.1 Composition of the Studied Ferrite System

A series of mixed ferrites of composition were fabricated by solid state reaction technique keeping in view of their ionic radial and valences for maintaining the charge neutrality.

In the present work, conventional ceramic method has been employed for a series composition of Ni-Cu-Zn ferrites are synthesized, characterized and investigated. The powder preparation process and sintering facility available at the Material Science Division, Atomic Energy Centre, Dhaka has been utilized for the preparation of samples. General formula for sample is objectives of the present research work are to synthesize Ni-Cu-Zn ferrites of composition $Ni_{0.28}Cu_{0.10}Zn_{0.62}Fe_2O_4$+ x wt.% additives. The properties of Ni-Cu-Zn with addition of additives like V_2O_5 and Bi_2O_3 samples are influenced considerably by sintering temperature and compositions.

In the present research work are to synthesize Ni-Cu-Zn ferrites of composition $Ni_{0.28}Cu_{0.10}Zn_{0.62}Fe_2O_4$+0.xwt.% additives such as

(i) $Ni_{0.28}Cu_{0.10}Zn_{0.62}Fe_2O_4$+ x wt.% V_2O_5 [x = 0.2, 0.4, 0.6 and 0.8] and

(ii) $Ni_{0.28}Cu_{0.10}Zn_{0.62}Fe_2O_4$+ x wt.% Bi_2O_3 [x = 0.2, 0.4, 0.6 and 0.8]

3.1.1 Method of Sample preparation

Sample preparation technique is an important part for ferrites sample. Knowledge and control of chemical composition, homogeneity and microstructure are very crucial. Sample preparation of polycrystalline ferrites with optimum desired properties is still a complex and difficult task. Ferrites with optimized properties have always demanded delicate handling and cautions approach in materials synthesis and appropriate knowledge of thermodynamics control of the chemical composition and homogeneity. As most of the properties needed for ferrite applications are not intrinsic but extrinsic, preparations of samples has to encounter added complexity. There are many processing methods such as solid state reaction method [3.1]; high energy ball milling [3.2]; sol-gel [3.3]; chemical co-precipitation method [3.4]; microwave sintering method [3.5]; auto combustion method [3.6] etc for the preparation of polycrystalline ferrite decompose at the elevated temperature if we

want to melt them under normal conditions. This happens because the oxygen splits off at higher temperature reducing Fe^{3+} to Fe^{2+}. This necessarily implies that ferrite preparation by melting, as in the case of metals, is not possible. The normal methods of preparation of ferrites comprise of the conventional ceramic method i.e. solid state reaction method involving ball milling of reactions following by sintering at elevated temperature range and non-conventional method, also called wet method chemical co-precipitation method and sol-gel method etc examples of wet method. The general preparation procedure of ferrites comprises of the following operation as shown in figure 3.1. The block diagram and the detail of which are described subsequently.

```
┌──────────────┐      ┌──────────────┐      ┌──────────────┐
│  Oxide Raw   │ ───> │ Weighing by  │ ───> │ Dry mixing by│
│  Materials   │      │different Mole│      │ Agate Mortar │
│              │      │  percentage  │      │              │
└──────────────┘      └──────────────┘      └──────────────┘
                                                    │
                                                    v
┌──────────────┐      ┌──────────────┐      ┌──────────────┐      ┌──────────────┐
│ Presintering │ <─── │  Briquetting │ <─── │    Drying    │ <─── │  Wet mixing  │
│              │      │              │      │              │      │   by Ball    │
│              │      │              │      │              │      │   milling    │
└──────────────┘      └──────────────┘      └──────────────┘      └──────────────┘
      │
      v
┌──────────────┐      ┌──────────────┐      ┌──────────────┐      ┌──────────────┐
│   Milling    │ ───> │  Pressing to │ ───> │   Sintering  │ ───> │   Finished   │
│              │      │   Desired    │      │              │      │    Product   │
│              │      │    shape     │      │              │      │              │
└──────────────┘      └──────────────┘      └──────────────┘      └──────────────┘
```
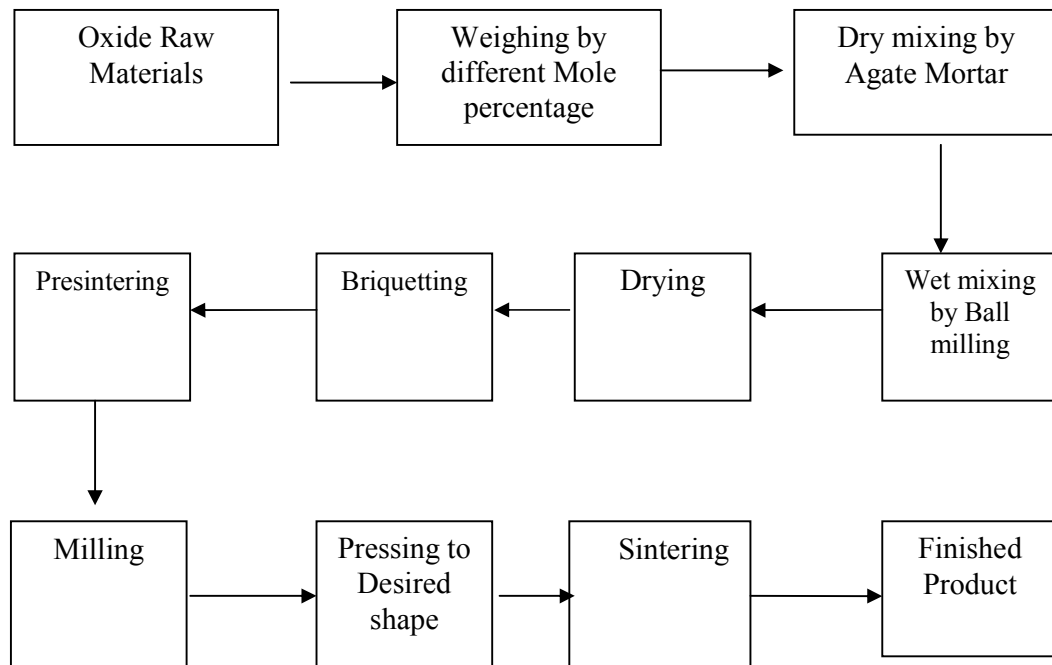
Figure 3.1: Flow chart of ferrite preparation.

The overall preparation process generally comprised of the following four major steps:

(i) Preparing a mixture of desired composition

(ii) Pre-firing the mixture to form ferrite

(iii) Converting the "raw ferrite" into powder and pressing the powder into the required shapes

(iv) Sintering

One thing is to be remembered that, the sintering process is irreversible in terms of microstructure, so that constant care could be maintained to keep conditions constant

45

prior to and during sintering. A brief discussion given below will give us the idea about the above mentioned four major steps.

3.1.2 Preparing a Mixture of Materials

The extent of the work in this step varies greatly, depending on the starting materials. When component oxides are used, the corresponding step involves a mere mixing of the oxides by wet milling for 6 hours. To avoid iron contamination, mixing is done with stainless steel balls in a steel ball milling machine and a fluid such as distilled water is used to prepare the mixture into slurry. The purity of raw materials used in the present work is analytical research grade oxides supplied by the manufacturer E. Mark of Germany.

The raw materials for the preparation of Ni-Cu-Zn ferrite were oxide of iron, nickel, copper and zinc. Fe_2O_3 and whatever oxides, MO are required are taken in powder form with the captions in the ratio corresponding to that in the final product. Metal carbonate may also be used; during the later firing, Co_2 will be given off and they will be converted to oxides. The constituent in required stoichiometric proportions were weighed first and then thoroughly mixed using ceramic mortar and pestle.

3.1.3 Pre-firing the Mixture to form ferrite

The slurry prepared in step 1 is dried, palletized and then transferred to a porcelain crucible for pre-firing in a constant temperature of 900℃ for 6 hours. This was performed in a furnace named Gallen Kamp at Materials Science Division AECD. The cooling and heating rates were $4^{o}C/min$. The presintering is very crucial because in this step of sample preparation of ferrite is formed from its component oxides. The solid state reactions, leading to the formation of ferrites, actually achieved by counter diffusion. This means that the diffusion involves two or more species of ions, which more in opposite direction initially across the interface two contacting particles of different component oxides. As far as the final composition of the ferrite is concerned step-2 is most crucial because subsequent steps would not change the composition substantially. For this reason, it is important to understand how a ferrite is formed from its component oxides.

During the pre-firing stage, the reaction of Fe_2O_3 with metal oxide (metal is divalent) takes place in the solid state to form ferrite.

For Ni-ferrite

$NiO + Fe_2O_3 \longrightarrow NiFe_2O_4$

For Ni-Zn ferrite

$(1 - x)NiO + xZnO + Fe_2O_3 \longrightarrow Ni_{1-x}Zn_xFe_2O_4$
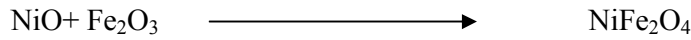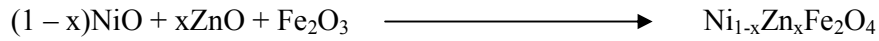
The reaction of the Ni-Cu-Zn ferrite finally

$0.28NiO + 0.62ZnO + 0.10CuO + 2Fe_2O_3 \longrightarrow$

$$Ni_{0.28}Cu_{0.10}Zn_{0.62}Fe_2O_4$$
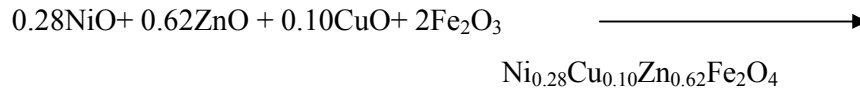
Finally $Ni_{0.28}Cu_{0.10}Zn_{0.62}Fe_2O_4 + x$ wt.% additives such as

(i) $Ni_{0.28}Cu_{0.10}Zn_{0.62}Fe_2O_4 + x$ wt.% V_2O_5 [x = 0.2, 0.4, 0.6 and 0.8] and

(ii) $Ni_{0.28}Cu_{0.10}Zn_{0.62}Fe_2O_4 + x$ wt.% Bi_2O_3 [x = 0.2, 0.4, 0.6 and 0.8]

In order to produce chemically homogeneous and magnetically better material, this pre-fired lump material was crushed. This oxide mixture was then milled thoroughly for 6 - 8 hours to obtain homogeneous mixture. It is to be mentioned that the size can be reduced to ≈ 1 micron by prolong normal ball milling. However some fraction of the particles in that case may be reduced to even sub micron level. The ferrite is formed essentially in the pre-firing step but the 'raw' ferrite formed has poor quality. In order to produce chemically homogeneous, dense and magnetically better material of desired shape and size, sintering at an elevated temperature is needed.

3.1.4 Converting Raw Ferrite into Powder and Pressing Powder

Besides reducing the particle size to ≈ 1 micron, grinding also eliminates intra particle pores and homogenizes the ferrite by mixing. To promote successful sintering in the next steps, the powder must be well characterized after grinding with respect to such factors, as particle size and distribution, particle shape, homogeneity, absorbed gases, impurities and intra-particle porosity. Iron contamination due to continuous wear of the mill wall and steel ball need to be closely watched and minimized. Now to the ground homogeneous powder, polyvinyl alcohol is added as a binder. Pressing the powder into compacts of desired shapes is done either by conventional method in a die-punch assemble or by hydrostatic or isostatic compaction. By conventional method in a die-punch assembly a uniformly dense body is difficult owing to the friction gradient of the powder at the wells of the die and between the particles themselves.

Figure 3.2: Hydraulic press used to make different shaped samples.
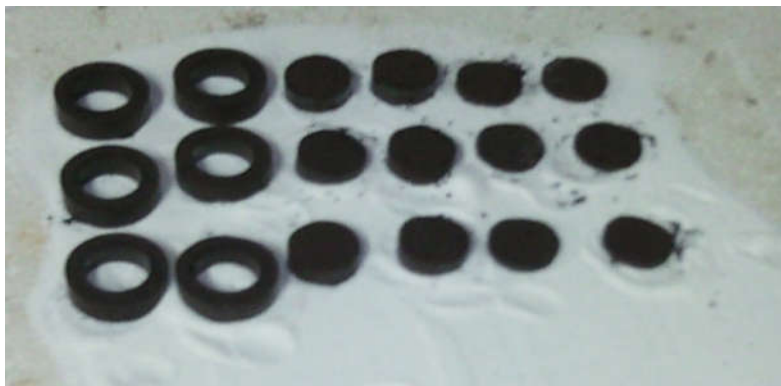
Figure 3.3: Toroid and disk shapes

Mainly, we made three types of samples cylindrical, tablet and toroidal. Specimen was prepared by a hydraulic press with a pressure at $1 - 10 \text{ton/cm}^2$, 14-140MPa. The die was designed and made in the workshop of AECD. This is made of nonmagnetic stainless steel.

3.1.5 Sintering

Sintering commonly refers to posses involved in the heat treatment of powder compacts at elevated temperatures where diffusion mass transport is appreciable. Sintering is the final and a very critical step of preparing properties. The sintering time, temperature and the furnaces atmosphere play very important role the magnetic property of final materials. Sintering commonly refers to processes involved in the heat treatment by which a mass of compacted powder is transformed into a highly densified object by heating it in a furnace below its melting point. Ceramic processing is based on the sintering of powder compacts rather than melting /solidifications /cold working (characteristic for metal) because:

(i) Ceramics melt at high temperatures

(ii) As solidified microstructures cannot be modified through additional plastic deformation and re-crystallization due to brittleness

(iii) The resulting coarse grains would act as fracture initiation of ceramics.

(iv) Low thermal conductivities of ceramics (< 30 - 50 W/mk) in contract to high thermal conductivity of metals (in the range 50-300 w/mk) cause large temperature gradients, and thus thermal stress and shock in melting solidification of ceramics.

This is a heat treatment by which a mass of compacted powder is transformed into a dense object. This is the final and critical step of sample preparation. Sintering involves the thermal treatment of a powder or compact at a temperature below the melting point of the main constituent, for the purpose of increasing its strength by bonding together of the particles. The thermodynamics driving force is the reduction in the specific surface area of the particles. In this process atomic mobility of the compact is sufficient to permit the decrease the free energy associated with the grain boundaries. The sintering mechanism usually involves atomic transport over particle surfaces, along grain boundaries and through the particle interiors. Sintering may result in densification, depending on the predominant diffusion pathway. It is used in the fabrication of metal and ceramic components, the agglomeration of ore fines for

further metallurgical processing and occurs during the formation of sand stones and glaciers. Sintering must fulfill three requirements.

- To bind the particles togather so as to impart sufficient strength to product.
- To dense the grain compacts by elimination of the pores
- To homogenize the materials by completing the reaction left unfinished in the preferring step.

The first two requirements are closely related as far as their mechanisms are concerned. The following figure shows the simple way to bond tour spherical particles to form neck at the contacts by volume diffusion.
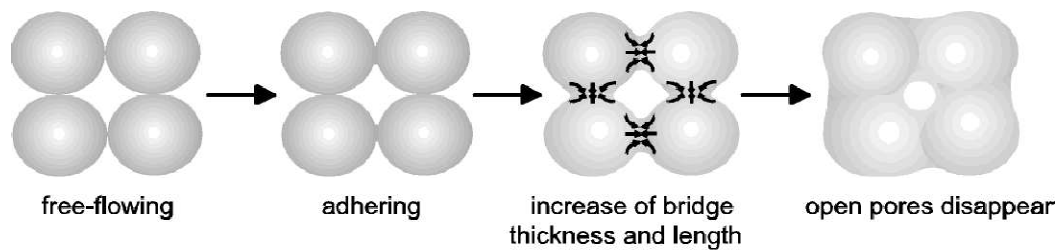
Figure 3.4: Volume diffusions.

One the basis of volume diffusion induced under surface tension, an important equation for the initial stage of sintering process is given by:

$$\frac{\Delta L}{L} = \left[\left(\frac{AD^*\gamma\Omega}{r^3 KT} \right) t \right]$$

(3.1)

Where, $\frac{\Delta L}{L}$ is the shrinkage of the compact, Ω is the volume of a single vacancy, D^* is the co-efficient of self diffusion for the slowest species, γ is the surface energy, γ is the average radius of the particles, t is sintering time and A is a constant with the approximate value of unity. The above equation indicates that sintering fulfills the requirements (a) and (b) more efficiently when compact features high surface energy and self diffusivity and the particles are fine.

For densification, Bruke made two important observations. One is that the formation of neck only makes the initial stage sintering; an intermediate stage begins when grain growth occurs with the compact density at around 60% of the theoretical value and ends when the pore phase become discontinuous and the density reaches a value of approximately 95%. Another observation of Bruke [3.7] deals with the final stage of sintering. Of discontinuous grain grows occur at the intermediate stage,

migration of grain boundaries will leave the remaining isolated pores trapped inside the grains, thus preventing further shrinkage of these intra particle pores and practically stopping the sintering process. In this operation, the cooling rate slays an important role on which structural modification is mainly based. Sintering of crystalline solids follows the following empirical relationship regarding rate of grain growth [3.8]

$$D = Kt^n \qquad\qquad (3.2)$$

Where d is the mean grain diameter, t is sintering time, n is about $\frac{1}{3}$ and K is a temperature dependent parameter.

In the present thesis we have used a programmable furnance NABER (Model HT 08/16 Germany) at AECD. The temperature of the furnace could be maintained within the accuracy of $\pm 1°C$.

For sintering we followed more or less the following program.
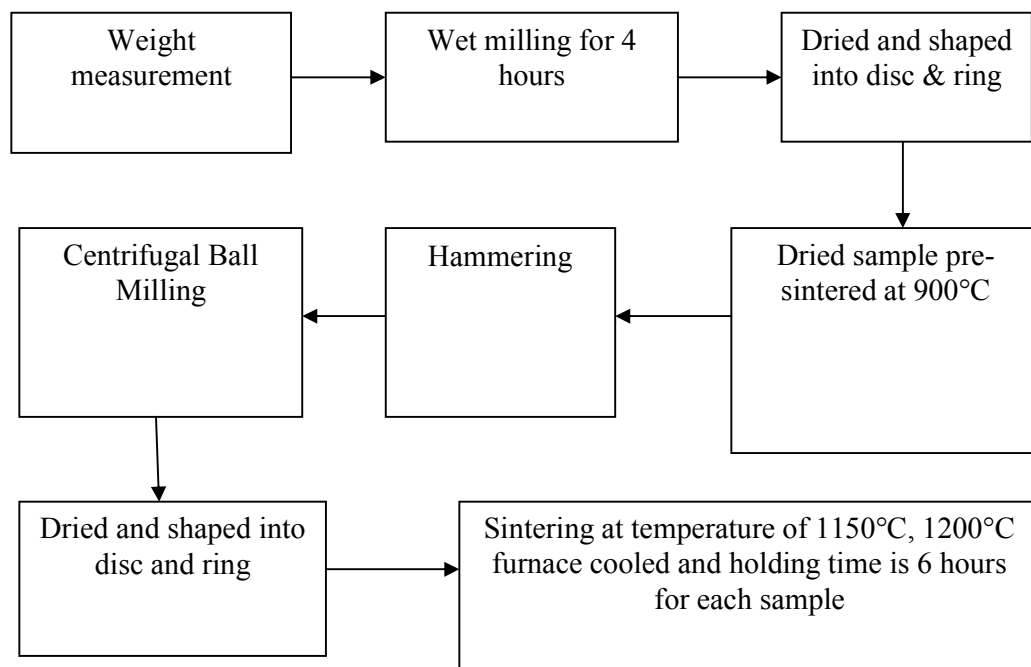
Figure 3.5: Flow chart of sintering

Why do we need sintering?

The principal goal of sintering is the reduction of compact porosity. Sometimes the initial spaces between compacted grains of ceramics are called

"voids", to differentiate them from the isolated spaces = pores, which occur in the final stages of sintering. The largest changes occur in:

* To bind the particles together so as to impart sufficient strength to the products.

* To density the green compacts by eliminating the pores.

* To homogenize in materials by completing the reactions left unfinished in the pre-sintering step.

* To make strength of elastic modulus.

* To make hardness and fracture toughness.

* To make homogeneous distribution of grain number, grain size and shape.

* To improve the average pore size and shape.

* To get a stable chemical composition and crystal structure.

Sintering is a widely used but very complex phenomenon. The fundamental mechanisms of sintering are still a matter of controversy. Experimental quantification of techniques, such as: dilatometer, buoyancy, gas absorption, proximity, indirect methods (e.g. hardness) and quantitative microscopic etc. The description of the sintering process has been derived from model experiments and by observing powder compact behavior at elevated temperatures. The following phenomena were observed:

(i)   Increase of inter-particle contact area with time.

(ii)   Rounding-off of sharp angles and points of contact.

(iii)   In most cases, the approach of particle centers and overall densification.

(iv)   Decreases in volume of interconnected pores.

(v)   Continuing isolation of pores.

(vi)   Grain growth and decrease in volume of isolated pores.

3.2 X-ray Diffraction

X-ray diffraction (XRD) provides precise knowledge of the lattice parameter as well as the substantial information on the crystal structure of the material under study. To study the crystalline structure of solids, X-ray diffraction (XRD) is a versatile and non-destructive technique that provides detailed information about the materials. A crystal lattice is a regularly arranged three-dimensional distribution

52

(cubic, rhombic etc.) of atoms in space. They are fashioned in such a way that they from a series of parallel plane separated from one another by a distance d (inter-planer or inter –atomic distance) which varies according to the nature of the material. XRD is a rapid analytical technique primarily used for phase identification of a crystalline material and can provide information on unit cell dimensions. The analyzed material is finely ground, homogenized and average bulk composition is determined.

X-rays are the electromagnetic waves whose wavelength is in the neighborhood of 1Å. The wavelength of an X-ray is that the same order of magnitude as the lattice constant of crystals and it is this which makes X-ray so useful in structural analysis of crystals. When X-ray beam is incident on a material, the photons primarily interact with the electrons in atoms and get scattered. Diffracted waves from different atoms can interfere with each other and the resultant intensity distribution is strongly modulated by this interaction. If the atoms are arranged in a periodic fashion, as in crystals, the diffracted waves will consist of sharp interference maxima (peaks) with the same symmetry as in the distribution of atoms. Measuring the diffraction pattern therefore allows us to deduce the distribution of atoms in a material. It is to be noted here that, in diffraction experiments, only X-rays diffracted via elastic scattering are measured.

The peaks in an X-ray diffraction pattern are directly related to the atomic distance. Let us consider an incident X-ray beam interacting with the atoms arranged in a periodic manner as shown in two dimensions in figure: 3.6. The atoms, represented as spheres in the illustration, can be viewed as forming different sets of planes in the crystal. For a given set of lattice planes with an inter-plane distance of d, the condition for a diffraction (peak) to occur can be simple written as

$$2d \sin n\theta = n\lambda$$

(3.3)

This is known as Braggs's law.

In the equation (3.3), λ is the wavelength of the X-ray, θ is the scattering angle, and n is an integer representing the order of the diffraction peak. The Bragg's Law is one of the most important laws used for interpreting X - ray diffraction data. From the law, we find that the diffraction is only possible when $\lambda < 2d$ [3.9].

In the present work A PHILIPS PW3040 X'Pert PRO X-ray diffractometer was used to study the crystalline phases of the prepared samples in the Materials Science division, Atomic Energy Centre, Dhaka.
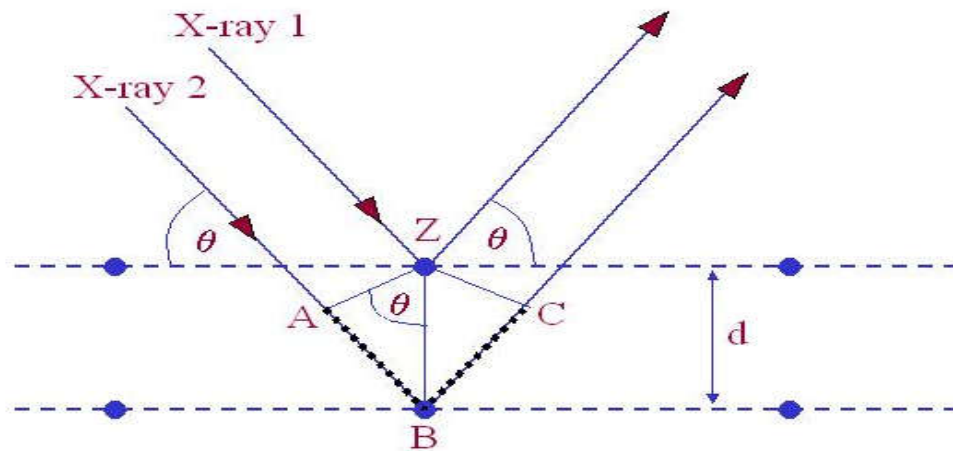
Figure 3.6: Bragg's diffraction pattern
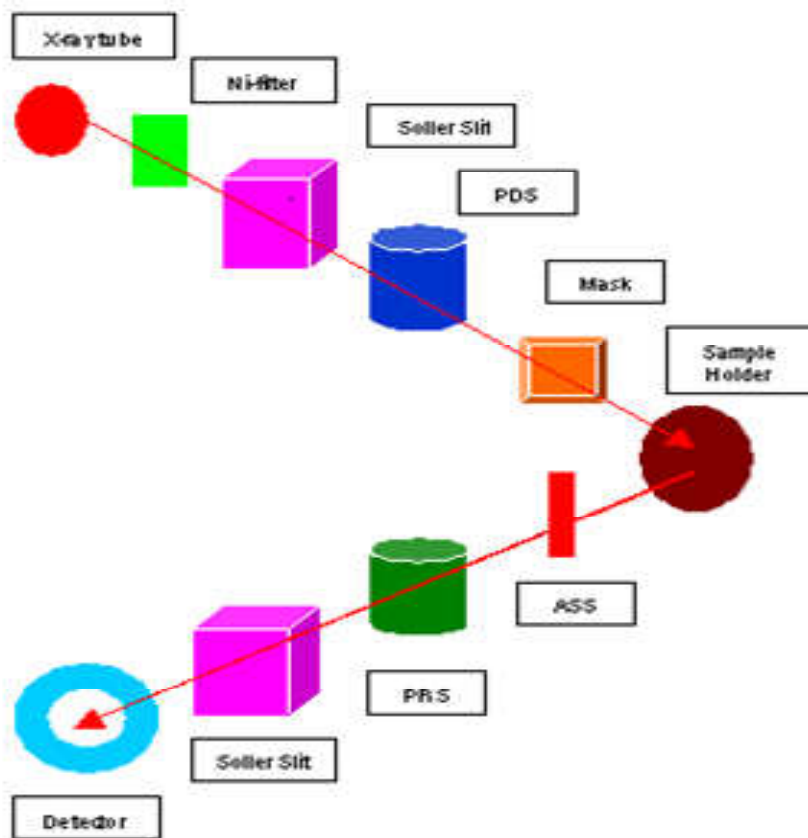
Figure: 3.7: Block diagram of the PHILIPS PW3040 X'Pert PRO XRD system

Figure 3.7 shows the inside view of the PHILIPS X'Pert PRO XRD system. The powder diffraction technique was used with a primary beam powder of 40 kV and 30 mA for Cu-K$_\alpha$ radiation. A nickel filter was used to reduce Cu-K$_\beta$ radiation and finally Cu-K$_\alpha$ radiation was only used as the primary beam. The experimental has been performed at room temperature. A *2θ* scan was taken from 25° to 75° to get possible fundamental peaks with the sampling pitch of 0.02^o and time for each step data collection was 1.0 sec. Both the programmable divergence and receiving slits were used to control the irradiated beam area and output intensity from the powder sample, respectively. An anti scatter slit was used just after the tube and in front of the detector to get parallel beam only. All the data of the sample were stored in the computer memory and later on analyzed them using computer "software" X'Pert HJGHS CORE". For XRD experiment each sample was set on a glass slide and fixed the sample by putting adhesive typed the two ends of the sample.

For each composition, the cylindrical samples of weight more than 2 gm are converted into powder. For XRD experiment each sample was set on a glass slide and fixed the sample by putting adhesive tape at the two ends of the sample X-ray diffraction patterns were carried out to confirm the crystal structure. Instrumental broadening of the system was determined from θ - 2θ scan of standard Si. At (311) reflections position of the peak, the value of instrumental broadening was found to be 0.07°. This value of instrumental broadening has subtracted from the pattern. After that using the X-ray data, the lattice constant (a) and hence the X-ray densities were calculated.

3.2.1 Different Parts of the PHILIPS X' Pert PRO XRD System

Figure: 3.8 shows the inside view of the X'- pert PRO XRD system. A complex of instruments of X- ray diffraction analysis has been established for both materials research and specimen characterization. These include facilities for studying single crystal defects, and a variety of other materials problems.

The PHILIPS X' Pert PRO XRD system comprised of the following parts

    (i)   Cu-Tube" with maximum input power of 60 kV and 55 mA

    (ii)   "Ni- Filter" to remove Cu-K$_\alpha$ component

    (iii)   "Solar slit" to pass parallel beam only

(iv)   "Programmable Divergent slits(PDS)" to reduce divergence of beam and control irradiated beam area

(v)   "Mask" to get desired beam area

(vi)   "Sample holder" for powder sample.

(vii)   "Anti Scatter slit (ASS)" to reduce air scattering back ground.

(viii)   "Programmable Receiving slit (PRS)" to control the diffracted beam intensity and

(ix)   Solar slit to stop scattered beam and pass parallel diffracted beam only.

Figure 3.8: Internal arrangement of a PHILIPS X' Pert PRO X-ray diffractometer.

3.2.2 Interpretation of the XRD data

The XRD data consisting of θ_{hkl} and d_{hkl} values corresponding to the different crystallographic planes are used to determine the structural information of the samples like lattice parameter and constituent phase. Lattice parameters of $Ni_{0.28}Cu_{0.10}Zn_{0.62}Fe_2O_4 + $ x wt.% V_2O_5 and $Ni_{0.28}Cu_{0.10}Zn_{0.62}Fe_2O_4 + $ x wt.% Bi_2O_3 ferrites samples were determined. Normally, lattice parameter of a composition is

determined by the Debye-Scherrer method after extrapolation of the curve. In this method at least five fundamental reflections are required to determine lattice parameter. In the present case, ten reflection planes are prominent at XRD patterns and we would like to understand additives as sintering aid influence of Ni-Cu-Zn ferrite. We determine lattice spacing (inner planer distance) d using this reflection from the equation:

$$2d_{hkl} \, \mathrm{Sin}\theta \, = \, \lambda$$

$$\text{i.e. } d_{hkl} \, = \, \frac{\lambda}{2\sin\theta} \tag{3.4}$$

Where λ is the wavelength of the X-ray, θ is the diffraction angle and n is an integer representing the order of the diffraction.

The lattice parameter for each peak of each sample was calculated by using the formula:

$$a = d_{hkl} \times \sqrt{h^2 + k^2 + l^2} \tag{3.5}$$

Where h, k, l are the indices of the crystal planes. We get d_{hkl} values from the computer using software "X'- Pert HJGHS CORE". So we got ten 'a' values for ten reflection planes such as a a_1 , a_2 a_3 ….. etc. To determine the exact lattice parameter for each sample, Nelson-Riley method was used. The Nelson-Riley function [3.10] f (θ), can be written as

$$F(\theta) = \frac{1}{2}\left[\frac{\cos^2\theta}{\sin\theta} + \frac{\cos^2\theta}{\theta}\right] \tag{3.6}$$

Now drawing the graph of 'a' vs F(θ) and using linear fitting of those points will give us the lattice parameter 'a_0'. This value of 'a_0' at F(θ) = 0 or θ = 90° .These 'a_0's are calculated with an error estimated to be $\pm$ 0.0001Å.

3.2.2.1 X-ray Density and Bulk Density

X-ray density, (ρ_x) was also calculated usual from the lattice constant. The relation between ρ_x and 'a' is as follows [3.11]

$$\rho_x = \frac{ZM}{Na^3} \tag{3.7}$$

Where M is the molecular weight of the corresponding composition, N is the Avogadro's number (6.023×10^{23} mole^{-1}), 'a' is the lattice parameter and Z is the number of molecules per unit cell,(Z = 8 for the spinel cubic structure).

Bulk Density

The bulk density (ρ_B) is measured by the formula

$$\rho_B = \frac{m}{V}$$

(3.8)

Where m is the mass of the disc sample and v is its volume.

3.2.2.2 Porosity

Porosity is a parameter which is inevitable during the process of sintering of oxide materials. It is noteworthy that the physical and electromagnetic properties are strongly dependent on the porosity of the studied samples. Therefore an accurate idea of percentage of pores in a prepared sample is prerequisite for better understanding of the various properties of the studied samples to correlate the microstructure property relationship of the samples under study. The porosity of a material depends on the shape, size of grains and on the degree of their storing and packing. The difference between the bulk density ρ_B and X-ray density ρ_x gave us the measure of porosity. Percentage of porosity has been calculated using the following relation [3.12]

$$P = (1 - \frac{\rho_B}{\rho_x}) \times 100\%$$

(3.9)

3.3 Measurement of Curie Temperature by Observing the Variation of Initial Permeability with Temperature

For ferrimagnetic materials in particular, for ferrite it is customary to determine the Curie temperature by measuring the permeability as a function of temperature. According to Hopkinson effect [3.13] which arises mainly from the intrinsic anisotropy of the material has been utilized to determine the Curie temperature of the samples. According to this phenomenon, the permeability increases gradually with temperature and reaching to a maximum value just before the Curie temperature.

Curie temperature measurements were done by using Hewlett Packard 4192A LF Impedance Analyzer shown in figure 3.9. Impedance parameters absolute value of impedance ($|Z|$), absolute value of admittance ($|Y|$), phase angle (θ), resistance (R), reactance (X), conductance (G), susceptance (B), inductance (L), capacitance (C), dissipation (D) and quality factor (Q). Measurement range of $|Z|$/R/X is 0.1mΩ to 1.2999 MΩ, $|Y|$/G/B is 1 ns to 12.999 s; θ is -180° to +180°; L is 0.1mH to 1.000 kH; C is 0.1PF

58

to 100.0 mF, D is 0.0001 to 19.999; Q is 0.1 to 1999.9. All have a basic accuracy of 0.1% and resolution of $4\frac{1}{2}$ digits. Number of display digits dependence on measuring frequency and OSC level setting. We made use of the excellent experimental facilities available at the Materials Science Division, Atomic Energy Centre, Dhaka.

The temperature dependent permeability was measured by using induction method. The specimen formed the core of the coil. The number of turns in each coil was 5. We used a constant frequency (100 kHz) of a sinusoidal wave, AC signal of 100mV. HP 4192A impedance analyzer with continuous heating rate of $\approx$ 5 K / min with very low applied ac field of $\approx 10^{-3}$Oe. By varying temperature, inductance of the coil as a function of temperature was measured. Dividing this value of L_o (inductance of the coil without core material), we got the permeability of the core i.e. the sample. When the magnetic state inside the ferrite sample changes from ferromagnetic to paramagnetic, the permeability falls sharply. From this sharp fall at specific temperature the Curie temperature was determined. For the measurement of Curie temperature, the sample was kept inside a cylindrical oven with a thermocouple placed at the middle of the sample. The thermocouple measures the temperature inside the oven and also of the sample.
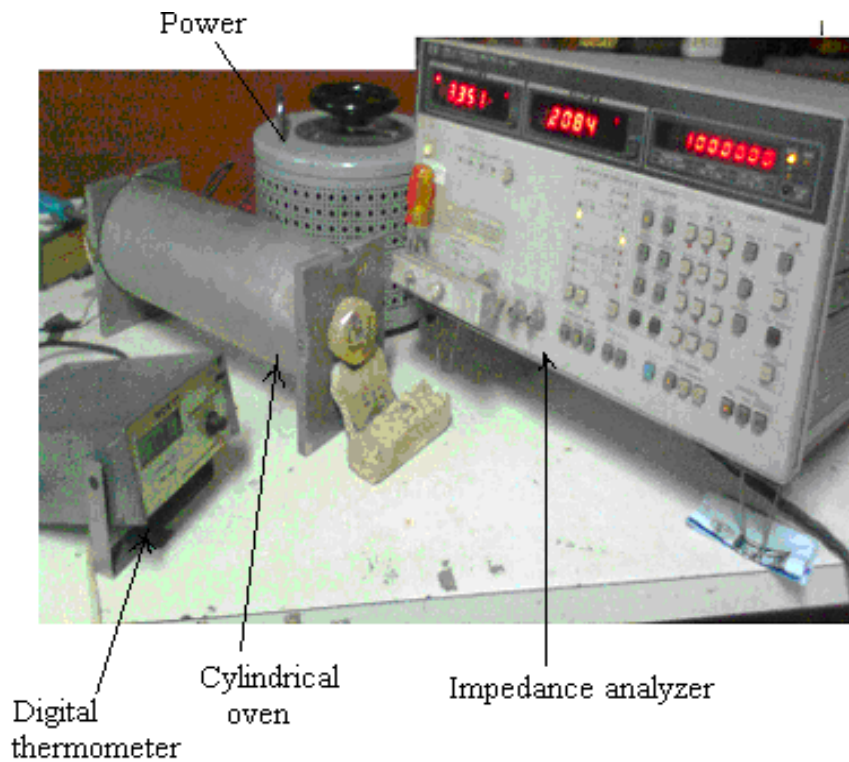
Figure 3.9: Impedance Analyzer Model-Hewlett-Packard 4192A.

The sample was kept just in the middle part of the cylindrical oven in order to minimize the temperature gradient. The temperature of the oven was then raised slowly. If the heating rate is very fast then the temperature of the sample may not follow the temperature inside the oven and there can be misleading information on the temperature of the samples. The thermocouple showing the temperature in that case will be erroneous. Due to the closed winding of wires the sample may not receive the heat at once. So, a slow heating rate can eliminate this problem. The cooling and heating rates are maintained as approximately 0.5°C min^{-1} in order to ensure a homogeneous sample temperature. Also a slow heating ensures accuracy in the determination of Curie temperature.

The oven was kept thermally insulated from the surroundings. The temperature was measured with a digital thermometer attached close to the sample and put inside the furnace where the temperature fluctuation is almost negligible. Then the permeability versus temperature curve was plotted from which the Curie temperature was calculated.

3.3.1 Permeability

From the frequency dependence of complex permeability, evolution of permeability and magnetic loss component at different stages of ferrite sample as affected by thermal treatment at different temperature was determined using toroids shape sample prepared with insulating Cu wire. The 4192 LF Impedance analyzer directly measure the value of inductance, L and loss factor.

$$D = \tan\delta \qquad (3.10)$$

From inductance the value of real part of complex permeability, μ' can be obtained by using the relation

$$\mu' = \frac{L}{L_0} \qquad (3.11)$$

where L is the inductance of the toroid and L_o is the inductance of the coil of same geometric shape in vacuum, L_o is determined by using the relation,

$$L_0 = \frac{\mu_0 N^2 S}{\pi \bar{d}} \qquad (3.12)$$

Here μ_o is the permeability of the vacuum, N is the number of turns (here N = 5), S is the cross-sectional area of the toroid shaped sample, S = dh, where, $d = \frac{d_1 \sim d_2}{2}$ and $\bar{d}$ is

the average diameter of the toroid sample given as $\bar{d} = \frac{d_1 + d_2}{2}$ \qquad (3.13)

where, d_1 and d_2 are the inner and outer diameter of the toroid samples.

3.3.2 Mechanisms of Permeability

Mechanisms of permeability can be explained as the following way: a demagnetized magnetic material is divided into number of Weiss domains separated by block walls. In each domain all the magnetic moments are oriented in parallel and the magnetization has its saturation value M_s. In the walls the magnetization direction changes gradually from the direction of magnetization in one domain to that in the next. The equilibrium positions of the walls results from the interactions with the magnetization in neighboring domains and from the influence of pores; crystal boundaries and chemical in homogeneities which tend to favor certain wall positions.

3.3.3 Technique of Measurements of Permeability

Measurements of permeability normally involve the measurements of the change in self inductance of a coil presence of the magnetic core. The behavior of a self inductance can now be described as follows. Suppose we have an ideal lossless air coil of inductance L_o. On insertion of magnetic core with permeability μ, the inductance will be μL_o. The complex impedance Z of this coil can be expressed as,

$$Z = R + jX = j\omega L_o(\mu' - j\mu'') \tag{3.14}$$

where the resistive part is

$$R = \omega L_o\mu' \tag{3.15}$$

and the reactive part is

$$X = \omega L_o\mu'' \tag{3.16}$$

The radio frequency (RF) permeability can be derived from the complex impedance of a coil Z (equation 3.14). The core is usually toroidal to avoid demagnetization effects. The quantity L_o is derived geometrically.

3.3.4 Frequency Characteristic of Ferrite Samples

The frequency characteristics of the cubic ferrite sample i.e. the permeability spectra were investigated using a Hewlett Packard Impedance Analyzer of Model No.4192A provide the value of inductance, L and loss factor, $D = \tan\delta$. The measurements of inductances were taken in the frequency range of 1 kHz to 13 MHz. The values of measured parameters obtained as a function of frequency and the real (μ') and imaginary part (μ'') of permeability and the loss factor are calculated. μ' is calculated by using the equation 3.11 and equation 3.12 and μ'' is calculated by using the following equation

$$\mu'' = \mu' \tan\delta \qquad\qquad (3.15)$$

3.4 Magnetization Measurement

Magnetization in ferrite samples originated due to the difference in the magnetic moments for the two sub-lattices. The larger the difference, the greater is the resultant magnetization, because of the anti-parallel arrangements of the moments in two sub-lattices. The magnetic moment of each sub-lattice arises due to the presence of magnetic ions such as Fe^{3+}, Fe^{2+}, Zn^{2+}, Cu^{2+}, Ni^2 etc. in our case, only iron ion has magnetic moment since Mg non-magnetic. Different ions occupy different two sites. So, as a whole, the two sub-lattices have their individual resultant magnetic moments. The differences in magnetic moment between the two sub-lattices give rise to net magnetic moment which in turn yields magnetization. In the present study magnetization has been performed a Vibrating Sample Magnetometer (VSM).

3.4.1 Vibration Sample Magnetometer

The principle of vibrations sample magnetometer (VSM) is the measurement of electromotive force induces by magnetic sample when it is vibrate at a constant frequency in the presence of a static and uniform magnetic field. A small part of the (10 - 50 mg) was weighted and made to avoid movements inside the sample holder shown in Figure 3.10. VSM is a versatile and sensitive method of measuring magnetic properties developed by S. Foner [3.14] and is based on the flux change in a coil when the sample is vibrate near it.

The simplest of these is the rotating coil which rotates at a fixed angular velocity. Therefore the amplitude of the generated voltage by rotating coil is proportional to the magnetic induction and therefore the amplitude can be used to measure magnetic induction or magnetic field in free space. The signal can be read directly as an AC voltage or converted to a DC voltage which is proportional to the amplitude.

Figure 3.11 shows VSM of Model EV7 system. The magnetic properties measurement system model EV7 is a sophisticated analytical instrument configured specially for the study of the magnetic properties of the small samples over a broad range of temperature from 103K to 800K and magnetic field from -20kOe to +20kOe. The VSM is designed to continuously measure the magnetic properties of materials as a function of temperature and the field. In this type of magnetometer, the sample is

vibrated up and down in a region surrounded by several pick up coils. The magnetic sample is thus acting as a time-changing magnetic flux, varying the electric flux is accompanied by an electric field and the field induces a voltage in pick up coils. This alternating voltage signal is processed by a control unit system, in order to increase the signal to noise ratio. The result is a measure of the magnetization of the sample.
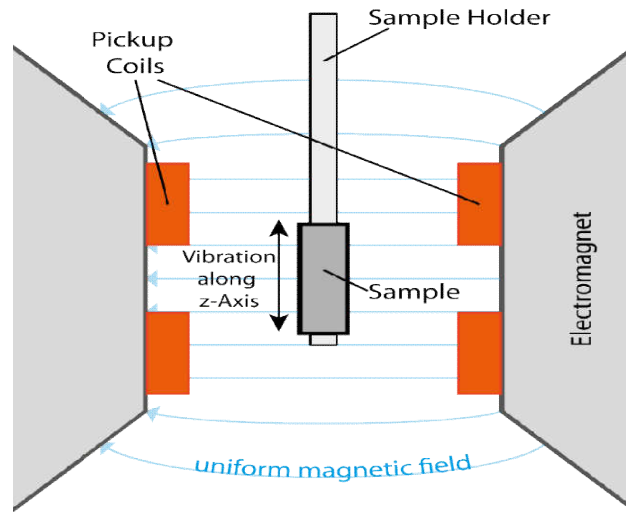
Figure 3.10: Vibrating Sample Magnetometer - sample holder and detection mechanism

By using a compact gradiometer pickup coil configuration, relatively large oscillation amplitude (1- 3mm peak) and a frequency of 40 Hz, the system is able to resolve magnetization changes of less than 10^{-6} emu at a data rate of 1 Hz. The VSM option for the PPMS consists primarily of a VSM line a motor transport (head) for vibrating the sample, a coil set puck for detection, electronics for driving the linear motor transport and detecting the response from the pickup coils. If a sample is placed in a uniform magnetic field, created between the poles of electromagnet, a dipole moment will be induced. If the sample vibrates with sinusoidal motion sinusoidal electrical signal can be induced in suitable placed pick-up coils. The signal has same frequency of vibration and its amplitude will be proportional to the magnetic moment.

The sample is attached to the end of a sample rod that is driven sinusoidally. The center of oscillation is positioned at the vertical center of a gradiometer pickup coil. The precise position and amplitude of oscillation is controlled from the VSM motor module using an optical linear encoder signal read back from the VSM linear

motor transport. The voltage induced in the pickup coil is amplified and lock-in detected in the VSM detection module.
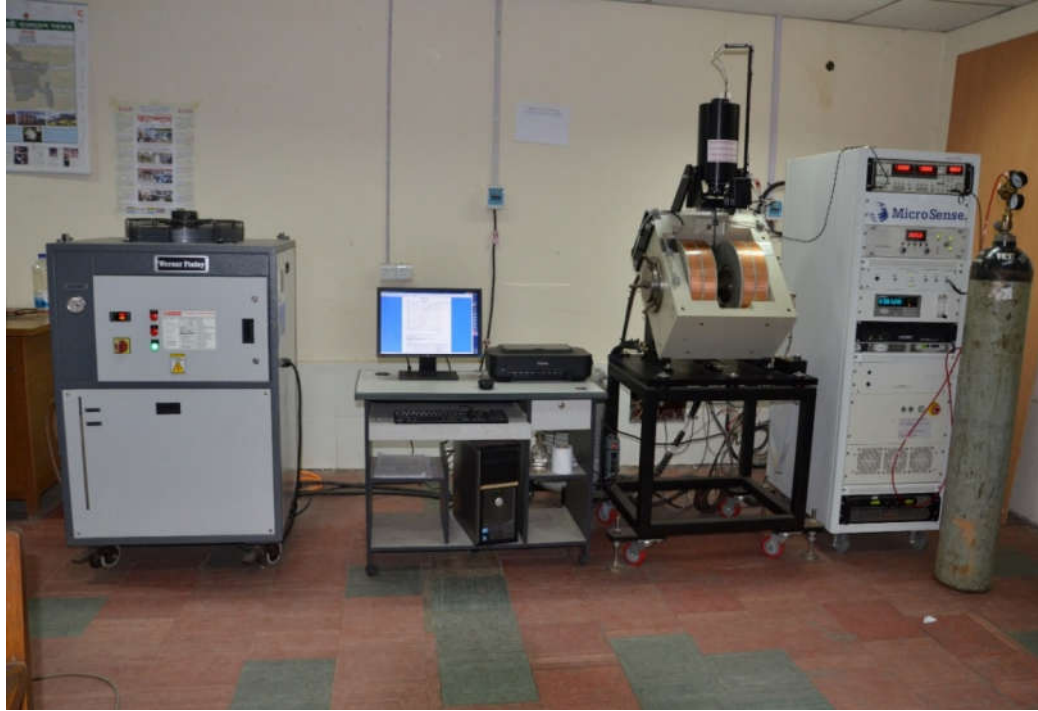
Figure 3.11: Vibrating Sample Magnetometer at Materials Science Division, AECD

The VSM detection module uses the position encoder signal as a reference for the synchronous detection. This encoder signal is obtained from the VSM motor module, which interprets the raw encoder signals from the VSM linear motor transport. The VSM detection module detects the in-phase and quadrature-phase signals from the encoder and from the amplified voltage from the pickup coil.

The sample is fixed to sample holder located at the end of a sample red mounted in a electromechanical transducer. The transducer is driver by a power amplifier which itself is driver by an oscillator at a frequency of 90Hz. So, the sample vibrates along the 2-axis perpendicular to the magnetizing field. The latter induce a signal in the pick-up coil system that is fed to a differential. The output of the differential amplifier is subsequently fed into a tuned amplifier and an internal lock in amplifier that receives signal supplied by the oscillator. The output of the lock-in amplifier, or the output of the magnetometer itself, is a DC signal proportional to the magnetic moment of the sample being studied. Calibration of the VSM is done by

measuring the signal of a pure Ni standard of Known saturation magnetic moment placed in the saddle point. The basic instrument included the electromechanical system and the electronic system including in personal computer. Laboratory electromagnet coils of various maximum field strengths may be used.

3.5   DC and AC Resistivity

Resistivity is an intrinsic property of a material .The technical importance of ferrites lies primarily in their high resistivity. The electrical resistivity measurements carried out by a two probe method on silver painted sample a Keithley Electrometer using pellet samples of diameter 8.3-8.8mm and of thickness 1.2 - 2.5 mm by applying silver electrodes on the surfaces. Samples were prepared by sintering the samples for $Ni_{0.28}Cu_{0.10}Zn_{0.62}Fe_2O_4$+ x wt.% V_2O_5 [x = 0.2, 0.4, 0.6 and 0.8] and

$Ni_{0.28}Cu_{0.10}Zn_{0.62}Fe_2O_4$+ x wt.% Bi_2O_3 [x = 0.2, 0.4, 0.6 and 0.8] ferrites for 6hours. The samples were polished using metallurgical polishing machine with the help of silicon carbide papers with grit size 600. After that the samples were clean with acetone and then again polished with special velvet type polishing cloth named as α-gam, for finer polishing using fine alumina powder of grain size 0.05 micron dispersed in a liquid. The powders were of various sizes starting with 1 micron to 0.05 micron. Samples are then cleaned in a ultrasonic cleaner and dried in surface at 150°C for several hours. Then the samples are again cleaned with acetone and silver paste was added to both the sides of the polished pellet samples together with two thin copper wires of 100 micron diameter for conduction. Again the samples are dried at 150°C to eliminate any absorbed moisture.

The DC and AC resistivity were measured as a function of frequency in the range 1 kHz-13MHz at room temperature by Electrometer Keithley model 6514 and impedance analyzer. Both the resistivity has been calculated using the formula:

$$\rho = \frac{RA}{l} = \frac{\pi r^2 R}{l}.$$ (3.16)

where R is the resistance of the Pellet, r is the radius of the pellet and l is the thickness of the pellet .

Ferrites are semiconductors and their resistivity decreases with increasing temperature according to the relation $\rho = \rho_\alpha e^{E_a / KT}$ (3.17)

65

where K the Boltzmann constant, T is the absolute temperature, E_a represents an activation energy which according to Verway and De Boer is the energy needed to release an electron from the ion to jump to the neighboring ion, thus giving rise to electrical conductivity. If we plot $\log \rho$ vs $\dfrac{1}{T}$ for various ferrites, a straight line is found in a wide temperature range with a slope corresponding to E_p according to the relation

$$E_p = 0.198 \times 10^{-3} \frac{d(\log \rho)}{d(1/T)} \tag{3.18}$$

3.5.1 Dielectric Constant

Dielectric measurement as a function of frequency in the range 100Hz-13MHz at room temperature were carried out by using Hewlett Packrat impedance analyzer in conjunction with a laboratory made furnace which maintain the desired temperature with the help of a temperature controller The real part of dielectric constant was calculated using the formula

$$\varepsilon' = \frac{cd}{\varepsilon_o A} \tag{3.19}$$

where c is the capacitance of the pellet in Farad, d the thickens of the pellet in meter , A the cross-sectional area of the flat surface of the pellet in m^2 and ε_o the constant of permittivity for free space.

3.6 Experimental Procedure for Microstructure Study

Magnetic properties of the Ni-Cu-Zn sample are strongly dependent upon the sensitive control of the microstructure permeability is directly proportional to the grain size of the samples. At least up to a critical diameter of the grains causes the permeability to increase monotonically. Resistivity and density of the ferrite samples are also dependent on the porosity of the samples. Resistivity of the samples increases with the trapped intra-granular pores. Hence the microstructure studies of the samples are required for making prediction about the result of permeability and resistivity of the ferrite samples. For microstructure study the ferrite samples were polished step by step. Primarily the samples were polished by using Megaserv Universal Polisher; model No C200/5V, Volts 240, Amp. 0.75 Secondly, using another polishing machine 99 phoenix .Aue, Enfield, CT06082 USA, Model No LABPOL 8/12, keeping a aped

of 300 - 450 rev/sec for about 1 hour using different grades of Al_2O_3 fine powders mixing with water. In the tertiary stage the polished samples were classed ultrasonically for $\frac{1}{2}$ hour using an ultrasonic cleaner FEITSCH @ Laboratte, Model 17:202, No 1030. After the fine polishing and ultrasonic cleaning the samples were etched thermally under suitable temperature for the different samples down below 150 to 100°C of the sintering temperature for 2 minutes in air for every sample. As the thermal etching was finished the samples were readily for the microstructure study. The microstructure measurements of the samples were done by using Philips XL30 Scanning Tunneling Microscope at AECD, Dhaka, Bangladesh. The following figure 3.10 shows the pictorial diagram of SEM.

The SEM microstructures of samples sintered at 1100°C (furnace cooled) were studied by using Philips XL30 Scanning Tunneling Microscope. To observe the microstructure the ferrite samples were ground and then polished with fine Al_2O_3 powder followed by thermal etching near to the sintering temperature 2 minutes. When the etching was completed, the grains were seen clearly by the SEM and photographed.

Figure 3.12: Scanning Electron Microscope

RESULTS AND DISCUSSION

4.0 Introduction

Ni-Cu-Zn ferrite materials with V_2O_5 and Bi_2O_3 additives are prepared by the conventional ceramic technique. The use of sintering additives was found to be an effective method in practical manufacturing to lower the sintering temperature with degrading the electromagnetic properties [4.1]. To obtain materials with high permeability as well as high quality factor, a key step is to tailor the additives composition to produce densification with limited grain growth. During the grain growth, the dislocation of the additives into the ceramic is assisted by solution re-precipitation process, which reduces the volume fraction of intergranular phases. The compositions of additives, melting temperature, reactions between the additives and ferrites, and microstructural evolution during the liquid-phase sintering are all very important parameters to characterize and understand any attempt to precisely control the magnetic properties [4.2-4.3]. Many researchers used Bi_2O_3 [4.4-4.5], V_2O_5 [4.6-4.7], MoO_3 [4.8-4.9], Glass [4.10], PbO [4.11] and WO_3 [4.12] as sintering aids in Ni-Cu-Zn ferrite.

These additives liquid phase are which either due to the melting of additives or eutectic liquid phase formation between the additives and ferrites. Amount of liquid phase increases with increasing amount of sintering aids which results in increased densification. However, excessive amount of sintering additives will deteriorate electromagnetic properties of ferrites. In addition, deriving as a liquid phase to promote the densification, it is important to recognize that the additives components may also play an important role in the contribution to the magnetic properties of the sintered ferrites. Hsu *et. al.* [4.13] stated that 0.5mol.% (~0.20wt.%) V_2O_5 addition had better densification in Ni-Cu-Zn ferrites. In Jeong *et. al.* [4.14] study, 0.25% MoO_3 addition had given highest bulk density and maximum initial permeability. This is primarily true if the permeability is diluted by the presence of a continuous low permeability grain boundary showed the presence of vanadium inside the ferrite grains.

In these study of the present work are to synthesize Ni-Cu-Zn ferrites of composition $Ni_{0.28}Cu_{0.10}Zn_{0.62}Fe_2O_4$ + x wt.% the concentration sintering additives were varied 0.2wt.% to 0.8wt.% for V_2O_5 and Bi_2O_3. The green samples containing

different additives were sintered at temperatures $1150^{\circ}C$ and $1200^{\circ}C$ with 6 hours holding time. Effects of those sintering additives on the densification behavior were investigated. The X-ray diffraction analysis proves that the additives do not affect the final crystal phase of the Ni-Cu-Zn ferrite in our testing range. The V_2O_5 additives more easily enter the crystal lattice of the Ni-Cu-Zn ferrite than the Bi_2O_3 additive. These characteristics evidently affect the electrical and magnetic properties such as Scanning Electron Microscope (SEM), magnetic phase transition were determined by permeability versus temperature, structural, transport and magnetic properties of sintered specimens were also measured.

4.1 X-ray Diffraction Analysis of Ni-Cu-Zn doped with V_2O_5

The phase formation behavior of $Ni_{0.28}Cu_{0.10}Zn_{0.62}Fe_2O_4$ + x wt.% V_2O_5 [x = 0.2, 0.4, 0.6 and 0.8] sintered at $1150^{\circ}C$ and $1200^{\circ}C$ for 6 hours were studied by X-ray diffraction(XRD) patterns exhibited that all the samples were indentified as a single phase of cubic spinel structure. The XRD patterns for all the samples were indexed for fcc spinel structure and the Bragg planes are shown in the patterns. The XRD patterns of the samples are given in figure 4.1 and figure 4.2. The peaks (111), (220), (311), (222), (400), (422), (511) and (440) correspond to spinel phase are characteristic of spinel structures with single phase. The lattice parameter 'a' corresponding to each plane was calculated by using X-ray data. The average values of 'a' were found by plotting 'a' against Nelson-Riley function.

4.1.1 Lattice Parameters

The values lattice parameter obtained from each plane are plotted against Nelson –Riley function [4.15]

$$F(\theta) = \frac{1}{2}\left[\frac{cos^2\theta}{sin\theta} + \frac{cos^2\theta}{\theta}\right] \tag{4.1}$$

Where θ is the Bragg's angle, by extrapolating the lattice parameter values to $F(\theta) = 0$ or $\theta = 90°$. The variation of the lattice parameter 'a' as a function V_2O_5 additive content x shown in figure 4.3(a) and figure 4.3(b). A decrease in lattice constant is observed with the increase of V_2O_5 content x in the lattice. The linear decrease in lattice constant with doped V_2O_5 indicates that the present system obeys the Vegard's law [4.16].
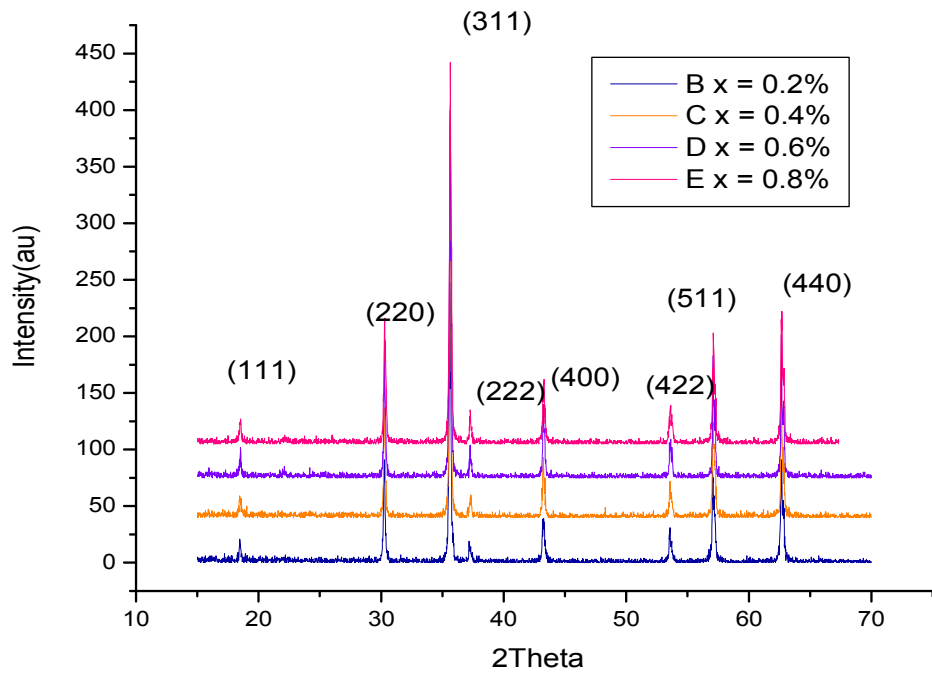
Figure 4.1: X-ray diffraction patterns of $Ni_{0.28}Cu_{0.10}Zn_{0.62}Fe_2O_4$ + x wt.% V_2O_5 [x = 0.2, 0.4, 0.6 and 0.8] sintered at 1150°C for 6 hours
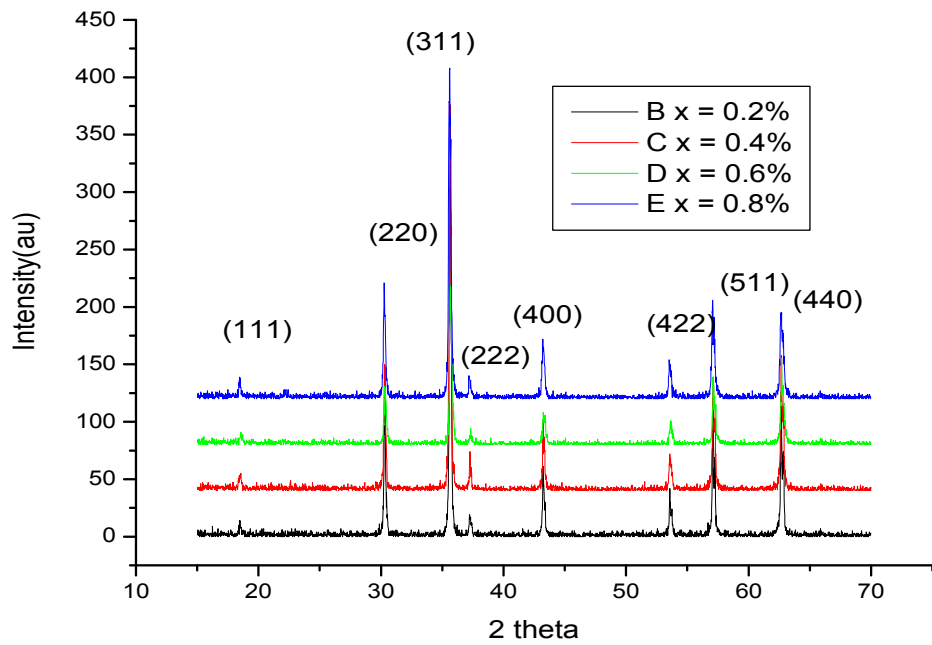
Figure 4.2: X-ray diffraction patterns of $Ni_{0.28}Cu_{0.10}Zn_{0.62}Fe_2O_4$ + x wt.%V_2O_5 [x = 0.2, 0.4, 0.6 and 0.8] sintered at 1200°C for 6 hours

This decrease can be obtained to the vacancy created by Fe^{3+} deficiency with increasing its V_2O_5 content. The unit cell is expected to reduce its size by contraction of the lattice resulting in decrease of lattice parameter gradually.
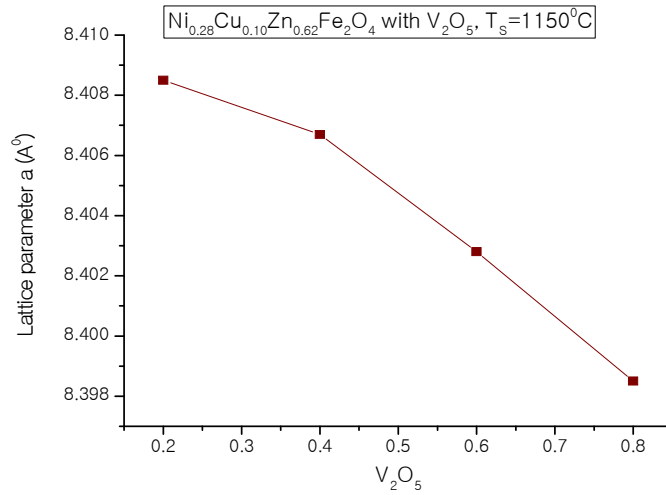
Figure 4.3(a): Variation of lattice parameter 'a' as a function of $Ni_{0.28}Cu_{0.10}Zn_{0.62}Fe_2O_4$ + x wt.% V_2O_5 (x = 0.2, 0.4, 0.6 and 0.8) sintered at 1150^oC for 6 hrs

Figure 4.3(b): Variation of lattice parameter 'a' as a function of $Ni_{0.28}Cu_{0.10}Zn_{0.62}Fe_2O_4$ + x wt% V_2O_5 (x = 0.2, 0.4, 0.6 and 0.8) sintered at 1200^oC for 6 hrs

71

4.1.2 Density and Porosity

The variation of density as a function V_2O_5 additives content are shown in figure 4.4(a) and figure 4.4(b). The bulk density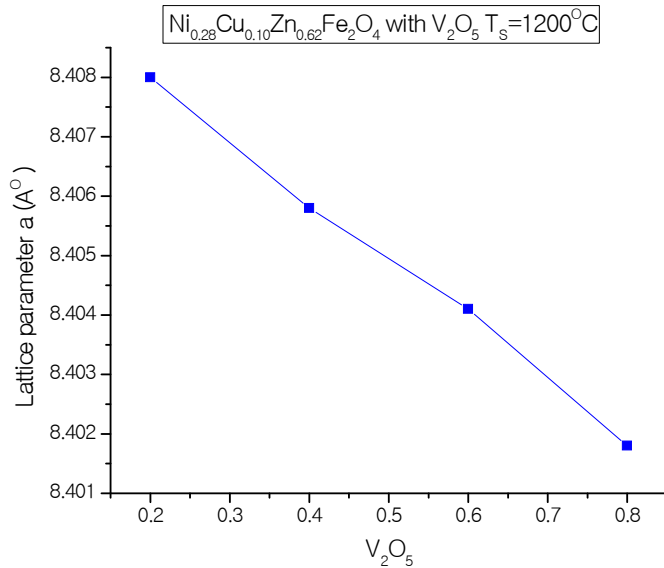, d_B was measured by usual mass and dimensional consideration whereas X-ray density, ρ_x was calculated from the molecular weight and volume of the unit cell for each sample by using the equation (4.2) and equation (4.3).

Bulk density, $\rho_B = \frac{m}{V} = \frac{m}{\pi r^2 h}$ g/cm^3 (4.2)

X-ray density, $\rho_x = \frac{8M}{Na^3}$ g/cm^3 (4.3)

Porosity $\quad P = 1 - \frac{\rho_B}{\rho_x}$ (4.4)

The ρ_B is lower than the ρ_x. This may be due to the existence of pores, which were formed and developed during the sample preparation or sintering process. It is worthwhile to mention that density plays an important role on the magnetic properties especially on the structure sensitive extrinsic properties such as permeability and flux density. Table 4.1 and Table 4.2 are shows the results of lattice parameter, theoretical density, bulk density and calculated porosity of are samples sintered at 1150°C/6hrs. and 1200°C/6hrs. There are observed Table 4.1 and Table 4.2 that porosity nearly same as fluctuated.

Table 4.1 Data of lattice parameter (a), X-ray density (ρ_x), bulk density (ρ_B), porosity (P%), molecular weight (M) of V_2O_5 (x = 0.2, 0.4, 0.6 and 0.8 %) of $Ni_{0.28}Cu_{0.10}Zn_{0.62}Fe_2O_4$+ x wt.% V_2O_5 ferrites sintered at 1150^{0}C for 6 hrs

V_2O_5 content(x%)	a (Å)	(ρ_x) (g/cm^3)	(ρ_B) (g/cm^3)	P%	M (g)
0.2	8.4085	5.34	3.84	28.08	239.38
0.4	8.4060	5.36	3.85	28.17	239.74
0.6	8.4028	5.37	3.87	27.93	240.10
0.8	8.3985	5.39	3.82	29.12	240.47

Figure 4.4(a): Comparison of the X-ray density and bulk density for the sample with V_2O_5 of $Ni_{0.28}Cu_{0.10}Zn_{0.62}Fe_2O_4$ +x wt% V_2O_5 (x = 0.2, 0.4, 0.6 and 0.8 %) ferrites sintered at 1150^0C for 6 hrs.
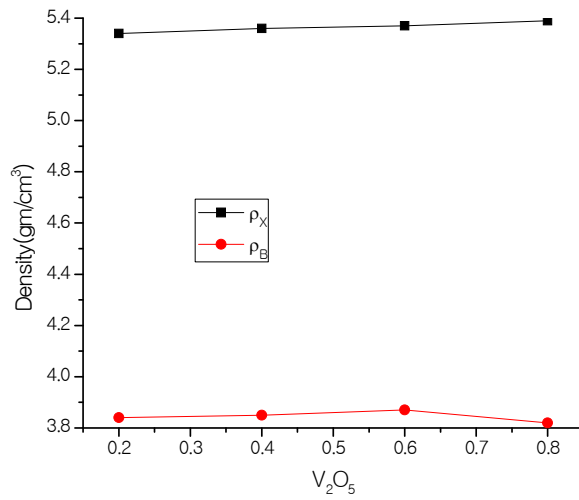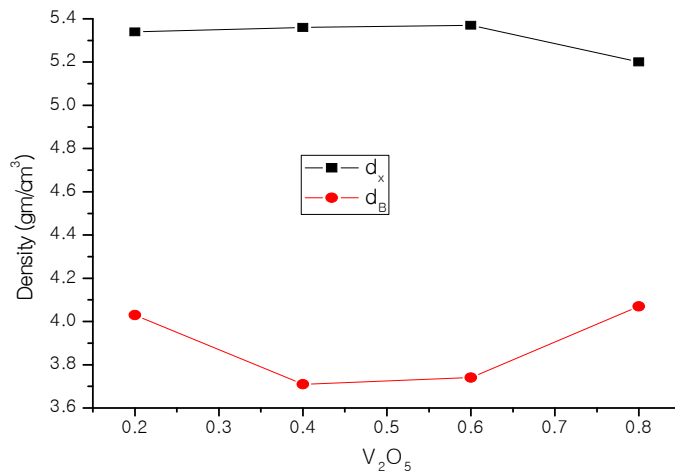

Figure 4.4(b): Comparison of the X-ray density and bulk density for the sample with V_2O_5 of $Ni_{0.28}Cu_{0.10}Zn_{0.62}Fe_2O_4$ + x wt% V_2O_5 (x = 0.2, 0.4, 0.6 and 0.8) ferrites sintered at 1200^0C for 6 hrs.

Table 4.2: Data of lattice parameter (a), X-ray density (ρ_x), bulk density (ρ_B), porosity (P%), molecular weight (M) of V_2O_5 (x = 0.2, 0.4, 0.6 and 0.8 %) of $Ni_{0.28}Cu_{0.10}Zn_{0.62}Fe_2O_4$ +x wt% V_2O_5 ferrites sintered at 1200^0C for 6 hrs

V_2O_5 Content (x%)	a (A^0)	ρ_x (g/cm^3)	ρ_B (g/cm^3)	P%	M (g)
0.2	8.4085	5.34	3.83	28.08	239.38
0.4	8.4060	5.35	3.85	25.67	239.74
0.6	8.4028	5.37	3.85	28.30	240.10
0.8	8.3985	5.39	3.86	29.31	240.47

4.2 X-ray Diffraction Analysis of Ni-Cu-Zn doped with Bi_2O_3

The phase formation behavior of $Ni_{0.28}Cu_{0.10}Zn_{0.62}Fe_2O_4$ +x wt% Bi_2O_3 [x = 0.2, 0.4 and 0.8] sintered at 1150^oC for 6 hours were studied by XRD. All the samples show crystallization with well defined diffraction lines. The powder XRD patterns exhibited that all the samples were identified as a single phase of sipnel structure. The XRD patterns for all the samples were indexed for fcc spinel structure and the Bragg planes are shown in the patterns. The XRD patterns of the samples are shown in figure 4.5. The peaks (111), (220), (311), (222), (400), (422), (511) and (440) corresponds to phase which are characteristics of spinel structures with a single phase. The lattice parameter 'a' corresponding to each plane was calculated by using the X-ray data.

4.2.1 Lattice Parameters

The values of the lattice parameter obtained from each plane are plotted against Nelson-Riley function F(θ) from equation (4.1). The variation of the lattice parameter 'a' as function of Bi_2O_3 additive content x is shown in figure 4.6. The linear decreases in lattice constant with additive Bi_2O_3 doped with Ni-Cu-Zn ferrite indicates that the present system obeys Vegard's law.
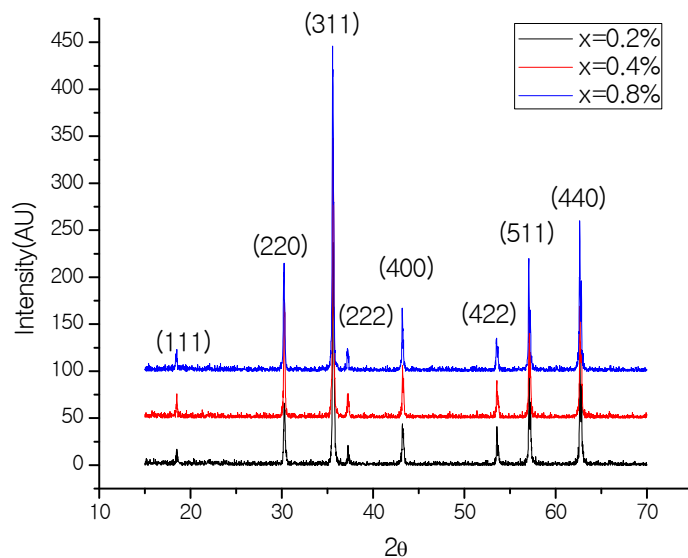
Figure 4.5:   X-ray diffraction patterns of $Ni_{0.28}Cu_{0.10}Zn_{0.62}Fe_2O_4$ + x wt.% Bi_2O_3
[x = 0.2, 0.4and 0.8] sintered at 1150^oC for 6 hours
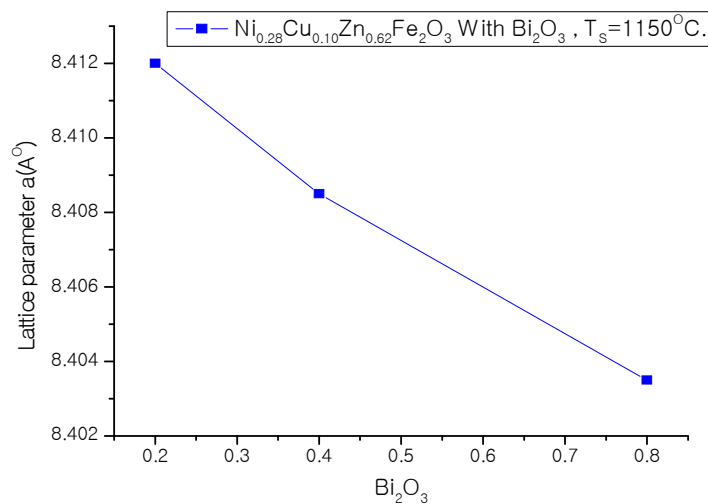
Figure 4.6:   Variation   of   lattice   parameter   'a'   as   a   function   of
$Ni_{0.28}Cu_{0.10}Zn_{0.62}Fe_2O_4$ + x wt.% Bi_2O_3 (x = 0.2, 0.4& 0.8%) sintered
at 1150^oC for 6 hrs

4.2.3 Density and Porosity

The variation of density with doped additive Bi_2O_3 is shown in figure 4.7. The bulk density (ρ_B) is lower than the X-ray density (ρ_x). This may be due to the existence of pore, which are inevitable during ceramic processing and formed and developed during the sample preparation or the sintering process. This enhancement of bulk density is due to activated diffusion process triggered by the excess vacancies created by Bi_2O_3 additives. Table 4.3 shows the results of lattice parameter, theoretical density, bulk density calculated porosity. The porosity which is intrinsic for any oxide materials plays an important role in deciding the magnetic and electrical properties.
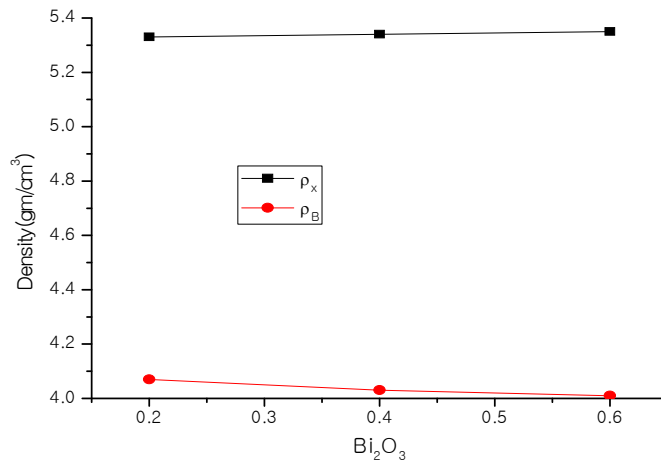
Figure 4.7:   Comparison of the X-ray density and bulk density for the sample with Bi_2O_3 of $Ni_{0.28}Cu_{0.10}Zn_{0.62}Fe_2O_4$ +x wt% Bi_2O_3 (x = 0.2, 0.4& 0.8 %) ferrites sintered at 1150^0C for 6 hrs.

Table 4.3: Data of lattice parameter (a), X-ray density (ρ_x), bulk density (ρ_B), porosity (P%), molecular weight (M) of Bi_2O_3 (x = 0.2, 0.4, 0.6 & 0.8) of $Ni_{0.28}Cu_{0.10}Zn_{0.62}Fe_2O_4$+ x wt.% Bi_2O_3 ferrites sintered at 1150^0C for 6 hrs

Bi_2O_3 content(x%)	a (Å)	(ρ_x) (g/cm^3)	(ρ_B) (g/cm^3)	P%	M (g)
0.02	8.4120	5.33	4.07	23.63	239.019
0.04	8.4085	5.34	4.03	24.53	239.021
0.08	8.4035	5.35	4.01	25.04	239.025

76

4.3 SEM Analysis of Ni-Cu-Zn doped with V_2O_5 Ferrites

Microstructure significantly affects the magnetic and electrical properties of ferrites. Domain behavior and its relation to microstructure of magnetic materials and electrical properties are grain size necessarily to maintain a single domain can be obtained from the microstructure study of ferrite samples. Figure 4.8(a-d) shows the SEM microstructure of $Ni_{0.28}Cu_{0.10}Zn_{0.62}Fe_2O_4$ + x wt% V_2O_5 (x = 0.2, 0.4, 0.6 and 0.8) ferrites sintered at 1150^oC for 6 hours.

(a)

(b)

(c)

(d)

Figure 4. 8 (a – d):   SEM micrographs of the system $Ni_{0.28}Cu_{0.10}Zn_{0.62}Fe_2O_4$ + x wt% V_2O_5 (x = 0.2, 0.4, 0.6 and 0.8) sintered at 1150^0C for 6 hrs

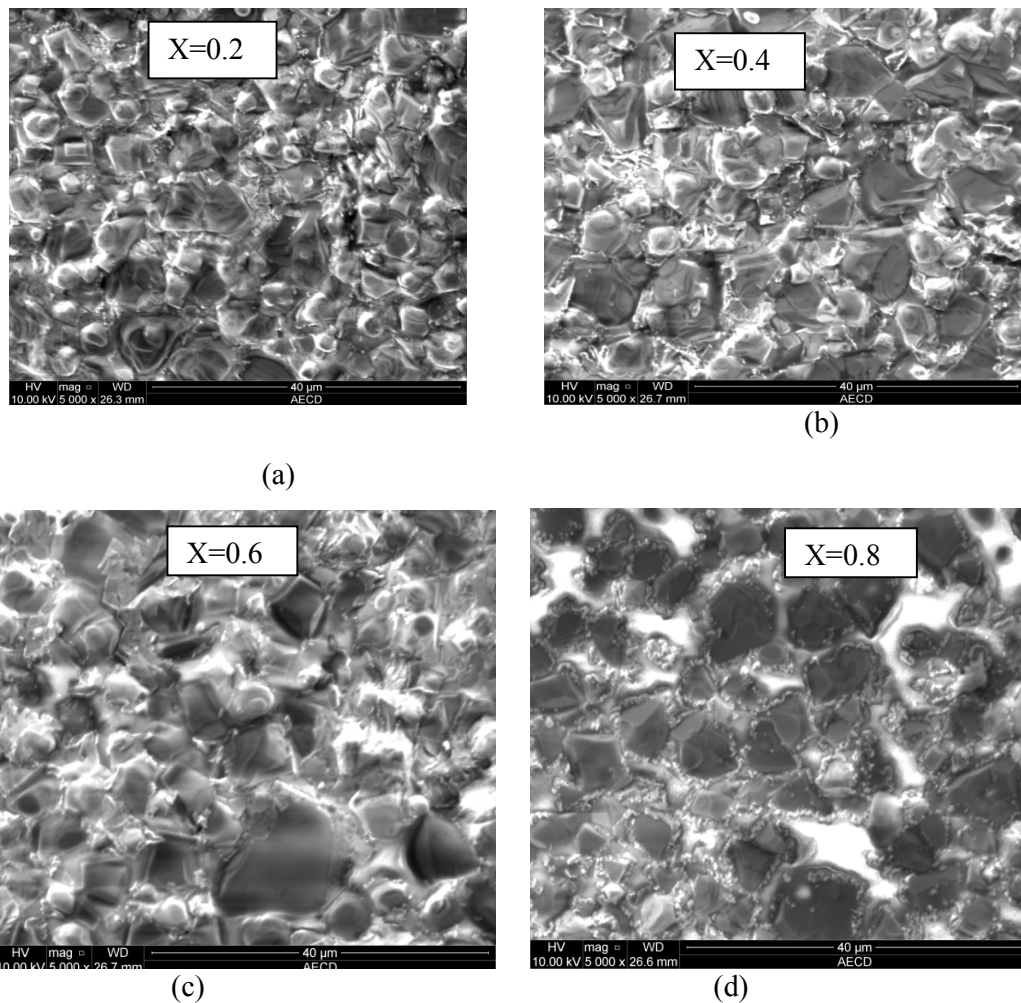A rapid grain growth of limited number of grains size much larger than those of the average grain population was observed. It might be due to lower melting point of V_2O_5 having liquid phase sintering effect. The liquid phase are act as driving force during sintering facilitating higher densification and grain growths. The behavior of grain growth reflects the composition between driving force for grain boundary movement and retarding force that drives the grain boundaries to grow over pores, thereby decreasing the pore volume and making the material dense. Abnormal grain growth occurs if this driving force is inhomogeneous. During our investigation it has also been noticed that the grain size of the samples increases with the increase of V_2O_5 additive content. The grains that grow consume their neighbors, grow larger and add more sides.

4.3.1 SEM Analysis of Ni-Cu-Zn doped with Bi_2O_3 Ferrites

Figure 4.9 (a –d) shows the SEM microstructure of $Ni_{0.28}Cu_{0.10}Zn_{0.62}Fe_2O_4$ + x wt% Bi_2O_3 (x = 0.2, 0.4, 0.6 and 0.8) ferrites sintered at 1150^oC for 6 hours. Influence of Bi_2O_3 doped microstructure of the Ni-Cu-Zn ferrites by the formation of liquid phase during sintering. It facilitates the grain growth by increasing the additives Bi_2O_3 content inter diffusion as a results of its segregation to the grain boundaries. For the samples with small grains, pores are formed at the grain boundaries whereas samples with large grains, the majority of pores are trapped inside the grains at large distance from the grain boundaries as well as some pores may migrate to the grain boundary, which might affect the permeability, density and resistivity of Ni-Cu-Zn ferrites. During the liquid phase sintering grain growth occurs via a dissolving/solution-precipitation process. Energetically, small grains are less stable than large grains due to their higher specific surface areas. As consequences small grains would be dissolved in the liquid-phase layers. Once the concentration of the dissolved phase reached a critical level, precipitation would take place. It seems that small grains have to "Swim" through a barrier (liquid phase layer) to combine with large grain. A gradual increase in grain size distribution is observed with increased doped Bi_2O_3 additive contents.

The crystal grain growth depends on grain boundaries migrating and larger crystal grains swallowing the small ones. During the growth the more different in size of the crystal grains, the more beneficial for longer crystal grains to swallow smaller up to 0.4 wt.% doped Bi_2O_3. After > 0.4 wt.% Bi_2O_3 additive contents

abnormal grain growth occurs if this driving force is inhomogeneous. Moreover, the strength of the driving force depends upon the diffusivity of individual grains, sintering temperature and porosity.

(a)   (b)

(c)   (d)
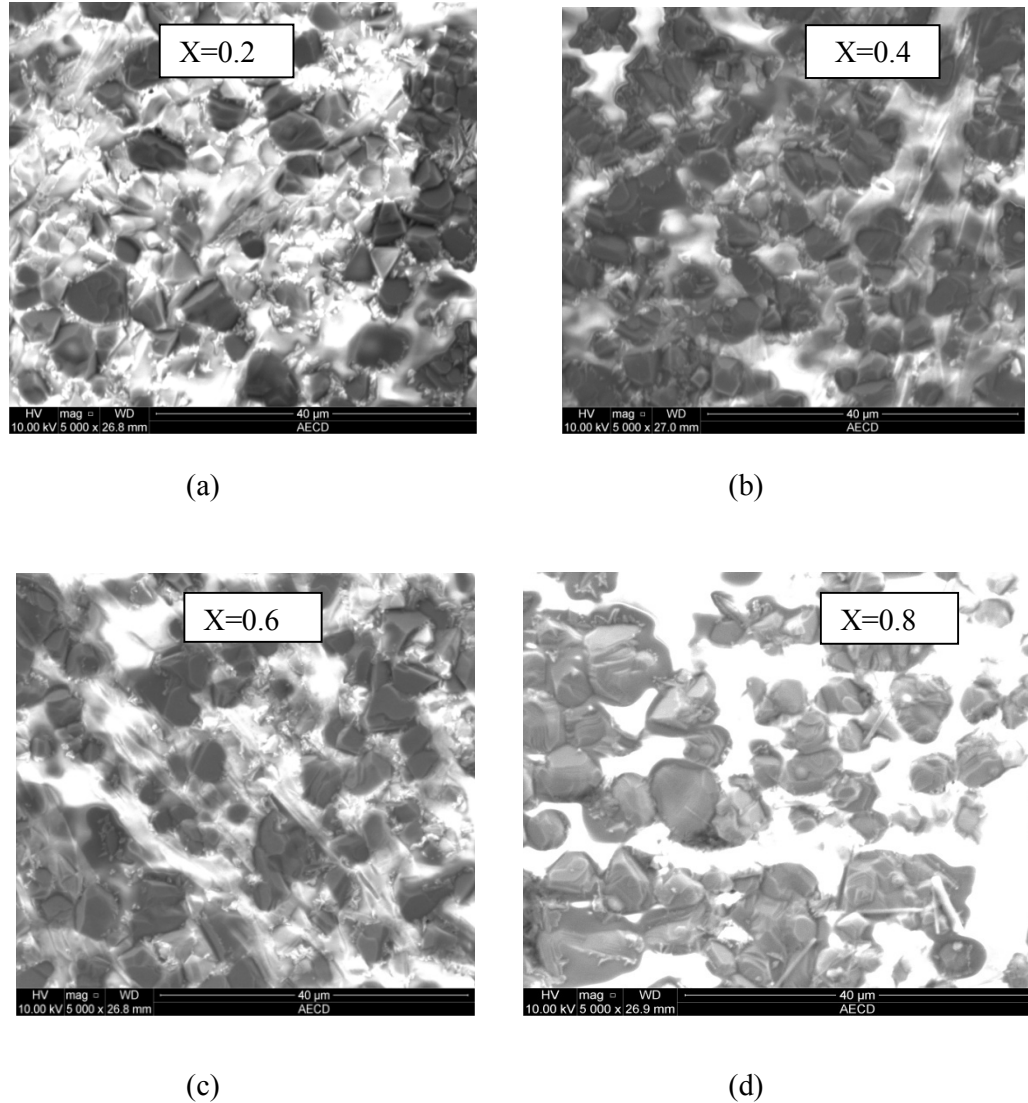
Figure 4. 9 (a – d): SEM micrographs of the system $Ni_{0.28}Cu_{0.10}Zn_{0.62}Fe_2O_4$ + x wt% Bi_2O_3 (x = 0.2, 0.4, 0.6 and 0.8) sintered at 1150^0C for 6 hrs

4.4 Magnetic Properties

4.4.1 Temperature Dependence of Initial Permeability in Ni-Cu-Zn doped with V_2O_5 Ferrite

Figure 4.10 (a – d) and figure 11(a – d) shows the temperature dependence of initial permeability $\mu^/$ for toroid shaped samples with composition $Ni_{0.28}Cu_{0.10}Zn_{0.62}Fe_2O_4$ + x wt% V_2O_5 (x = 0.2, 0.4, 0.6 and 0.8) sintered at

1150°C/6hr and 1200°C/6hr respectively, which is measured at a constant frequency (100 kHz) of an ac signal by using Impedance Analyzer. Since the initial permeability is directly related to the magnetization and to the ionic structure, then the thermal spectra of permeability can taken as a test of the formation and homogeneity of the ionic structure of the samples. It is observed that the initial permeability increases with the increase in additives V_2O_5 up to 0.6 after than decreases. This is because doped V_2O_5 in these compositions not only increase the magnetic moment and but also lower anisotropy [4.17].

(a)   (b)

(c)   (d)

Figure 4.10(a – d): Temperature dependence of permeability for $Ni_{0.28}Cu_{0.10}Zn_{0.62}$
        Fe_2O_4 + x wt%V_2O_5 (x = 0.2, 0.4, 0.6 and 0.8%) sintered at
        1150^0C for 6 hrs

(a)

(b)

(c)

(d)

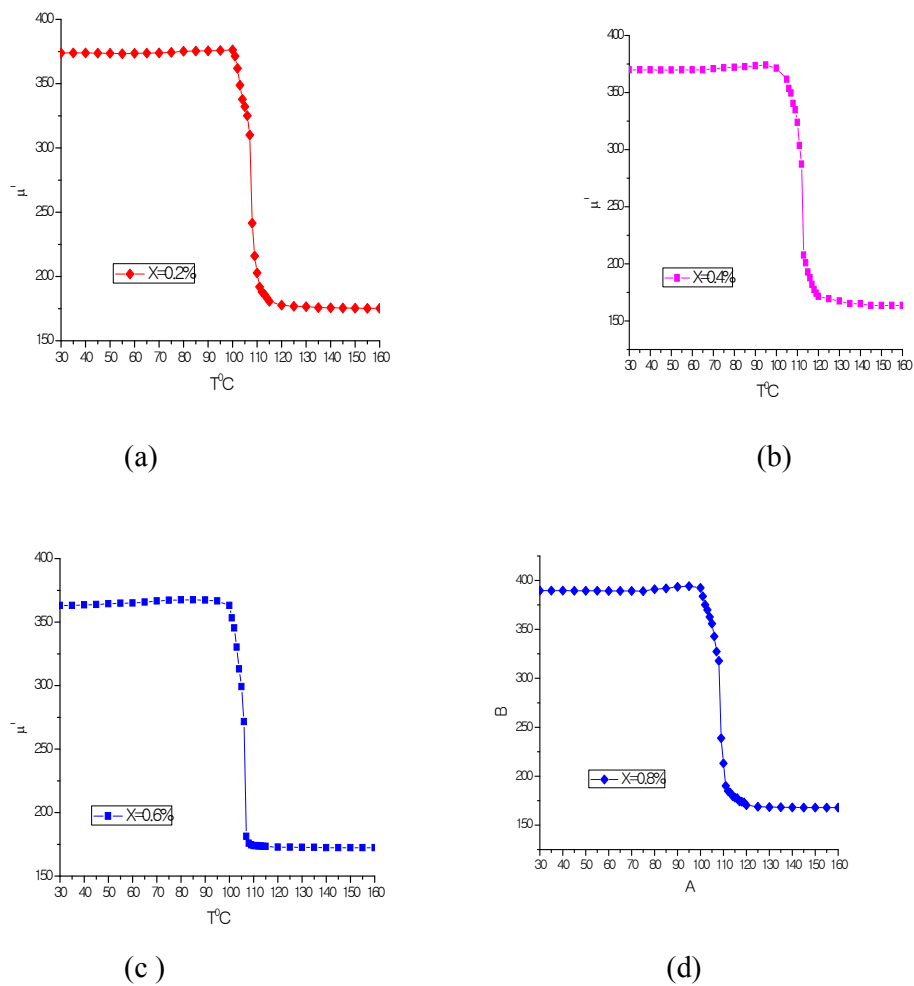Figure 4.11(a – d) :   Temperature dependence of permeability for $Ni_{o.28}Cu_{0.10}Zn_{0.62}$ Fe_2O_4 + x wt.%V_2O_5 (x = 0.2, 0.4, 0.6 and 0.8) sintered at 1200^0C for 6 hrs
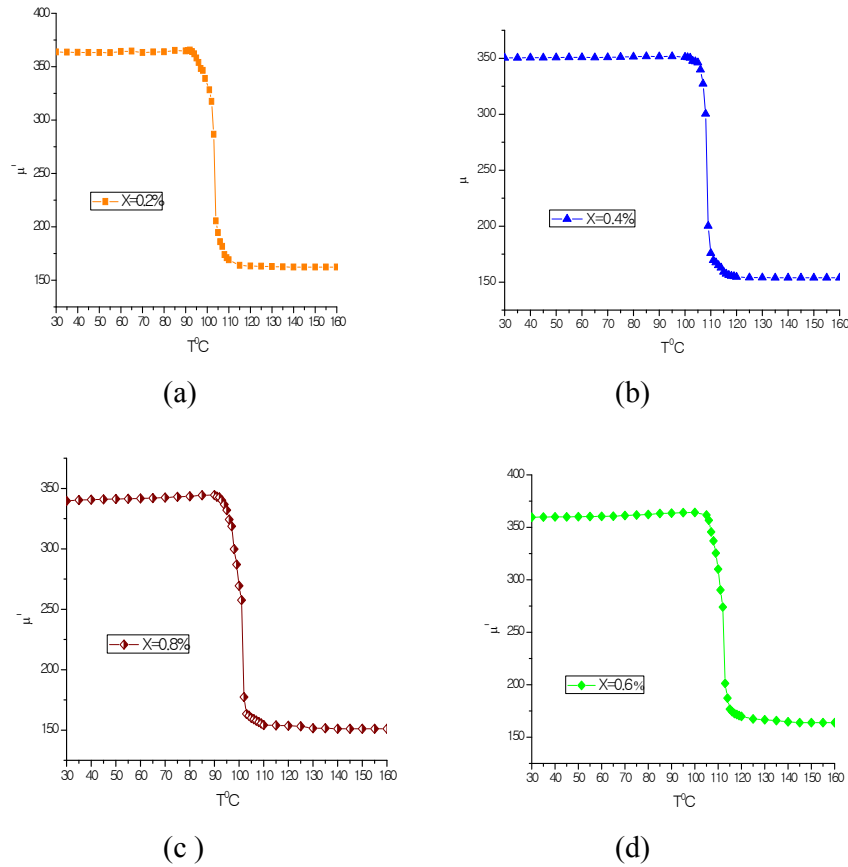
It is observed from figure 4.10 (a) to (d) that the permeability falls sharply when the magnetic state of the ferrite samples changes from ferromagnetic to paramagnetic state. The Curie temperature (T_c) $\mu^/$ attains its maximum value and then drops off sharply to minimum value at the Curie point can be used as a measure of the degree of compositional homogeneity [4.18], which also be confirmed by XRD that no impurity phases could be detected. The T_c of the samples are shown in Table 4.4. From Table 4.4 it is observed that T_c slowly and gradually increases with increasing additive V_2O_5 doped up to x = 0.6 after decrease. These initially increasing T_c due to strengthening of A – B exchange interaction due to increase number of Fe^{3+} ions at A site as well as decrease of lattice parameters of the studied samples. This increases linkage between the magnetic ions and exchange coupling that determined the magnitude of T_c.

The T_c temperature gives an idea of an amount of energy takes to break up the long range ordering in the doped additive V_2O_5 materials. According to the T_c data, it reveals that T_c data during sintering temperature are very close to each other in both cases small difference in the T_c in sintering temperature at constant holding time 6 hours may occur due to the reduced thermal disturbance taking place.

Table 4.4:   Data of Curie temperature (T_C) and Initial permeability at 100kHz of the samples $Ni_{0.28}Cu_{0.10}Zn_{0.62}Fe_2O_4$+ x wt.% V_2O_5 (x = 0.2, 0.4, 0.6 and 0.8%) sintered at 1150^oC and1200^oC for 6 hrs.

V_2O_5	T_S=1150°C		T_S=1200°C	
	T_C(^{o}C)	μ_i at constant 100 (kHz)	T_C (^{o}C)	μ_i at constant 100 (kHz)
0.2	108	226	104	228
0.4	113	278	109	278
0.6	116	222	113	222
0.8	109	194	102	198

4.4.1.1 Frequency Dependence Complex Initial Permeability doped with Samples V_2O_5

The complex permeability is given by $\mu = \mu^/ - i\mu^{//}$, $\mu^/$ is the real permeability (in phase) and $\mu^{//}$ the imaginary permeability (90° out of phase). From Figure 4.12(a) and Figure 4.12(b) show the variation on real part of complex permeability ($\mu^/$) spectra as a function of frequency range 1kHz to 120MHzs for $Ni_{0.28}Cu_{0.10}Zn_{0.62}$ Fe_2O_4+ x wt.% V_2O_5 (x = 0.2, 0.4, 0.6 and 0.8) sintered at 1150°C and 1200°C for 6 hours. For all the samples sintered at 1150°C and 1200°C, the values of initial permeability increase with increasing V_2O_5 doped up to 0.4 after decreasing. From these figures, it is seen that the real part of the permeability $\mu^/$ remained almost constant until the frequency is raised to a certain value 3 – 4MHz and then droops to a very low values at higher frequencies. The imaginary part of initial permeability $\mu^{//}$ gradually increased with frequency and attain a broad maximum at a certain frequency where the real part of permeability rapidly decreases shown in figure 4.13(a) and figure 4.13(b).

It is observed that $\mu^/$ is fairly constant with frequency up to certain low frequency (initial permeability μ_i are shown in table 4.4) rises slightly and then falls

rather rapidly to a very low value at a high frequency. As decreasing $\mu^{/}$ at higher frequencies is due to the fact that at higher frequencies impurities between grains and intragranular pores act as pining points and increasingly hinder the motion of spin and domain walls thereby decreasing their contribution to permeability [4.18]. The imaginary component $\mu^{//}$ first rises slowly and then suddenly rises with steep slope which passes through a maxima known as resonance frequency before falling to lower value.
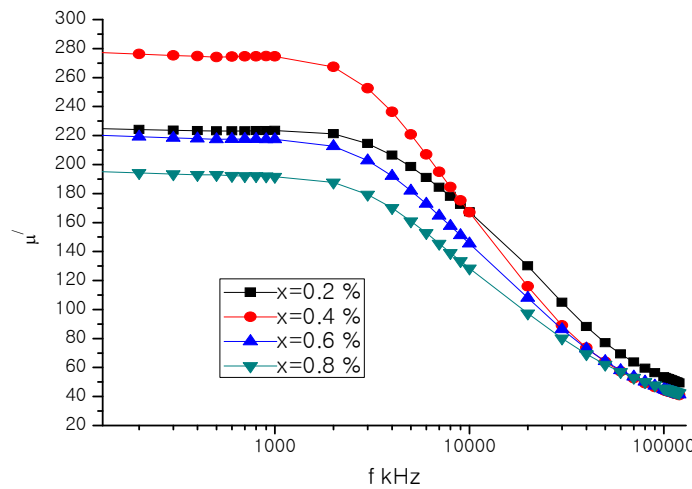
Figure 4.12(a): Frequency dependence of the real part of the permeability, $\mu^{/}$ of $Ni_{0.28}Cu_{0.10}Zn_{0.62}Fe_2O_4 + x$ wt%V_2O_5 (x = 0.2, 0.4, 0.6 and 0.8) sintered at 1150 ^{0}C for 6 hrs.
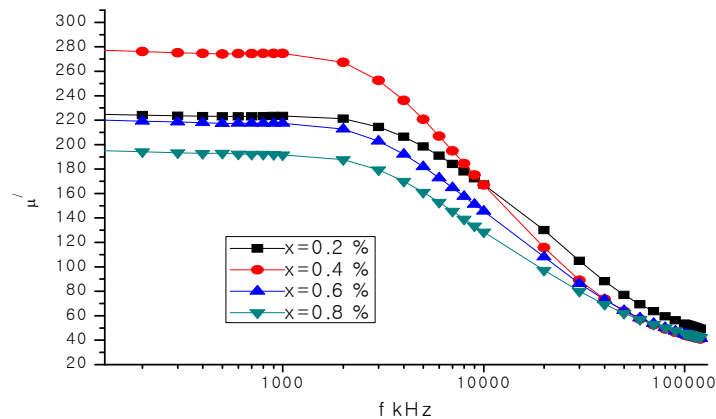
Figure 4.12(b): Frequency dependence of the real part of the permeability, $\mu^{/}$ of $Ni_{0.28}Cu_{0.10}Zn_{0.62}Fe_2O_4 + x$ wt%V_2O_5 (x = 0.2, 0.4, 0.6 and 0.8) sintered at 1200 ^{0}C for 6 hrs.

83
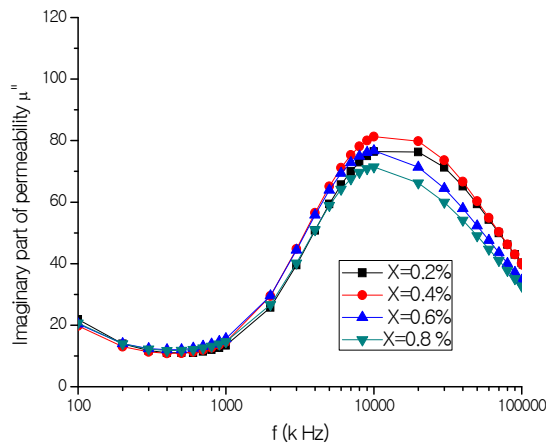
Figure 4.13(a): Frequency dependence complex permeability, $\mu^{//}$ of Ni$_{0.28}$Cu$_{0.10}$Zn$_{0.62}$Fe $_2$O$_4$ + x wt%V$_2$O$_5$ (x = 0.2, 0.4, 0.6 and 0.8) sintered at 1150^{0}C for 6 hrs.
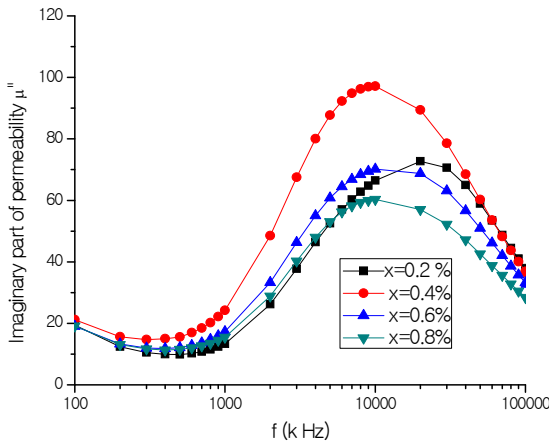
Figure 4.13(b): Frequency dependence complex permeability, $\mu^{//}$ of Ni$_{0.28}$Cu$_{0.10}$Zn$_{0.62}$Fe$_2$O$_4$ + x wt%V$_2$O$_5$ (x = 0.2, 0.4, 0.6 and 0.8) sintered at 1200^{0}C for 6 hrs.

Initial permeability (μ_i) shows flat profile from 1kHz to 4MHz indicating good low frequency stability for these sample. These dispersion occurs because the domain wall motion plays a relatively important role when the spin rotation reduces [4.19]. At low frequencies a ferrite induction is a low loss constant self-inductor where μ_i = 278 is highest at Ni-Cu-Zn ferrite doped 0.4wt.% V$_2$O$_5$ and this core

sample is mostly inductive, rejecting the electromagnetic interference (EMI) signal to the source. The constant value of permeability over a wide frequency range, which is named the zone of utility of ferrite, is desirable for various applications such as broad band transformation and wide band read writes head for video recording.

4.4.1.2 Frequency Dependence of Quality Factor doped with Samples V_2O_5

Figure 4.14(a) and figure 4.14(b) represents the frequency dependence of quality factor of $Ni_{0.28}Cu_{0.10}Zn_{0.62}Fe_2O_4$+ x wt.% V_2O_5 (x = 0.2, 0.4, 0.6 and 0.8) ferrites sintered temperature at 1150^oC and 1200^oC at 6 hours constant holding time. The quality factor, were calculated from the magnetic loss tangent measured on the coil wound torodial samples. The variation of the quality factor with frequency showed a similar trend for all the samples. Quality factor increases with increases of frequency showing peak and then decreases with further increases of frequency. It is seen that quality factor deteriorates beyond 10 - 120MHz i.e. the loss tangent is minimum up to 10 - 120MHz. It is found that the maximum and minimum quality factor at same both sintering temperature.

Figure 4.14(a): Frequency quality factor of $Ni_{0.28}Cu_{0.10}Zn_{0.62}Fe_2O_4$ + x wt%V_2O_5 (x = 0.2, 0.4, 0.6 and 0.8) sintered at 1150^0C for 6 hrs.
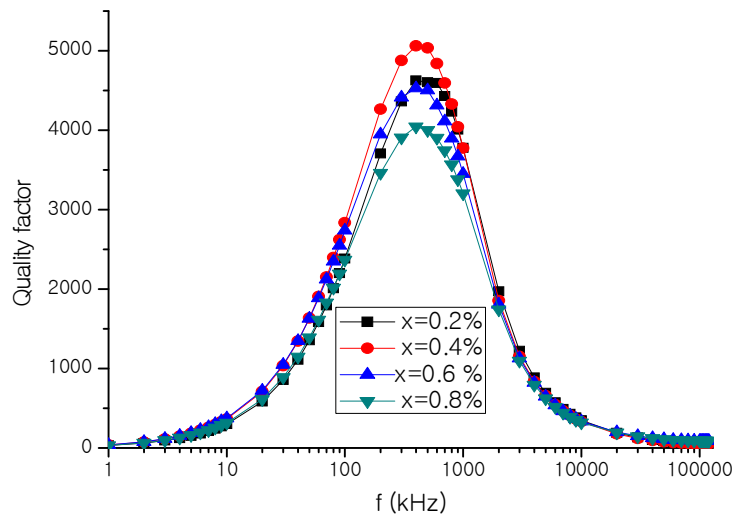
Figure 4.14(b): Frequency quality factor of $Ni_{0.28}Cu_{0.10}Zn_{0.62}Fe_2O_4$ + x wt%V_2O_5 (x = 0.2, 0.4, 0.6 and 0.8) sintered at 1200^0C for 6 hrs.
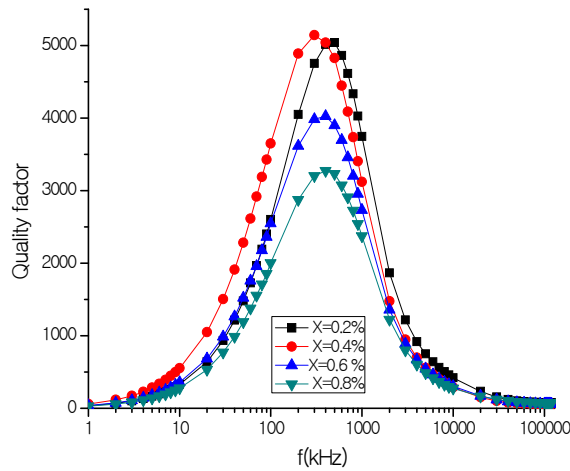
Low quality factor is required for high frequency magnetic applications. The loss is due to lag of domain wall motion with respect to the applied alternating magnetic field and is attributed to variations domain wall defects [4.19]. The peak corresponding to maxima in quality factor shifts to low frequency range as various doped V_2O_5 counted increases. Figure 4.14(a) and figure 4.14(b) shows the relative quality factor and relative loss factor of the same sample and both sintering temperature. Both of these two quantities are shown here for a better understanding for merit of the prepared materials for an inductor device application. For all curves, it is noticeable that the higher values of the relative quality factor in general lie within the range of 30 kHz to 1MHz frequencies. Thus the frequency range for application area might be chosen.

4.4.2 Temperature Dependence of Initial Permeability in Ni-Cu-Zn doped with Bi_2O_3 Ferrite

Figure 4.15(a - d) and figure 4.16(a - d) shows the temperature dependence of initial permeability for toroid shaped samples of $Ni_{0.28}Cu_{0.10}Zn_{0.62}Fe_2O_4$+ x wt.% Bi_2O_3 (x = 0.2, 0.4, 0.6 and 0.8) ferrites sintered temperature at 1150^oC and 1200^oC at 6 hours, which is measured at constant frequency 100kHz of an ac signal by using

Impedance Analyzer. It is observed that the initial permeability decreases with increases in doped Bi_2O_3 additives, while it falls abruptly close to the Curie point. From these are figure shows that permeability falls sharply when the magnetic state of the ferrite samples changes from ferromagnetic to paramagnetic. When the anisotropy constant reaches to zero just below the Curie temperature (T_c), $\mu^/$ its maximum value and drops off sharply to minimum value at Curie point.
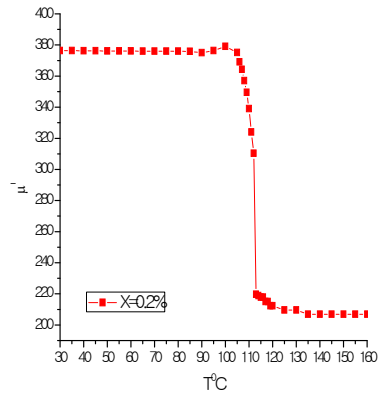
(a)
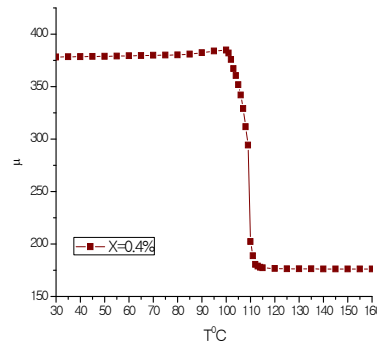
(b)
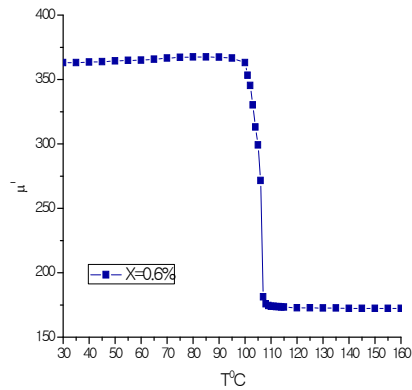
(c)
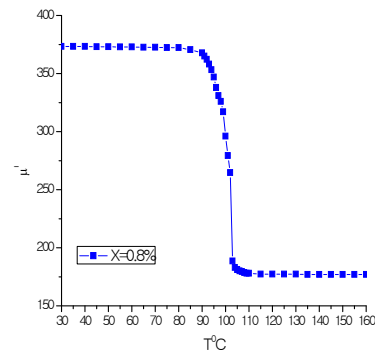
(d)

Figure 4.15(a – d):   Temperature   dependence   of   initial   permeability   for $Ni_{0.28}Cu_{0.10}Zn_{0.62}$ Fe_2O_4 + x wt%Bi_2O_3 (x = 0.2, 0.4, 0.6 and 0.8%) sintered at 1150^0C for 6 hrs
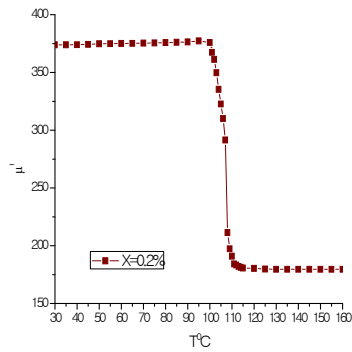
(a)
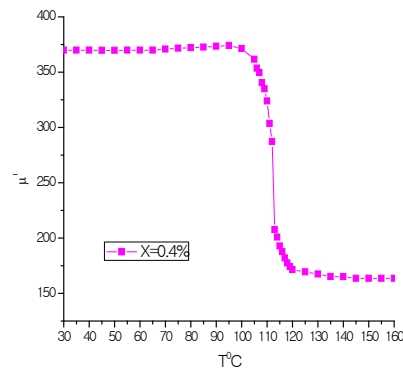
(b)
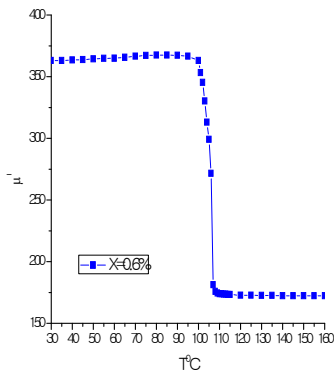
(c)
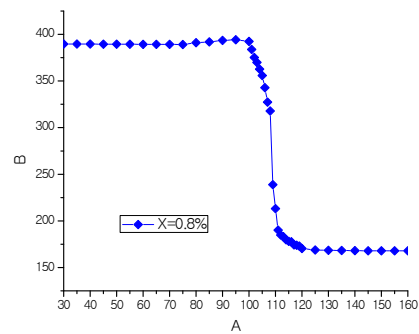
(d)

Figure 4.16(a – d):   Temperature   dependence   of   initial   permeability   for
                       $Ni_{0.28}Cu_{0.10}Zn_{0.62}$ Fe_2O_4 + x wt%Bi_2O_3 (x = 0.2, 0.4, 0.6 and
                       0.8%) sintered at 1200^0C for 6 hrs

        The T_c mainly depends upon the strength of A-B exchange interaction. As the
A-B exchange interactions increases with the density and the magnetic moment of
the magnetic ions. On other hand, greater amount of thermal energy is required to
offset the effects of exchange interaction. It is observed Table 4.5 that T_c decrease
continuously with increase of doped Bi_2O_3 additives in Ni-Cu-Zn ferrites. This
decreases the number of bonds or linkages between the magnetic ions that determine
the magnitude of the T_c.

Table 4.5:   Data of Curie temperature (T_C) and Initial permeability at 100kHz of the samples $Ni_{0.28}Cu_{0.10}Zn_{0.62}Fe_2O_4$+ x wt.% Bi_2O_3 (x = 0.2, 0.4, 0.6 and 0.8%) sintered at 1150^oC and1200^oC for 6 hrs.

Bi_2O_3	$T_S=1150^OC$		$T_S=1200^OC$	
	$T_C{}^oC$	μ_i at constant 100 (kHz)	$T_C{}^oC$	μ_i at constant 100(kHz)
0.2	113	280	109	239
0.4	110	238	107	238
0.6	107	236	101	237
0.8	102	222	97	236

4.4.2.1 Frequency Dependence Complex Initial Permeability doped with Samples Bi_2O_3

Figure 4.17(a) and figure 4.17(b) shows the variation real part of complex permeability ($\mu^/$) spectra in $Ni_{0.28}Cu_{0.10}Zn_{0.62} Fe_2O_4$+ x wt.% Bi_2O_3 (x = 0.2, 0.4, 0.6 and 0.8) sintered at 1150^oC and1200^oC for 6 hours. The permeability of all composition were stable up to 1MHz and the cot off frequencies of samples were above 120MHz, the maximum frequency limit of the instrument. The dispersion was to the much higher permeability of composition 0.2wt.% Bi_2O_3 compared to other. However, the permeability decreased with higher Bi_2O_3 (> x = 0.2) substitution. This might be due to the presence of higher amount $BiFeO_3$ phase. From the figure 4.17(a) and figure 4.17(b), the range of operating frequency in the x = 0.2 sintered at 1150^oC/6h sample wider than that in the other at 1200^oC/6h, which shows the compositional stability and quality of the ferrite samples.

Figure 5.18(a) and figure 5.18(b) shows the imaginary component $\mu^{//}$ first rises slowly and then increases quite abruptly making a peak at a certain frequency, where the real component $\mu^/$ is failing sharply. Moreover as the sintering temperature increases dispersion of $\mu^{//}$ - f spectra also shifts to the lower frequency range as result of increasing density and grain size, as prepared by Nakamura [4.20]. Generally application range of frequency is best suited below the frequency from where the $\mu^{//}$ starts rising sharply.
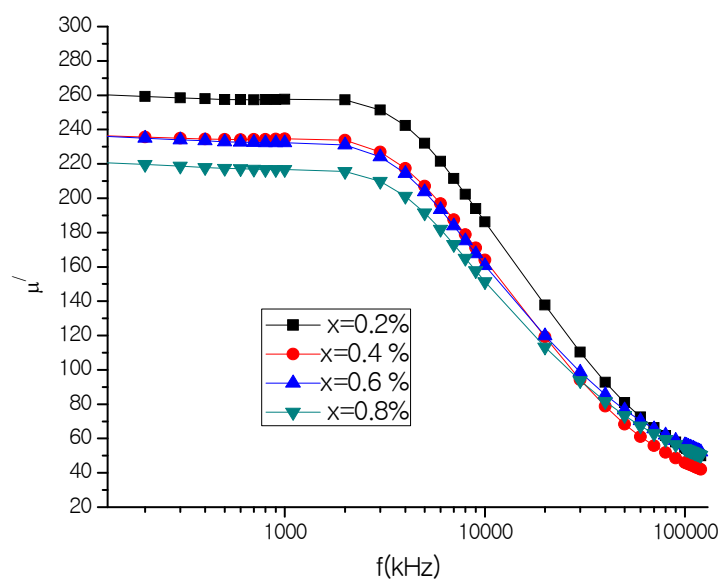
Figure 4.17(a): Frequency dependence of the real part of the permeability, $\mu^{/}$ of $Ni_{0.28}Cu_{0.10}Zn_{0.62}Fe_2O_4$ + x wt.% Bi_2O_3 (x = 0.2, 0.4, 0.6 and 0.8) sintered at $1150\,^0C$ for 6 hrs.
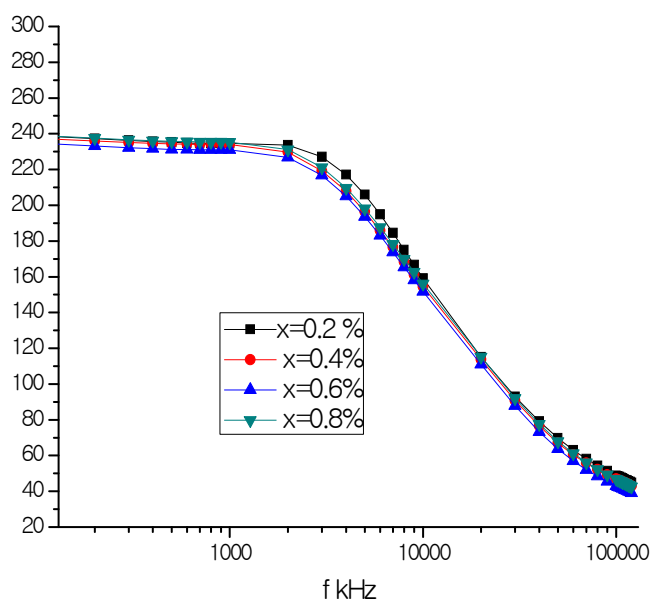
Figure 4.17(b): Frequency dependence of the real part of the permeability, $\mu^{/}$ of $Ni_{0.28}Cu_{0.10}Zn_{0.62}Fe_2O_4$ + x wt.% Bi_2O_3 (x = 0.2, 0.4, 0.6 and 0.8) sintered at 1200^0C for 6 hrs.
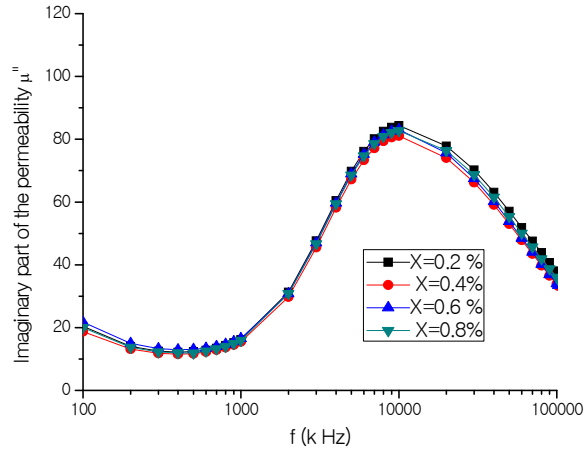
Figure 4.18(a): Frequency   dependence   complex   permeability, $\mu^{//}$ of
Ni$_{0.28}$Cu$_{0.10}$Zn$_{0.62}$Fe $_2$O$_4$ + x wt% Bi$_2$O$_3$ (x = 0.2, 0.4, 0.6 and 0.8) sintered at 1150^{0}C for 6 hrs.
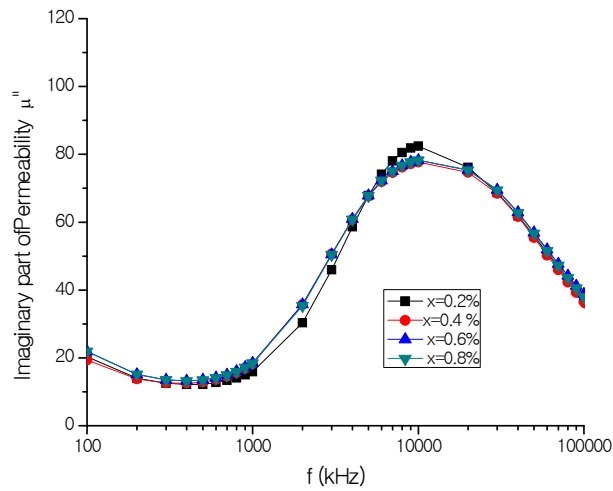
Figure 4.18(b): Frequency dependence of the real part of the permeability, $\mu^{/}$ of Ni$_{0.28}$Cu$_{0.10}$Zn$_{0.62}$Fe$_2$O$_4$ + x wt.% Bi$_2$O$_3$ (x = 0.2, 0.4, 0.6 and 0.8) sintered at 1200 ^{0}C for 6 hrs.

For a device application, the frequency range up to which the material can be used an inductor is always much less than the frequency at which $\mu^{//}$ attains its maximum value. This means that high frequency and high permeability cannot go together or in other words if we want to use the ferrite inductor for high frequency application, then the permeability of the device materials must be sacrificed. Again if a device needs very high $\mu^{/}$ then it must be used ferrite materials having lower resonance frequency i.e. the device is suitable for lower frequency range application. It is observed Table 4.5, the initial permeability (μ_i) and T_c decreases with increases of doped Bi_2O_3 and magnetic loss tangent ($\tan\delta$) which could be explained by a combination of low density small grain size and more lattice defects.

4.4.1.2 Frequency Dependence of Quality Factor doped with Samples Bi_2O_3

Frequency dependence of quality factor of the samples with doped Bi_2O_3 at sintered 1150^oC and 1200^oC for 6 hours were measured and figure 19(a) and figure 19(b) shows that the results. Factor signifies the merit of the material from the application point of view. The variation of the quality factor with frequency showed a similar trend all the samples. Quality factor increases with increases of frequency showing peak and then decreases with further increase of frequency. It is seen that quality factor deteriorates beyond 8 – 120MHz. A very high value of relative quality factor or extra ordering low value of loss tangent is found. The resonance frequency peaks are the results of the absorption of energy due to matching of the oscillation frequency of the magnetic dipoles and the applied frequency.

The resonance frequency was determined from the maximum of imaginary part of permeability of these ferrites. The highest value of quality factor is found for the samples doped 0.4wt.% Bi_2O_3 which indicates the highest value of quality factor. For all curves, it is noticeable that the higher values of the relative quality factor in general lie within the range of 20 kHz to 2MHz frequencies. Thus the frequency range for application area is chosen.
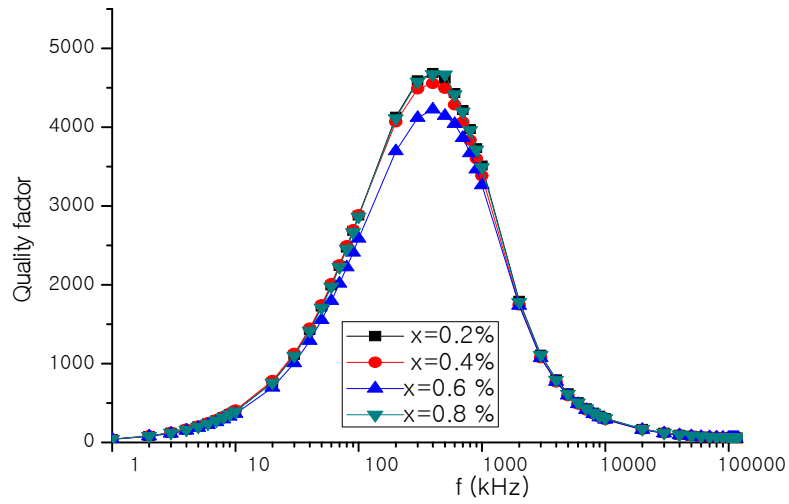
Figure 4.19(a): Frequency quality factor of $Ni_{0.28}Cu_{0.10}Zn_{0.62}Fe_2O_4$ + x wt% Bi_2O_3 (x = 0.2, 0.4, 0.6 and 0.8) sintered at 1150^0C for 6 hrs.
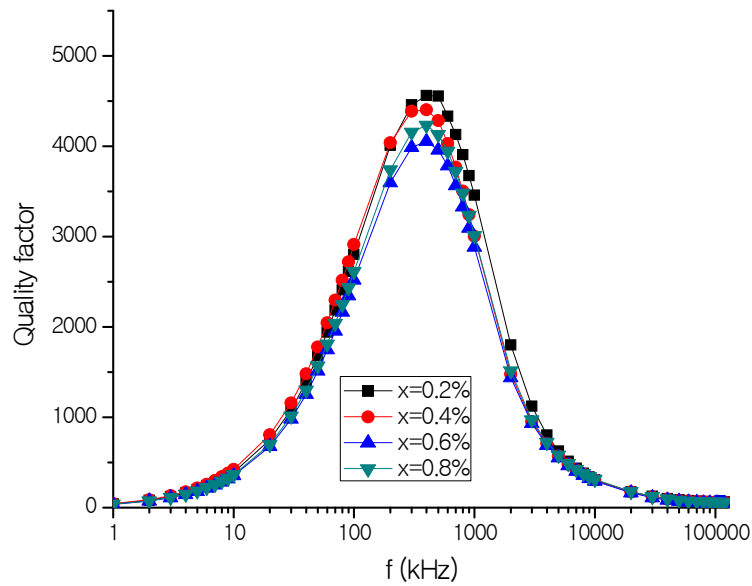
Figure 4.19(b): Frequency quality factor of $Ni_{0.28}Cu_{0.10}Zn_{0.62}Fe_2O_4$ + x wt% Bi_2O_3 (x = 0.2, 0.4, 0.6 and 0.8) sintered at 1200^0C for 6 hrs.

4.5   Field Dependence of Magnetization of Ni-Cu-Zn doped with V_2O_5 Ferrites

The magnetization as a function of applied magnetic field up to 10 kOe measured with vibrating sample magnetometer (VSM) at room temperature $Ni_{0.28}Cu_{0.10}Zn_{0.62}Fe_2O_4$ + x wt% V_2O_5 (x = 0.2, 0.4, 0.6 and 0.8) sintered at 1150^0C and 1200^oC for 6 hours has been measured and are presented in figure 4.20(a) and figure 4.20(b). It is observed that magnetization increases sharply at very low field (H < 1 kOe) which corresponds to magnetic domain reorientation due to domain wall displacement and there after increase slowly up to saturation due to spin rotation.

Table 4.6:   Saturation magnetization of $Ni_{0.28}Cu_{0.10}Zn_{0.62}Fe_2O_4$ + x wt.% V_2O_5 sintered at 1150^0C & 1200^oC for 6 hrs.

X Content V_2O_5	$T_S=1150^oC$ M(emu/g)	$T_S=1200^oC$ M(emu/g)
0.2	41.68	*42.86*
0.4	42.50	39.28
0.6	46.03	44.03
0.8	40.89	44.43

It is observed from figure 4.20(a) , figure 4.20(b) and Table 4.6 that saturation magnetization (M_s) increases up to x = 0.6 and then it decreases with x content at sintered 1150^oC but not follow the order sintered at 1200^oC.

All the figure follows the magnetization process of magnetization toward the saturation value is connected with the magnetic anisotropy effect. Actual saturation could not be attained even with magnetic field as high as 10kOe. The insignificant decreases of M_s may be experimental uncertainty. The magnetization process is connected with soft magnetic of behavior of magnetic material. Hence the present systems V_2O_5 doped Ni-Cu-Zn ferrites, frustration and randomness increases or decreases in M_s and shows significant departure from Nell's collinear model.
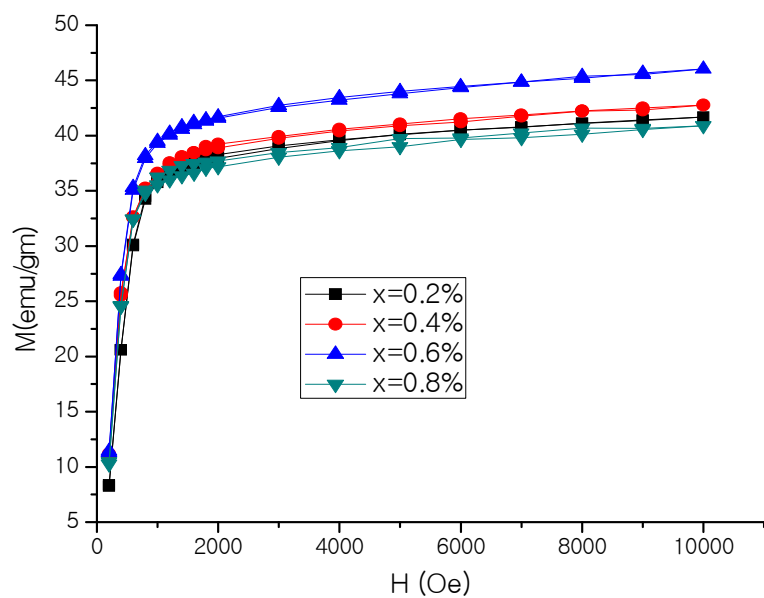
Figure 4.20(a): Field dependence of magnetization of $Ni_{0.28}Cu_{0.10}Zn_{0.62}Fe_2O_4 + x$ wt.% V_2O_5 (x = 0.2, 0.4, 0.6 and 0.8%) sintered at 1150^0C for 6 hrs
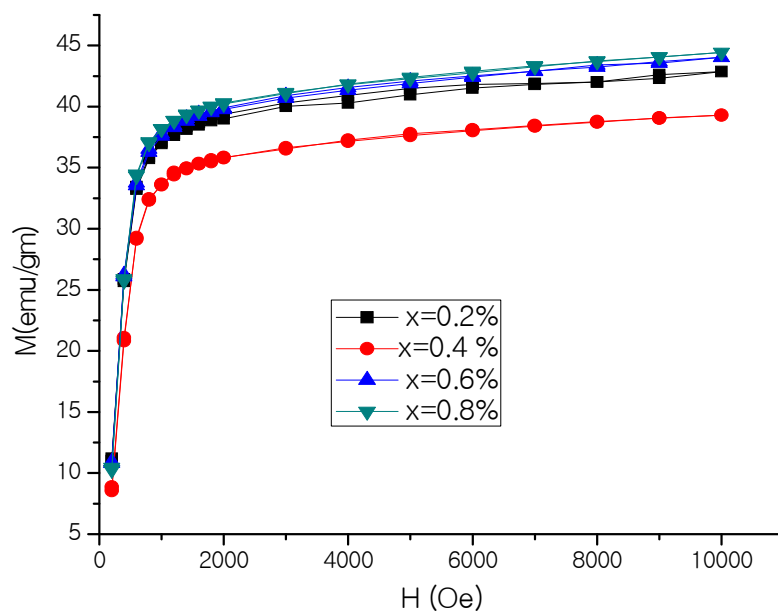
Figure 4.20(b): Field dependence of magnetization of $Ni_{0.28}Cu_{0.10}Zn_{0.62}Fe_2O_4 + x$ wt.% V_2O_5 (x = 0.2, 0.4, 0.6 and 0.8%) sintered at 1200^0C for 6 hrs.

4.5.1 Field Dependence of Magnetization of Ni-Cu-Zn doped with Bi$_2$O$_3$ Ferrites

Figure 4.21(a) and figure 4.21(b) shows the variation of M$_s$ of the Ni$_{0.28}$Cu$_{0.10}$Zn$_{0.62}$Fe$_2$O$_4$ + x wt% Bi$_2$O$_3$ (x = 0.2, 0.4, 0.6 and 0.8) ferrites as a function of applied magnetic field up to 10kOe. It is from the figures that virgin M$_s$ is increases with increasing x content follows at sintered temperature 1200°C but not follow 1150°C as shown in Table 4.7.

Table 4.7:   Saturation magnetization of Ni$_{0.28}$Cu$_{0.10}$Zn$_{0.62}$Fe$_2$O$_4$ + x wt.% Bi$_2$O$_3$ sintered at 1150^{0}C & 1200°C for 6 hrs.

X Content Bi$_2$O$_3$	T$_S$=1150°C M(emu/g)	T$_S$=1200°C M(emu/g)
0.2	44.86	42.86
0.4	43.77	44.50
0.6	43.13	45.28
0.8	46.28	46.84
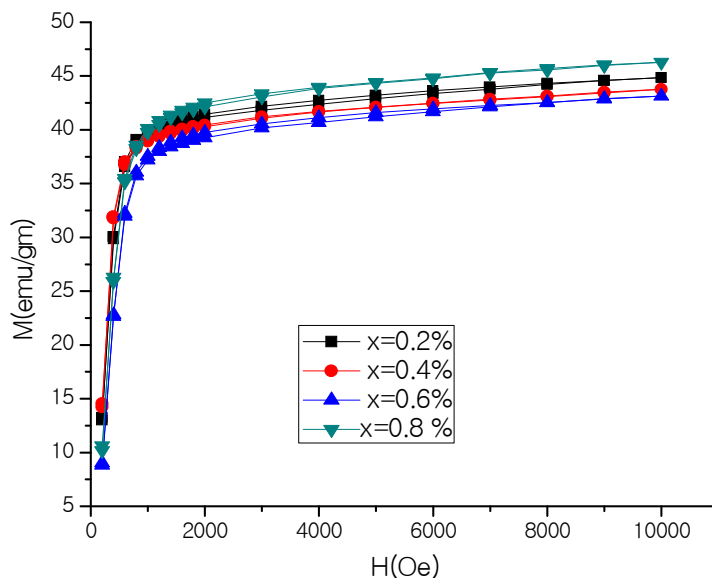
Figure 4.21(a):   Field dependence of magnetization of Ni$_{0.28}$Cu$_{0.10}$Zn$_{0.62}$Fe$_2$O$_4$ + x wt.% Bi$_2$O$_3$ (x = 0.2, 0.4, 0.6 and 0.8%) sintered at 1150^{0}C for 6 hrs
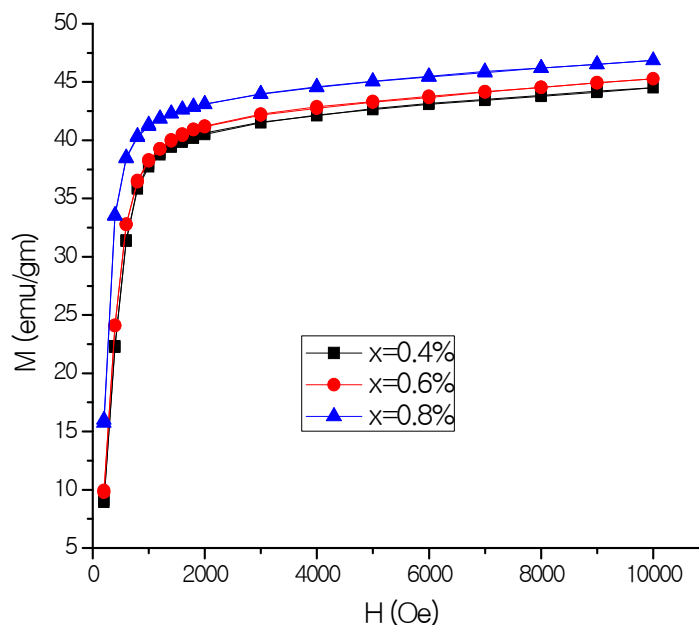
Figure 4.21(b): Field dependence of magnetization of $Ni_{0.28}Cu_{0.10}Zn_{0.62}Fe_2O_4$ + x wt.% Bi_2O_3 (x = 0.2, 0.6 and 0.8%) sintered at 1200^0C for 6 hrs

The observed variation in M_s can be explained on the basis of cation distribution and the exchange interactions between A and B-sites respectively. At sintered temperature 1150^oC, the initial decrease in M_s with increased additive Bi_2O_3 is due to the increase of resultant sublattice magnetic moment which can be explained on the basis of Neel's two sub lattice model. The magnetization of each composition depends on the distribution of Fe^{3+} ions between the two sublattices A and B, where Zn^{2+}, Cu^{2+} and Bi^{2+} ions are nonmagnetic. In perfect ferrites, the A-A, B-B and A-B nearest neighbor exchange coupling are normally antiferromagnetic and the A-B exchange coupling is usually heavily predominant. The slow decrease of M_s from the two sub lattice magnetization unlike ferromagnetic.

4.6   Electrical Transport Property

4.6.1 Temperature Dependence of DC Electrical Resistivity of Ni-Cu-Zn Ferrites doped with V_2O_5 and Bi_2O_3

Figure 22(a), (b) and figure 23(a), (b) are the shows the temperature dependence of DC resistivity for different composition. DC resistivity is an important parameter and depends upon several factors such as sintering temperatures, time and atmosphere including the grain structure. It is well known that resistivity of ferrites depend on their chemical composition [4.21] and heat treatment. Ferrite is a semiconductor, which means that its electrical resistivity decreases with temperature.

Its electrical resistivity is at least a million times that of a metal. These are very large resistivity means in turn that an applied alternating magnetic field will not induce eddy currents in a ferrite. This property makes ferrite the best magnetic materials for high frequency application where power losses from eddy currents must be minimized.

Figure 22(a): DC resistivity as a function of temperature of
Ni$_{0.28}$Cu$_{0.10}$Zn$_{0.62}$Fe$_2$O$_4$ + x wt.% V$_2$O$_5$ (x = 0.2, 0.4, 0.6 and 0.8) sintered at 1150°C for 6 hrs.

Figure 22(b): DC resistivity as a function of temperature of
Ni$_{0.28}$Cu$_{0.10}$Zn$_{0.62}$Fe$_2$O$_4$ + x wt.% V$_2$O$_5$ (x = 0.2, 0.4, 0.6 and
0.8) sintered at 1200° for 6 hrs.
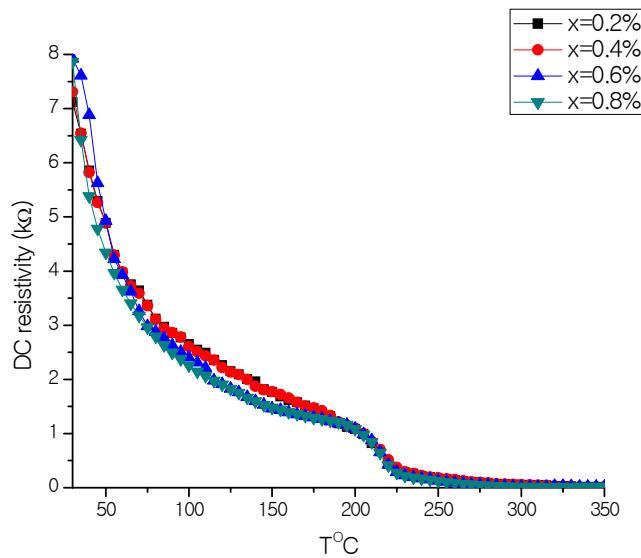
Figure 23(a): DC resistivity as a function of temperature of
Ni$_{0.28}$Cu$_{0.10}$Zn$_{0.62}$Fe$_2$O$_4$ + x wt.% Bi$_2$O$_3$ (x = 0.2, 0.4, 0.6 and 0.8)
sintered at 1150°C for 6 hrs.
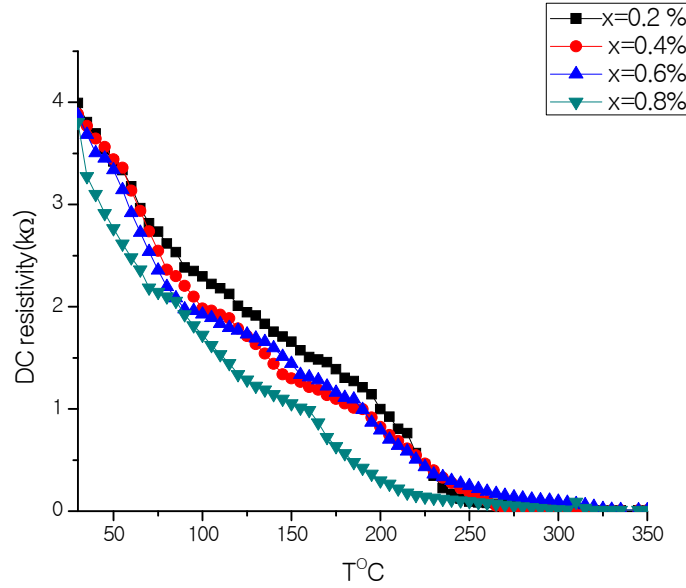
Figure 23(b): DC resistivity as a function of temperature of
Ni$_{0.28}$Cu$_{0.10}$Zn$_{0.62}$Fe$_2$O$_4$ + x wt.% Bi$_2$O$_3$ (x = 0.2, 0.4, 0.6 and 0.8)
sintered at 1200°C for 6 hrs.

4.6.2 Frequency Dependence of Dielectric Constant of Ni-Cu-Zn Ferrites doped with V$_2$O$_5$ and Bi$_2$O$_3$

Figure 24(a), (b) and figure 25(a), (b) are the variation of dielectric constant, $\epsilon^{/}$ with frequency for different composition of Ni$_{0.28}$Cu$_{0.10}$Zn$_{0.62}$Fe$_2$O$_4$+ x wt.% V$_2$O$_5$ and Ni$_{0.28}$Cu$_{0.10}$Zn$_{0.62}$Fe$_2$O$_4$ + x wt.% Bi$_2$O$_3$ ferrites sintered at 1150°C/6hrs and 1200°C/6hrs from 100Hz to 120MHz at room temperature respectively. It can be seen from all the figures that the dielectric constant is found to decrease continuously with increasing frequency for all the specimens exhibiting a normal dielectric behavior of ferrites. The dielectric dispersion is rapid at lower frequency region and it remains almost independent at high frequency region. The incorporation of V$_2$O$_5$ and Bi$_2$O$_3$ into Ni-Cu-Zn ferrites has no pronounced effect on the dielectric constant in high frequency, but significantly decreases the dielectric constant in the low frequency range.

The dielectric behavior of ferrites may be explained on the basis of the mechanism of the dielectric polarization process and is similar to that of the conduction process. The electronic exchange $Fe^{2+} \leftrightarrow Fe^{3+}$ gives the local displacement of the electrons in the direction of applied electronic field, which

100

induces the polarization in ferrites [4.22]. All the samples have high value of $\epsilon^{/}$ in the order of 2×10^5 at V_2O_5 and 4×10^5 at Bi_2O_3 as well as same x = 0.4wt.% content at low frequencies after all the samples are decreases.

All the figures shows the samples x = 0.4 and 0.6 showed the maximum dispersion while that the other samples are shown in dopes in V_2O_5 and Bi_2O_3. The presence of Fe^{2+} ions in excess amount favors the polarization effects. Thus, the more dispersion observed in the samples are with x = 0.4 and x = 0.6 can be attributed to the presence of Fe^{2+} ions in excess amount which could be formed at elevated sintering temperature. Similarly the weak dependence of dielectric constant on frequency can be due to the lack of Fe^{2+}/Fe^{3+} ions concentration. All the samples have high values of $10^5 - 10^6$ at low frequencies.
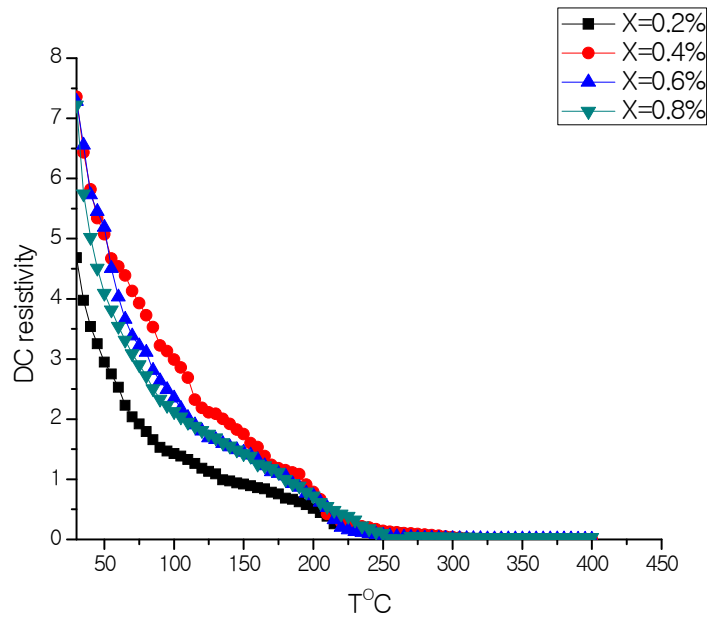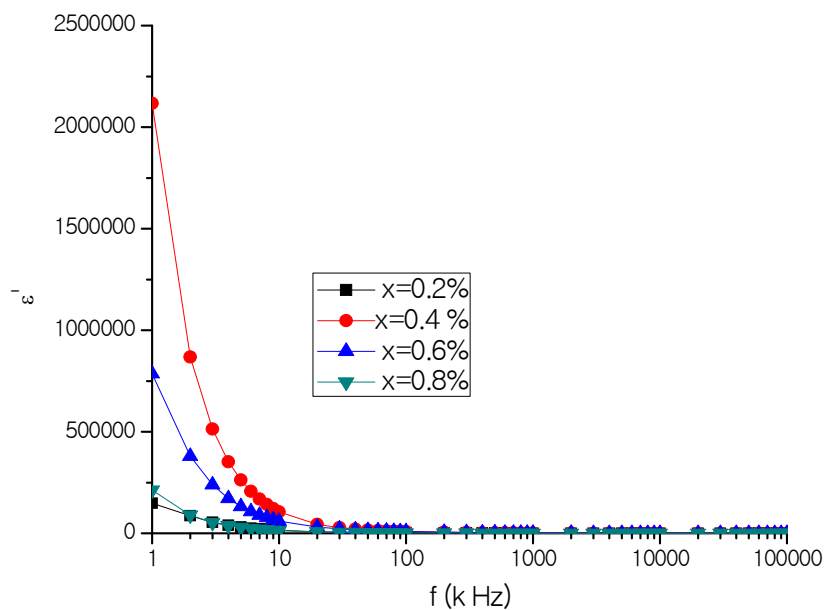

Figure 24(a):   Dielectric constant $\left(\epsilon^{/}\right)$ as a function of temperature of

$Ni_{0.28}Cu_{0.10}Zn_{0.62}Fe_2O_4$+ x wt.% V_2O_5 (x = 0.2, 0.4, 0.6 and 0.8)

sintered at 1150^oC for 6 hrs.

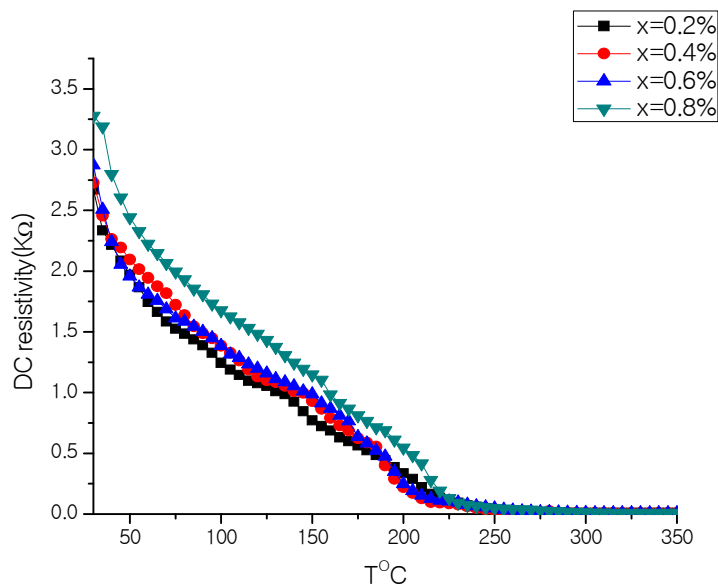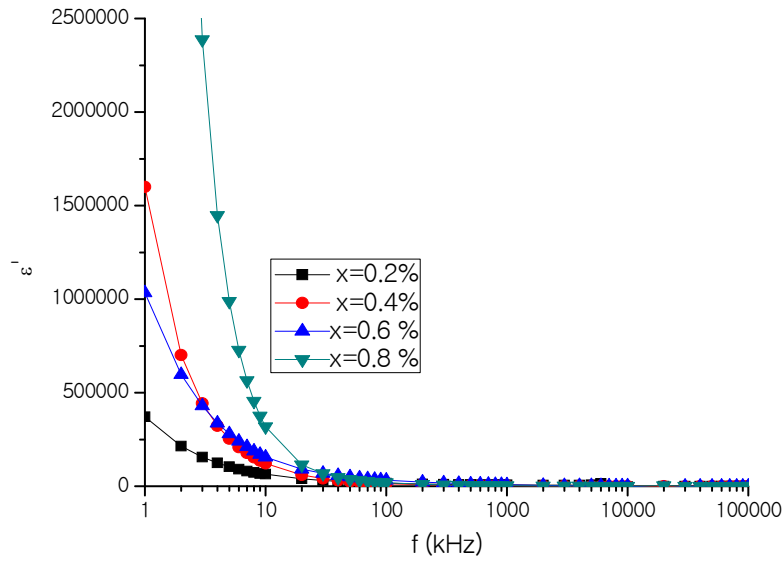Figure 24(b): Dielectric constant $\left(\in^{/}\right)$ as a function of temperature of $Ni_{0.28}Cu_{0.10}Zn_{0.62}Fe_2O_4+$ x wt.% V_2O_5 (x = 0.2, 0.4, 0.6 and 0.8) sintered at 1200° for 6 hrs.
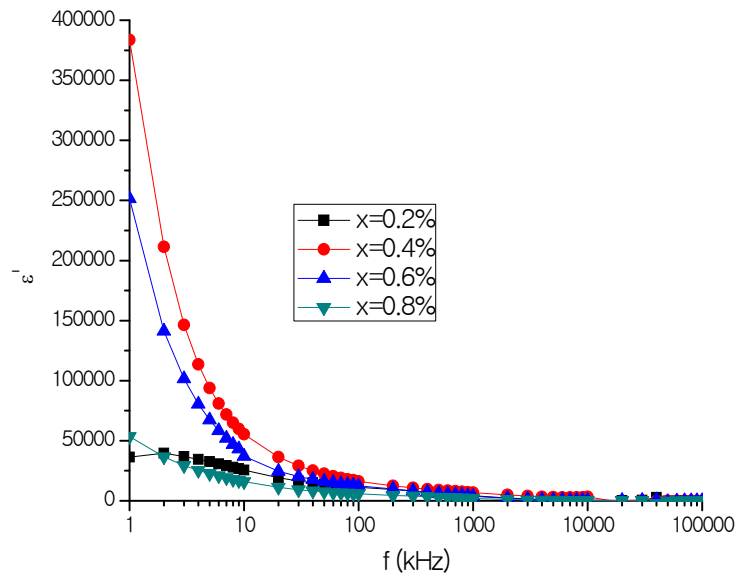
Figure 25(a): Dielectric constant $\left(\in^{/}\right)$ as a function of temperature of $Ni_{0.28}Cu_{0.10}Zn_{0.62}Fe_2O_4+$ x wt.% Bi_2O_3 (x = 0.2, 0.4, 0.6 and 0.8) sintered at 1150^oC for 6 hrs.
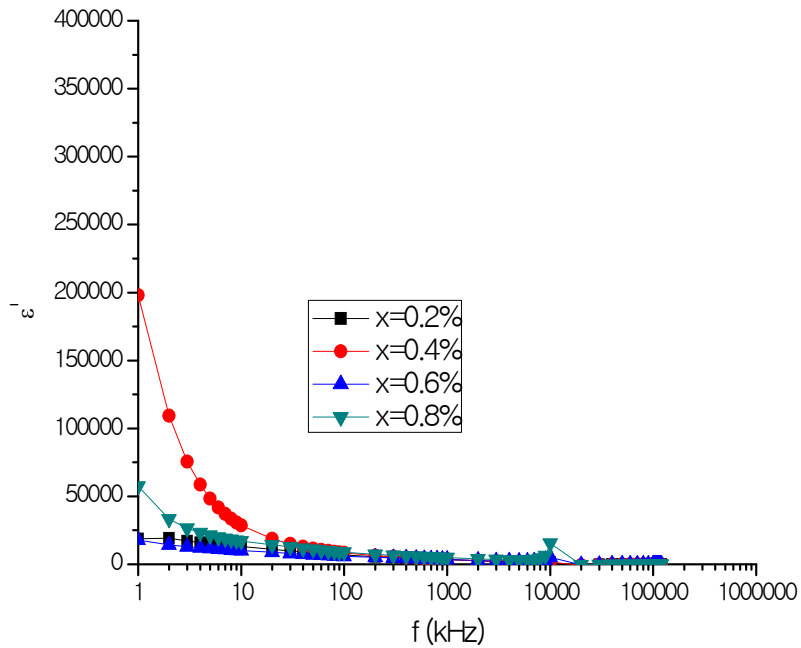
Figure 25(b): Dielectric constant $\left(\in'\right)$ as a function of temperature of
$Ni_{0.28}Cu_{0.10}Zn_{0.62}Fe_2O_4$ + x wt.% Bi_2O_3 (x = 0.2, 0.4, 0.6 and 0.8)
sintered at 1200° for 6 hrs.

The dielectric structure was supposed to be composed of the fairly well conducting ferrite grains. These are separated by the second thin layer of grain boundaries which are poorly conducting substances. These grain boundaries could be formed during the sintering process due to the superficial reduction or oxidation of crystallites in the porous materials as a result of their direct contact with the firing atmosphere [4.23]. The grain boundaries of lower conductivity and higher dielectric constant are found to be more effective at lower frequency while the ferrite grains of higher conductivity and lower dielectric constant are effective at high frequencies.

CONCLUSIONS

5.1 Conclusions

The present work has been focused on the synthesis study of structural electrical transport and electromagnetic properties of $Ni_{0.28}Cu_{0.10}Zn_{0.62}Fe_2O_4$ + x wt.% the concentration sintering additives were varied 0.2wt.% to 0.8wt.% for V_2O_5 and Bi_2O_3. The samples are prepared standard double sintering ceramic method, sintered at 1150^oC and 1200^oC for holding time 6 hours. The effects of dopiness as V_2O_5 and Bi_2O_3 as sintering aids on the densification kinetics and magnetic properties of the ferrites were also investigated. The XRD pattern confirmed the single phase cubic spinel structure of both additives.

Study the following findings and conclusions are can be summarized:

(i)   The linear decrease of lattice constant with additives V_2O_5 or Bi_2O_3 doped with Ni-Cu-Zn ferrite indicate that the present systems obeys Vegard's law.

(ii)   The bulk density is lower than the X-ray density, which is inevitable during ceramic processing and formed developing during the both samples are preparation or the sintering process.

(iii)   SEM micrographs indicate the rapid grain growth of limited number of grain size much larger than those of the average grain population that the grain size of the samples increases with increase of V_2O_5 additive content. The grains that grow consume their neighbors, grow larger and add more sides.

(iv)   Grain growths by increasing the additives Bi_2O_3 content inter diffusion as results of its segregation to the grain boundaries. During the growth the more different in size of the crystal grains, the more beneficial for longer crystal grains to swallow smaller up to 0.4wt.% Bi_2O_3. After > 0.4wt.% Bi_2O_3 additives contents abnormal grain growth occurs, if driving force is inhomogeneous.

(v)   Curie temperature (T_c) slightly increases with increasing V_2O_5 doped Ni-Cu-Zn ferrites up to x = 0.6 after decrease. This increases linkages between the magnetic ions and exchange coupling that determine the

magnitude of T_c and during sintering temperature are very close to each other in both cases small difference in the T_c.

(vi) T_c decreases continuously with the increase of Bi_2O_3 additives in Ni-Cu-Zn ferrites. This happened due to decreasing linkages between the magnetic ions and exchange coupling that determines the magnitude of the T_c and similar nature both sintering temperature as well as reduce value to effect are greater amount of thermal energy is required to offset of exchange interaction.

(vii)   The initial permeability (μ_i) increases with doped V_2O_5 and both sintering temperature attaining a same value of $\mu_i = 278$ for the sample $x = 0.4$ after decreasing. μ_i shows flat profile from 1 kHz to 4 MHz indicating good low frequency stability and this core sample is mostly inductive, rejecting the electromagnetic interference signal to source. This seen that the higher values of the quality factor lie between the range of 30 kHz to 1 MHz frequencies.

(viii)   The μ_i decreases with higher content doped Bi_2O_3 in Ni-Cu-Zn ferrites but the highest value of quality factor is found for the samples doped 0.4wt.% Bi_2O_3, which quality factor within the range 20 kHz to 2 MHz frequencies. Thus the frequency range for application area is chosen.

(ix)   Magnetization increases sharply at very low field (H < 1 kOe) which corresponds to magnetic domain reorientation due to domain wall displacement and there after increase slowly up to saturation due to spin rotation for both additive V_2O_5 or Bi_2O_3 doped in Ni-Cu-Zn ferrites. The magnetization process is connected with soft magnetic behavior of magnetic material. Saturation magnetization (M_s) increases up to $x = 0.6$ and after than, it decreases in V_2O_5 doped samples but M_s decreases up to $x = 0.6$ and after than it increases for Bi_2O_3 doped at sintering temperature 1150^oC/6hrs. The slow decrease or increase of M_s from two sublattices unlike ferromagnetic.

(x)   The DC electrical resistivity is found to decrease with temperature for all the samples which means these ferrites are semiconductor.

(xi)   Dielectric constant decreases with increasing frequency exhibiting normally dielectric behavior of ferrites like all the samples. All the figures shows the sample $x = 0.4$ and $x = 0.6$ showed the maximum dispersion

while that the other samples are shown in dopes V_2O_5 and Bi_2O_3 with Ni-Cu-Zn ferrites. The increases in frequency enhance the hopping frequency of charge carriers, resulting in an increase in the conduction process, thereby decreasing the dielectric constant. Dielectric structure to be composed of the fairly well conducting ferrite grain.

Finally analysis of the experimental results of $Ni_{0.28}Cu_{0.10}Zn_{0.62}Fe_2O_4 + x$ wt.% V_2O_5 or Bi_2O_3 series is appeared that the sample with x = 0.4 shows the properties sintered at both temperatures having constant permeability, low magnetic loss and maximum dielectric dispersion with visible grain size.

5.2   Scope for Future Work

With the development and advancement of ferrites a tremendous surge in research on miniaturization and high efficiency electronic devices is one rise soft ferrite materials are extensively used in inductors which form a basic requirement in high technology areas. Most effective additives introduced as sintering aids in Ni-Cu-Zn ferrites adequately suit these demands and are considered to shape the future of advanced technology.

The scopes of the future works are proposed as:

(i)   Different spinel ferrite systems to investigate the effect on lowering the sintering temperature are improving electromagnetic properties.

(ii)   To investigate the mechanism of sintering for different sintering aids.

(iii)   Fabrication and characterization of multilayer chip inductor using improved Ni-Cu-Zn ferrites as stated.

(iv)   AC and DC electrical properties may be studied.

(v)   SEM can be studied for better understand surface nature and domain wall motion.

Therefore future work on these types of systems may be carried out using electromagnetic properties such as permeability and resistivity is dependent on the densification and macrostructure of the ferrite. Substitution and additives of sintering aids in ferrites have been used as attractive approaches to enhance the electromagnetic properties.

REFERENCES

CHPATER-I

[1.1]   Goldman A.;   "Recent Advances in Ferrite Materials Technology", in Modern Ferrite Technology, Van Nostrand Recinhold, New York, 1990

[1.2]   Culity B. D. and Graham C. D.; "Introduction to magnetic materials", 2nd edition, A. Willey & Son Publication, U. S. A., 2009

[1.3]   Snoek   J.   L.;   "New   developments   in   Ferromagnetism   & Antiferromagnetism"; Annales de physique, 3, 137, 1948.

[1.4]   Suzuki T., Tanaka T. and Ikemizu K.; "High density recording capability for advanced particulate media", J. Magn. Magn. Mater. 235, 159, 2001.

[1.5]   Giannkopoulou T., Kompotiatis L., Kontogeorgakos A. and Kordas G.; "Microwave behavior of ferrites prepared via Sol-gel method", J. Magn. Magn. Mater. 246, 360, 2002.

[1.6]   Olsen E. and Thonstad J.; "Nickel ferrite as inert anodes in aluminum electrolysis", J. Appl. Electrochem., 29, 293-311, 1999.

[1.7]   Augustin C. O., Prabhakaran D. and Srinvasan L. K.; "The use of the inverted-blister test to measure the adhesion of an electrocoated paint layer adhering to a steel substrate", J. Mater. Sci. Lett., 12, 383, 1993.

[1.8]   Kulikowski J.; "Soft magnetic ferrites development or stagnation", J. Magn. Magn. Mater. Vol.41, pp.56-62, 1984.

[1.9]   Verma A., Goal T. C., Mendiratta R. G. and Gupta R. G.; "High-resistivity nickel-zinc ferrite by the citrate precursor method", J. Magn. Magn. Mater. Vol.192, pp.271-276, 1999.

[1.10]   Nakamura T., Miyaonoto and Yamada Y.; "Complex Permeability spectra of Polycrystalline Li-Zn ferrite and application of EM-wave absorber", J. Magn. Magn. Mater. Vol.256, pp.340-347, 2003.

[1.11]   Laksman A., Rao K. H. and Mendiratta R. G.; "Magnetic properties of In^{5+} and Cr^{3+} substituted Mg-MN ferrites", J. Magn. Magn. Mater. Vol.250, pp.92-97, 2002.

[1.12]   Hakim M. A., Manjurul Haque M., Huq M., Manjura Hoque Sk. And Nordblad P.; "Rcentrant Spin Glass and Spin Glass Behavior of Diluted Mg-Zn Ferrites", Cp 1003, Magnetic Materials, International Conference on Magnetic Materials (ICMM-2007) AIP, p-295, 2007.

[1.13]   Kin O. Low and Frank R. Sale; "Electromagnetic properties of gel-derived Ni-Cu-Zn ferrites", J. Magn. Magn. Mater. Vol.246, pp.30-45, 2002.

[1.14]   Manjurul Haque M., Huq M. and Hakim M. A.; "Thermal hysteresis of Permeability and Transport properties of Mn substituted Mg-Cu-Zn ferrites", Journal of Physics D:Applied Physics, Vol.41, 055007, pp.1-10, 2008.

[1.15]   Khan Z. H., Mahbubur Rahman M., Sikder S. S., Hakim M. A. and Saha D. K.; "Complex Permeability of Fe-deficient Ni-Cu-Zn ferrotes", Journal of Alloys and Compounds, Vol.584, 208-215, 2013.

[1.16]   Jean J. H. and Lee C. H.; "Effects of Lead (11) Oxide on Processing and Properties of Low –Temperature Cofirable Ni-Cu-Zn Ferrite", J. Am. Ceram. Soc, 82, 343-350, 1999.

[1.17]   Akther Hossain A. K. M., Mahhmud S. T., Seki M., Kawai T. and Tabata H.; "Structural, electrical transport and magnetic properties of $Ni_{1-x}Zn_xFe_2O_4$", J. Magn, Magn. Mater., 312, 210, 2007.

[1.18]   Stoppels D.; "Development in soft magnetic power ferrites", J. Magn, Magn. Mater., 160, 323, 1996.

[1.19]   Balayachi A., Dormann J. L. and Nogues M. "Critical analysis of magnetically semi disordered systems: Critical exponents at various transitions"; J. Phys.: Condens. Matter., 10, 1599, 1998.

[1.20]   Seo S. H. and Oh J. H.; "Effect of MoO_3 Addition of Sintering Behaviors and Magnetic properties of Ni-Cu-Zn Ferrite for Multilayer Chip Inductors", IEE Transactions on Magnetics, Vol.35, No.5, 1999.

[1.21]   Manjurul Haque M., Huq M. and Hakim M. A.; "Influence of CuO and sintering temperature on the microstructure and magnetic properties of Mg-Cu-Zn Ferrites", J. Magn. Magn. Mater., Vol.320, pp.2792-2799, 2008.

[1.22]   Amarenda K. S., Goel T. C. and Mendiratta; "Magnetic properties of Mn-Zn Ferrites", J. Applied Physics, Vol.92, pp.3872-3876, 2002.

[1.23]   Khan Z. H., Sikder S. S., Hakim M. A., Saha D. K. and Noor S.; "Structural and Magnetic properties of Cu-substitute Ni-Cu-Zn ferrites", Journal of Engineering Science, 02, 81-85, 2011.

[1.24]   Tsakloudi V., Elattherion E., Stoukises M. and Zaspalis V.; "Electromagnetic properties of Mn-doped Ni-Cu-Zn Ferrites", J. Magn. Magn. Mater., 318, 58, 2007.

[1.25]   Ahmed T. T., Rahman I. Z. and Tofail S. A. M.; "Effect of copper ion distribution on the magnetization of nano scaled Ni-Zn Ferrite", J. Magn. Magn. Mater., Vol.272-276, pp.2250-2252, 2004.

[1.26]   Herzer G., Vaznez M., Knobel M., Zhokov A., Reininger T. and Davies H. A.; "Present and future applications of nanocrystalline magnetic materials", J. Magn. Magn. Mater., 294, 252, 2005.

[1.27]   Khan Z. H., Mahabubur Rahman M. Sikder S. S., Hakim M. A., Shireen Akhter, Das H. N. and Anjuman B; "Thermal Hysteresis of Cu substitute $Ni_{0.28}Cu_{0.10+x}Zn_{0.62-x}Fe_{1.98}O_4$ ferrites", Advanced Chemistry letters, Vol.1, pp.1-6, 2013.

[1.28]   Low K. O. and Sale F. R.; "Electromagnetic properties of Gel-derived Ni-Cu-Zn ferrites", J. Magn. Magn. Mater., 246, 30-35, 2002

[1.29]   Khan Z. H., Mahabubur Rahman M. Sikder S. S., Hakim M. A. and Saha D. K.; "Complex Permeability of Fe-deficient Ni-Cu-Zn ferrites", Journal of Alloys and Compounds, 548, 208-215, 2013.

[1.30]   Haque M. M., Huq M. and Hakim M. A.; "Effect of Zn^{2+} substitution on the magnetic properties of $Mg_{1-x}Zn_xFe_2O_4$ ferrites"; Physica, B404, 3915, 2009.

[1.31]   Yue Z., Zhou J., Li L., Wang X. and Gui Z.; "Effect of copper on the electromagnetic properties of Mg-Cu-Zn ferrites prepared by Sol-gel auto-combustion method", Mater. Sci. Eng., B86, 64, 2001.

[1.32]   Rezlescu N., Rezlescu E., Popa P. D., Craus M. L., Rezlescu L.; J. Magn. Magn. Mater, 182, 199, 1998.

[1.33]   Rezlescu E., Rezlescu N., Popa P. D., Rezlescu L., Pasnicu C., Craus M.L.; Mat. Res. Bull. 33(6), 915, 1998.

[1.34]   Saroaut Noor, Hakim M. A., Sikder S. S., Manjura S. Haque, Kazi Hanium Marja and Per Nordblad; "Magnetic Behavior of Cd^{2+} & substituted Cobalt ferrites"; Journal of Physics and Chemistry of Solids; 73, pp 227-231, 2011.

[1.35]   Farea A. M. M., Shatendra Kumar, Khalid Majasam Batoo, Ali Yousef, Alimuddin; " Influence of frequency, temperature and composition on electrical properties of polycrystalline $Co_{0.5}Cd_xFe_{2.5-x}O_4$ ferrites"; Physica B403, 684, 2008.

[1.36]   Nomura T. and Nakano A.; Proc. 6th Int. Conf. on Ferrites, 1198, 1992.

[1.37]   Nakamura T. and Okano; "Low Temperature Sintered Ni-Zn-Cu Ferrite", J. Phys. IV France, 7, CI-91, 1997.

[1.38]   Yasuda K., Mochizuki and Takaya M.; Proceedings of the Eight International Conference of Ferrites (ICF8), p.1162, Kyoto 2000.

[1.39]   Yue Z., Zhou K., Li L., Zhang H. and Gui Z.; "Synthesis of nanocrystalline Ni-Cu-Zn ferrites powder by Sol-gel auto-combustion method", J. Magn. Magn. Mater., 208, 55-60, 2000.

[1.40]   Töpfer J. and Mürbe J.; Proceedings of the 9th International Conference of Ferrites (ICF9), P.885, San Francisco, 2004.

[1.41]   Hsu J. Y., Ko W. S. and Chen C. J.; "The effect of V_2O_5 on the sintering of Ni-Cu-Zn ferrites", IEEE Trans. Magn., 31, 3994, 1995.

[1.42]   Jean J. H. and Lee C. H.; "Effect of Lead (11) Oxide on Proceesing and Properties of Low Temperature Cofirable Ni-Cu-Zn Ferrite", J. Am. Ceram. Soc., 82, 343-350, 1999.

[1.43]   Jeong J., Han Y. H. and Moon B. C.; "Effect of B_{i2O3} addition on the microstructure and electromagnetic properties of Ni-Cu-Zn ferrites", J. Mater. Sci: Mater. Electronics, 15(5), 303-306, 2004.

[1.44]   Wang S. F., Wang Y. R. , Yang T. C. K., Chen C. F., Lu C. A. and Huang C. Y.; J. Magn. Magn. Mater., 220, 129, 2000.

[1.45]   Yang Y. H. and Wang S. F.; Int. J. Inorg. Mat. 3, 1189, 2001.

[1.46]   Su H., Zhang H. and Tang X.; Mater. Sci. Engg., B117, 231 2005.

[1.47]   Kawano K. , Sakurai N., Kusumi S. and Kishi H.;J. Magn. Magn. Mater., 297, 26, 2004.

[1.48]   Kong L. B. , Li Z. W., Lin G. Q. and Gan Y. B.; " Electrical and magnetic properties of magnetism ferrite ceramics doped with Bi_2O_3", Acta Materialia 55, 6561, 2007.

[1.49]   Ping Hu, Yang H., Pan D., Wang H., Tian J., Zhang S., Wang X. and Volinsky A. A.; "Heat treatment effects on microstructure and magnetic properties of Mn-Zn ferrite powders", J. Magn. Magn. Mater., 322, 173-177, 2010.

[1.50]   Jingling Sun, Jianbao Li and Geliang Sun; "Effects of La_2O_3 and Ga_2O_3 on some properties of Ni-Zn ferrites", J. Magn. Magn. Mater., 250, 20, 2002.

[1.51]   Naknao A., Nakahata I., Murse T.; J. Jpn. Soc. Powder Powder Metal: 48(2) 131, 2001.

[1.52]   Brabers V. A. M., Hirsch A. A., Vleuten W. C. V., Doremalen P.V. ; IEEE Trans. Magn. 14(5), 895, 1978.

[1.53]   Seo S. E. and Oh J. H.; IEEE Trans. Magn., 35(5), 3412, 1999

[1.54]   Gu M. and Liu G.; J. All. Compds., 475(1-2), 356, 2009.

CHAPTER-II

[2.1]   Smit J. and Wijn H. P. J.; "Ferrites", John Wiley & Sons, New York, 1959.

[2.2]   Ogasawara T. and Oliveira; "Microstructure and hysteresis curves of the barium hexaferrite from co-precipitation by organic agent", J. Magn. Magn. Meter. 217, 147, 2000.

[2.3]   Standly K. J.; "Oxide Magnetic Materials"; 2nd ed., Oxford University Press, 1972.

[2.4]   Rollin J. Parker; John Wiley and Sons, "Advances in Permanent Magnetism"; Inc., New York, 1990.

[2.5]   Bragg W. H.; "The structure of magnetic and the spinels"; 95, 561, 1915.

[2.6]   Cullity B. D. and Graham C. D.; "Introduction to Magnetic Materials", John Wiley & Sons, New Jersey, 1972.

[2.7]   Livingston J. D.; "Driving Forces: The Natural Magic of Magnets"; Harrand University Press: Cambridge, 1996.

[2.8]   Alex Goldman; "Modern Ferrite Technology", Van nosttrand Reinhold, New York, 1990.

[2.9]   Li F. S., Wang L., Wang J. B., Zhou Q. G., Zhou X. Z., Kunkel H. P. and Williams G.; J. Magn. Magn. Mater., 268, 332, 2004.

[2.10] Chen C. W.; "Magnetism and Matallurgy of Soft Magnetic Materials"; New York 1977.

[2.11] Neel L.; "Magnetic properties of ferrites: Ferrimagnetism and Antiferromagnetism", Annales de Phys. e, 3, 137-198, 1948.

[2.12] "International Tables for X-ray Crystallography"; The Kyvoch Press, Birmingam, England, 1965.

[2.13] Chan R. W., Haasen P. and Kramer E. J.; "Materials Science and Technology", Vol.3B, VCH Publishers Inc., New York, NY (USA) & Verlagsgesellschaft mbH, weinheim (Federal Republic of Germany), 1994.

[2.14] Omar M. A.; "Elementary Solid State Physics (Principles & Applications)", Addison –Wesley Amsterdam, 1962.

[2.15] Parasnis D. S., Harper and Brothers; "Magnetism: from lodestone to Polar Wandering", New York, 1961.

[2.16] Viswanathan B. and Murthy V. R. K.; "Ferrite Materials Science and Technology", Spring Verlag, Noarosa Publishing House, New Delhi, 1990.

[2.17] Craik D. J.; "Magnetic Oxide", Part1, John Wiley & Sons, Ltd., Bristol England.

[2.18] Verway E. J. W. and Heilmann E. L.; T. Cham. Phys., 15(4), 174 -180, 1947.

[2.19] Anderson P. W.; "in Magnetism", part 1, Eds., G. T. Rado and H. Suhl (Academic Press, New York, 1963.

[2.20] Reitz J. R., Milford F. J. and Chrisly R. W.; "Foundations of Electromagnetic Theory", 3rd Ed. Addison – Wesley London, 1979.

[2.21] Halliday D., Resnick R. and Walker J.; "Fundamentals of Physics", 6th Ed. John Wiley & Sons, New York, 2002.

[2.22] Knepicka S. and Novak P.; "Oxide spinels", In E. P. Wohlfarth, editor, Ferromagnetic Materials, Volume 3, Chapter 4, Pages 184-304, North-Holland, The Netherlands, 1982.

[2.23] Anderson P. W.; in Magnetism, Vol.1, Eds., G. T. Rado and H. Suhl (Academic Press, New York, 1963.

[2.24] Yafet Y. and Kittel C.; "Antiferromagnetic arrangements in ferrites", Phys. Rev. 87, 290,1952.

[2.25] Leyons D. H., Keplan T. A., Dwight K. and Menyuk N; "Classical theory of the ground spin state in cubic spinels", Phys. Rev. 126, 540, 1962.

[2.26] Land A.,; "Quantum Mechanics", Pitman London, 1951.

[2.27] Van Vleck J. H.; "Theories of Electric and Magnetic photonic Crystals", IEEE Antenna Propagant. SOC Symp. 2, 1395, 2004.

[2.28] Weiss P.; "L'hypothese du champ molecular et lu propriete ferromagnetic", Claredon press, Oxford, 1932.

[2.29] Vowles Hugh P.; "Early evolution of Powder Engineering", 17(2), 412, 1932.

[2.30] Fowler Michael; "Historical Begimmry of Theories of Electricity and Magnetism", Retrived, 2008.

[2.31] Alex Goldman; "Modern Ferrite Technology", Van Nosttrand Reinhold, New York, p.15, 1940.

[2.32] William D. Cattister; The University of Utah, Materials Science and Engineering 6th ed., Wiley 2003.

[2.33] Samokhvalov A. A. and Rustamov A. G.; Sov. Phys. Solid State, 6, 749, 1964.

[2.34] Bossmann A. J. and Crevecoeur C.; "Machanism of the electrical conduction in Li-doped NiO", Phys. Rev. 144, 763, 1966.

[2.35] Verway E. J., Haayman P. W. and Romeijin; "Physical Properties and Cation Arrangement of Oxides with Spinel Structure 11. Electronic conductivity", J. Chem. Phys. 15(4), 181-187, 1947.

[2.36] Van Uitert L. G.; "High-Resistivity Nickel Ferrites – The Effect of Minor Additions of Manganese or Cobalt", J. Chem. Phys. 24(2), 306-310, 1956.

[2.37] Jonker G. H.; "Analysis of the semiconducting properties of cobalt ferrite", J. Phys. Chem. Solids, 9(2), 165-175, 1959.

[2.38] Mandal S., Banerjee D., Bhattacharya R. N. and Ghosh A. A.; "Thermoelectric power of unconventional lead vanadate glass", J. Phys: Condens Matter 8, 2865-2868, 1996.

[2.39] Samokhvalov A. A. and Rustamov A. G.; Sov. Phys. Solid state, 6, 744, 1964.

[2.40] Bosman A. J. and Crevecour C.; "Mechanism of the Electrical Conduction in Li Doped NiO", Phys. Rev. 144 (2), 763-770, 1966.

[2.41] Jonker G. H. and Van Santen J. H.; "Magnetic Compounds with perovskite structure 111. ferromagnetic compounds of cobalt", J. Physica, 19(1-12), 120-130, 1953.

[2.42] Bhise R. V., Mahajan V. C., Patil M. G, Lotke S. D. and Pati S. A l; Indian J. Physics 33, 454-462, 1995.

[2.43] Bhise B. V., Ghatage A. K., Kulkarni B. M., Lotke S. D. and Patil S. A.; Bull. Mater. Sci; 19(3), 1996.

[2.44] Patil M. G., Mahajan V. C., Bhise B. V., Chendke S. M., and Patil S. A.; Phys. Stat. Sol. (a) 144, 415, 1994.

[2.45] Patil B. L., Patil A. B., Patil M. G., Mahajan V. C., Bhise B. V., Chandke S. M., Sawant S. R. and Patil S. A.; Materials Research Lab. Shivaji Univ. India.

Chapter III

[3.1] Kong L. B., Li Z. W., Lin G. Q. and Gan Y. B.; "Magneto-Dielectric properties of Mg-Cu-Co ferrites Ceramic: II Electrical, dialectical and magnetic properties", J. Am. Ceram. Soc., 90(7), 2014, 2007.

[3.2] Sharma S. K., Kumar R., Kumar S. Knobel M., Menses C.T., Kumar V. V. S., Reddy V. R. , Singh M. and Lee C. G.; " Role of inter partical interactions on the magnetic behavior of $Mg_{0.95}Mn_{0.05}Fe_2O_4$ ferrite nanoparticales"; J. Phys. Conden. Matter. , 20, 235214, 2008.

[3.3] Zahi S., Hashim M. and Daud A. R.; "Synthesis magnetic and microstructure of Ni-Zn ferrite by Sol-gen technique"; J. Magn. Magn. Mater., 308, 177, 2007.

[3.4] Hakim M. A., Saha D. K. and Fazle Kibria A. K. M. ; "Synthesis and temperature dependent structural study of nanocrystalline Mg- ferrite materials"; Bang. J. Phys., 3, 57, 2007.

[3.5] Bhaskar A., Rajini Kanth B. and Murthy S. R.; "Electrical properties of Mn added Mg-Cu- Zn ferrites prepared by microwave sintering method"; J. Magn. Magn. Mater.; 283, 109, 2004.

[3.6] Yue Z., Zhou J., Li L. and Gui Z.; " Effects of MnO_2 on the electro-magnetic properties of Ni-Cu-Zn ferrites prepared by sol-gel auto combustion"; J. Magn. Magn. Mater., 233, 224, 2001.

[3.7] Burke J. E. ; "Kinetics of High Temperature Processes", Kingery W. D. ed. (wiley, NY) 1959

[3.8] Slick P. I.; " Ferrites for Non-microwave applications", ferromagnetic materials, Ed. E. P. Wolfarth, North Holland Pub Co_2, 1980

[3.9] Kittel C.; Introduction to Solid State Physics, 7th edition, John Wiley and Sons, Inc., Singapore, 1996

[3.10] Nelson J. B., Riley D. P; "An experimental investigation of extrapolation methods in the derivation of accurate unit-cell dimensions of crystals", Proc. Phys. Soc. London 57, 160, 1945.

[3.11] Gadkari A. B., Shinde T. T. and Vasambekar P. N. ; "Structural and Magnetic properties of nanocrystalline Mg-Cd ferrites prepared by oxalate Co-precipitation methods"; J. Mater. Sci. Mater. Electron, 21(1), 96 - 103, 2010.

[3.12] Tahir Abbas, Islam M. U. and Ashraf M.; Ch. Mod. Phys. Letts. B, 9(22), 1419, 1995.

[3.13] Balayachi A., Dormann J. L. and Nogues M.; "Critical analysis of magnetically semi disordered systems: critical exponents at various transitions", J. Phys. Condens. Matter. 10, 1599, 1998.

[3.14] Simon Forner; "Versatile and sensitive Vibrating Sample Magnetometer", Rev. Sci. Instr. 30, P.548, 1959

Chapter IV

[4.1]   Wang S. F., Wang Y. R., Yang T. C. K., Chen C. F., Lu C. A. and Huang C. Y.; "Densification and magnetic properties of low fire Ni-Cu-Zn ferrites", J. Magn. Magn. Mater. 220, 129-138, 2000.

[4.2]   Nakamura T.; "Low-temperature sintering of Ni-Cu-Zn ferrite and its permeability spectra", J. Magn. Magn. Mater. 168, 285-29, 1997.

[4.3]   Lebourgeois R., Duguey S., Ganne J. P. and Heintz J. M.; "Influence of V_2O_5 on the magnetic properties of Ni-Cu-Zn ferrites", J. Magn. Magn. Mater. 312, 328, 2007.

[4.4]   Jeong J., Han H. Y. and Moon C. B.; "Effects of Bi_2O_3 addition on the microstructure and electromagnetic properties of Ni-Cu-Zn ferrites", J. Nat. In Elect., 15(5), 303, 2004.

[4.5]   Kawano K., Sakurai N., Kusumu S. and Kishi H.; "Magnetic permeability and microstructure of the Bi, Si oxides-doped Ni-Cu-Zn ferrite composite material", J. Magn. Magn. Mater. 297(1), 26-32, 2006.

[4.6]   Yan M., Hu J., Luo W. and Zhang W. Y.; "Preparation and investigation of low firing temperature Ni-Cu-Zn ferrites with high relative initial permeability", J. Magn. Magn. Mater. 303(1), 249, 2006.

[4.7]   Khan Z. H., Sikder S. S., Md. Masud Rana and Hakim M. A.; "Effect of V_2O_5 and Li_2O on the magnetic properties of Ni-Cu-Zn ferrites", International Conference on Advance in Physics in the 4th February 2013, Department of Physics, University of Dhaka, Bangladesh.

[4.8]   Su H., Zhang H., Tang X. and Xiang X.; "High permeability and high Curie temperature Ni-Cu-Zn ferrite", J. Magn. Magn. Mater. 283, 157, 2004.

[4.9]   Seo S. H. and Oh J. H.; "Effect of MoO_3 addition on sintering behaviors and magnetic properties of Ni-Cu-Zn ferrite for multilayer chip inductor", IEEE Trans. Magn., 35(5), 3412 – 3414, 1999.

[4.10] Wang S. F., Wang Y. R., Yang T. C. K., Wang F. J. and Lu C. A.; "Densification and properties of fluxed sintered Ni-Cu-Zn ferrites", J. Magn. Magn. Mater. 217, 35, 2000.

[4.11] Jean J. H., Lee C. H. and Kou W. S.; "Effects of Lead(II) Oxide on processing and properties of low-temperature Cofirable Ni-Cu-Zn ferrite", J. Am. Ceram. Soc. 82(2), 343 – 350, 1999.

[4.12] Park K. S., Nam J. H. and Oh J. H.; "Magnetic properties of Ni-Cu-Zn ferrites with addition of tungsten trioxide" J. Magn. Magn. Mater. 226-230, 1415, 2001.

[4.13] Hsu J. Y., Ko W. S. and Chen C. J.;"The effect of V_2O_5 on the sintering of Ni-Cu-Zn ferrites", IEEE Trans. Magn. 31(6), 3994, 1995.

[4.14] Su H., Zhang H. and Tang X.; "Effects of Bi_2O_3-WO_3 additions on sintering behaviors and magnetic properties of Ni-Cu-Zn ferrites", Mat. Sci. Engg. B117, 231, 2005.

[4.15] Nelson J. B., Riley D. P.; "An experimental investigation of extrapolation methods in the derivation of accurate unit-cell dimensions of crystals"; Proc. Phys. Soc. London 57, 160, 1945.

[4.16] Vegard L.; "Die constitution der mischkristalle und die raumfulling der atome", Z. Phys. 5, 17, 1945.

[4.17] Cullity B. D.; "Introduction to Magnetic Materials'; Addison –Wesley publishing company, Inc. 1972.

[4.18] Shrotri J., Kulkarni S. D., Deshpande C. E. and Date S. K.; "Effect of Cu substitution on the magnetic and electrical properties of Ni-Zn ferrite synthesized by soft chemical method", Mater. Chem. Phys., 59, 1, 1999.

[4.19] Overshott K.; "The causes of the anomalous Coss in amorphous ribbon materials", IEEE, Trans. Magn. 17, 2698, 1981.

[4.20] Nakamura T.; "Low temperature sintering of Ni-Cu-Zn ferrite and its permeability spectra", J. Magn. Magn. Mater. 168, 285, 1997.

[4.21] Gorter E. W.; "Saturation magnetization and crystal symmetry of ferromagnetic oxides", Philips Res. Rep. 9, 295, 1954.

[4.22] Iwauchi K.; "Dielectric properties of fine particles of Fe_3O_4 and some ferrites", Jpn. J. Appl. Phys. 10, 1520, 1971.

[4.23] Kumar Kunar B. and Srivastava G.; "Dispersion observed in electrical properties of titanium substituted lithium ferrites", J. Appl. Phys., 75, 6115, 1994.

CONFERENCE PUBLICATIONS

1. M. A. Gofur, Z. H. Khan, M. A. Hossain, S. S. Sikder, D. K. Saha and S. M. Hoque; "Effect of V_2O_5 Doping on Microstructure, Magnetic and Dielectric Behavior of Ni-Cu-Zn Ferrites", International Conference on Physics 2016, 10-12 March.

2. M. A. Gofur, M. A. Hossain, S. S. Sikder, D. K. Saha and M. N. I. Khan; "Effect of Sintering Temperature on Complex Permeability Ni-Cu-Zn Ferrite with V_2O_5 Addition", International Conference on Physics 2016, 10-12 March.

3. M. A. Gofur, M. A. Hossain, Z. H. Khan, S. S. Sikder, D. K. Saha; "Dielectric and Magnetic Properties of Ni-Cu-Zn Ferrite with V_2O_5 Addition", Conference on Whether Forecasting and Advances in Physics; Bangladesh Perspectives, 21 May 2016
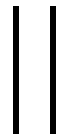
M. Phil. Thesis | | Md. Abdul Gofur | | December-2016